FACULDADE DE ENGENHARIA
DA UNIVERSIDADE DO PORTO

Mestrado em Engenharia Mecânica (MEM)

3D printer nozzle: effects of die dimension, geometry, and material on the quality of FFF printed parts in PLA

Joana Maria Tribuzi Magalhães Melo
(up201503568)

Advisor: Fernando Jorge Lino Alves (Dr.)

Co-Advisor: Leonardo Santana (Dr.)

Porto, 2022

(blank space)

Aos meus pais, às minhas irmãs e ao Nuno

(blank page

Resumo: as impressoras 3D de fabricação de filamentos fundidos (FFF) democratizaram a manufatura aditiva (AM) para uma ampla gama de usuários devido ao seu baixo custo e interface amigável. Um dos principais elementos dessas máquinas é o bico, responsável pela condução da energia térmica para o processamento da transformação do material de construção e para controlar o volume de extrusão e a resolução do processo de impressão, pois afeta as dimensões e geometrias dos filamentos extrudados. Nesse sentido, o bico desempenha um papel muito importante no índice econômico e técnico que definem a qualidade dos objetos impressos por FFF. Atualmente, existem muitos tipos de bicos no mercado o que torna a escolha deste componente pelo utilizador uma tarefa difícil. Assim, o objetivo deste estudo foi entender os efeitos de bicos, em materiais, diâmetros e geometrias de saída, na qualidade de extrusão, propriedades mecânicas à flexão e porosidade total das peças impressas em Ácido Polilático (PLA). O estudo foi realizado em três partes distintas. Numa primeira fase, foi feita uma análise utilizando três bicos com o mesmo diâmetro, neste caso 0,4 mm, mas variando seu material, (latão, aço temperado e vanádio). Nesta etapa, as amostras foram impressas com duas orientações de construção, “no plano” e na lateral, para avaliar os efeitos da vida últil dos bicos de latão e para avaliar a capacidade de fornecimento de energia térmica dos bicos, com maior e menor influência a cama aquecida da impressora. Numa segunda etapa, foram estudados os efeitos de bicos de latão em diferentes diâmetros (0,4; 0,6 e 0,8 mm) e dos parâmetros de controle da largura e espessura de camada na formação mesoestrutural dos componentes impressos. A avalição das peças na etapa 2 usou as mesmas respostas da primeira fase. Finalmente, uma análise dos efeitos do diâmetro do bocal e do material no inchamento do extrudido em testes de extrusão, foram realizados para cada bico. No terceiro caso de estudo, o LDPS/FEUP juntou-se à Palbit™ para conceber e construir um bocal calibrado de carboneto de tungstênio com uma cavidade de saída quadrada e analisar seus efeitos sobre as propriedades mecânicas, nível de porosidade e estabilidade de forma de objetos impressos em Ácido polilático (PLA). Primeiramente, os parâmetros de impressão foram calibrados para o novo bico, com a ajuda do desenho experimental de Taguchi. Em seguida, as variáveis de fatiamento foram mantidas constantes, e amostras foram fabricadas para testes de flexão, cubos para medição de porosidade e peças para digitalização 3D. Para fins de comparação, os mesmos parâmetros foram usados para construir os modelos mencionados com bico convencional de latão cilíndrico. Os bicos de aço temperado e latão de 0,6 mm foram os aqueles que forneceram os melhores resultados para a resposta avaliada em suas respectivas etapas. No entanto, o bico de latão de 0,4 mm pode ter sido danificado devido ao seu desgaste natural devido a longas jornadas de impressão que foi submetido em trabalho anterior. Com o segundo caso de estudo, concluiu-se que ao escolher um bico de impressora, o usuário deve considerar a vida útil do componente, a estabilidade de sua deposição bem como sua impressão repetibilidade de qualidade. Os resultados do terceiro caso de estudo mostraram que as propriedades mecânicas, módulo e tensão máxima à flexão, das amostras impressas com o bico quadrado foram ligeiramente inferiores

aos obtidos com o cilíndrico. Os níveis de porosidade foram equivalentes em ambos os bicos, indicando uma organização meso-estrutural, em relação aos vazios. Ambos os grupos de amostras apresentaram desvios de formas próximas, mostrando, portanto, níveis semelhantes de resolução. As baixas propriedades mecânicas obtidas com o bico quadrado podem estar relacionadas à sua influência na comportamento de cisalhamento e transferência de calor para o material a ser extrudido. Além disso, controlar o alinhamento da cavidade quadrada com os eixos x e y da plataforma de impressão não foi simples, o que pode ter afetado a orientação geométrica do extrudado durante a deposição. Os problemas mencionados podem ter afetado a força de adesão do filamentos inter e intracamadas.

Palavras-chaves: Fabricação por Filamentos Fundidos, PLA, vida útil, propriedades mecânicas, porosidade, material do bico, diâmetro do bico, geometria do bico.

Abstract: Fused Filament Manufacturing (FFF) 3D printers have democratized additive manufacturing (AM) for a wide range of users due to their low cost and user-friendly interface. One of the main elements of these machines is the nozzle, responsible for conducting the thermal energy for processing the transformation of the building material and for controlling the extrusion volume and the resolution of the printing process, as it affects the dimensions and geometries of the extruded filaments. In this sense, the nozzle plays a very important role in the economic and technical index that define the quality of objects printed by FFF. Currently, there are many types of nozzles on the market which makes the choice of this component by the user a difficult task. Thus, the objective of this study was to understand the effects of nozzles, on materials, diameters, and output geometries, on extrusion quality, mechanical properties at bending and total porosity of Polylactic Acid (PLA) printed parts. The study was carried out in three distinct parts. In a first phase, an analysis was carried out using three nozzles with the same diameter, in this case 0.4mm, but varying their material (brass, tempered steel and vanadium). In this step, the samples were printed with two construction orientations, “in the plane” and on the side, to evaluate the effects of the service life of the brass nozzles and to evaluate the thermal energy supply capacity of the nozzles, with greater and lesser influence. the printer's heated bed. In a second step, the effects of brass nozzles in different diameters (0.4, 0.6 and 0.8 mm) and the parameters of control of layer width and thickness on the mesostructural formation of the printed components were studied. The evaluation of the pieces in step 2 used the same answers as in the first phase. Finally, an analysis of the effects of nozzle diameter and material on extrudate swelling in extrusion tests was performed for each nozzle. In the third case study, LDPS/FEUP teamed up with Palbit™ to design and build a calibrated tungsten carbide nozzle with a square outlet cavity and analyze its effects on mechanical properties, porosity level and shape stability. objects printed in Polylactic acid (PLA). First, the printing parameters were calibrated for the new nozzle, with the help of Taguchi's experimental design. Then the slicing variables were held constant, and samples were fabricated for bending tests, cubes for porosity measurement, and parts for 3D digitization. For comparison purposes, the same parameters were used to build the aforementioned models with a conventional cylindrical brass nozzle. The 0.6 mm hardened steel and brass nozzles were the ones that provided the best results for the response evaluated in their respective stages. However, the 0.4mm brass nozzle may have been damaged due to its natural wear and tear from the long print runs it underwent in previous work. With the second case study, it was concluded that when choosing a printer nozzle, the user must consider the component's useful life, the stability of its deposition as well as its print quality repeatability. The results of the third case study showed that the mechanical properties, modulus and maximum flexural stress, of the samples printed with the square nozzle were slightly lower than those obtained with the cylindrical one. The porosity levels were equivalent in both nozzles, indicating a meso-structural organization, in relation to the voids. Both groups of samples showed deviations of close shapes, thus showing similar levels of resolution. The low mechanical properties obtained with the square nozzle may be related to its influence on the shear behavior

and heat transfer to the material to be extruded. Also, controlling the square cavity alignment with the print platform's x and y axes was not straightforward, which may have affected the geometric orientation of the extrudate during deposition. The mentioned problems may have affected the adhesion strength of the inter and intralayer filaments.

Keywords: Fused Filament Fabrication, PLA, lifespan, mechanical properties, porosity, nozzle material, nozzle diameter, nozzle geometry.

Acknowledgments:

I would like to take this opportunity to thank all the people who directly and/or indirectly were present during the development of the work of this dissertation, as well as throughout my academic career.

In this way, I thank:

To Doctor Jorge Lino, my advisor, for the attention and trust and encouragement shown throughout the entire work, as well as the effort so that I never encountered problems or lack of material and working conditions.

To Dr. Leonardo Santana, my co-supervisor, for his availability, for his tireless help, for the numerous meetings and for all the patience and enriching tips to make this work possible.

To Master Henrique Takashi, for his help, support, availability, and knowledge sharing.

To Doctor Bruno Areias for helping me to overcome some technical challenges throughout this work and for all the help provided.

To Master Ana Pais for always being available to help in my experimental trials and in adversities that arose along the way and for all the shared knowledge.

To Dr. Marco Marques, for the guidance and support provided within the laboratory.

To Engineer Diogo Vieira da Silva for providing the technical drawing of the square nozzle that was used. To Palbit™ for manufacturing and offering the square nozzle that was used in this study.

To Dona Emília for the help in the measurements and tests performed.

To Dr. Guilherme Mariz Oliveira Barra, from UFSC/Brazil, for providing the balance for measuring the density of the filaments.

To the LDPS for hosting me during these 6 months of dissertation and for the help provided by all the members in always helping me.

To INEGI, for the help in carrying out some of the tests.

To my parents, for providing conditions throughout my academic career.

To my sisters, for all their support and willingness to help.

To Nuno, for all the patience, understanding, help, support, and companionship over the years and especially throughout this work.

(blank page)

Acronym List

3D - Three Dimensional

ABS – Acrylonitrile Butadiene Styrene

AM – Additive Manufacturing

ASA – Acrylonitrile Styrene Scrylate

ANOVA - Analysis of Variance

ASTM – American Society for Testing and Materials

CAD – Computed Aided Design

CNC – Computer Numeric Control

FDM – Fused Deposition Modeling

FFF – Fused Filament Fabrication

FM – Flexion Module

FTIR – Fourier Transformed Infrared Spectroscopy

HIPS – High Impact Polystyrene

LDPS - Product and Services Development Laboratory

MFS – Maximum Flexural Strength

OS - Open Source

PETG – Polyethylene Ethylene Glycol Terephthalate

PLA – Polylactic Acid

STL – Standard Triangle (Tesselation) Language

TPU – Thermoplastic Polyurethane

Rw – Road width

(blank page)

List of Symbols

α – Significance level of statistical analysis (ANOVA)

T_g – Glass transition temperature

W_D – Dry sample mass for density measurement

W_i – Mass of the sample immersed in distilled water to measure the density

W_S – Mass of the wire used to measure the density

ρ – Density [kg/m^3]

φ – Porosity

(blank page)

Generated scientific disclosures

(1) MELO, Joana Tribuzi; SANTANA, Leonardo; IDOGAVA, Henrique Takashi; ALVES, Jorge Lino. 3D printer nozzle: effects of its diameter and material on the quality of extruded filament and FFF-printed parts. In: International Cappadocia Scientific Research Congress, 2021, Cappadocia (Online). **Oral presentation.**

(2) MELO, Joana Tribuzi; SANTANA, Leonardo; IDOGAVA, Henrique Takashi; ALVES, Jorge Lino, LOPES PAIS, Ana Isabel. Effects of nozzle material and its lifespan on the quality of PLA parts manufactured by FFF 3D Printing. **Submitted to Engineering Manufacturing Letters** in December 2021. Status: Accept Submission.

(3) ALVES, Jorge Lino; MELO, Joana Tribuzi; SANTANA, Leonardo; IDOGAVA, Henrique Takashi; Effects of a square profile extrusion die on the manufacturing of FFF parts. Status: Submitted.

(blank page)

Contents

List of Figures

List of Tables

(blank page)

1. Introduction

The Fused Filament Fabrication (FFF) process stands out as one of the most popular Additive Manufacturing (AM) technologies due to its ease of use and good cost-effectiveness. The FFF process is classified as an extrusion-based AM process, in which the raw material is a thermoplastic filament, which is gradually heated, extruded, and deposited selectively by a calibrated nozzle. The material extrusion and deposition will be repeated throughout the entire layer stacking process, until obtaining the final object [1], [2]. One of the main components of 3D printer in the FFF process is the nozzle, responsible for conducting thermal energy for the processing of the building material, and for controlling the extrusion volume, and resolution of the printing process since it affects the dimensions, and geometries of the extruded filaments. Thus, the nozzle plays a very important role in the technological properties of printed parts and the economic aspects of the FFF process [3], [4]. Due to the importance of this component, scientific studies are dedicated to evaluating the effect of the nozzle diameter in terms of mechanical properties, porosity, surface roughness, dimensional quality and density of printed parts [5], [6]. Other studies investigate the influence of nozzle diameter and output geometry on parameters related to material extrusion, such as pressure drop, extrusion time, geometric errors and bed width stability [7], [8]. There are also articles related to nozzle clogging (Tlegenov, Lu and Hong, [9]) and to its wear when using abrasive materials (Pitayachaval and Masnok, [10]).

The purpose of this study is to understand the effects of nozzles, in different materials, output diameters and geometries, on extrusion quality, flexural mechanical properties, total porosity of parts printed in Polylactic Acid (PLA) and in the Benchy calibration. Our goal is to obtain information to further the design of nozzles with different output geometries.

There are many studies on the behavior of the nozzle. It was observed, however, that few of them explore the influence of thermal conductivity of the nozzle's materials and its lifespan — when applied to printing with non-abrasive filaments, such as conventional one in PLA — in the final quality of the parts produced by FFF printers.

1.1. Motivation

The motivation for carrying out this work comes from the interest in three-dimensional printing technology, especially in low-cost equipment based on Fused Filament Fabrication (FFF) technology. Since they present increasingly accessible values, both in machines and in materials, they allow a vast number of people, technical or not, to produce prototypes of their ideas and carry out projects in a short time.

Another motivation was to continue the theme of Silva's internship report [11], because although he has designed a square profile nozzle, he had no chance to put it into practice, as well as test new nozzle geometries and on a practical context, since most of the studies with geometry variation that exist are focused on printing with cement in addition to that most are still in the simulation stage.

1.2. Research objectives

1.2.1. General objective

The general objective of this work was to evaluate the effects of the lifespan, dimensions, material, and geometry of the calibrated nozzle, that is, of the extruder head die, on the mechanical properties, total porosity, and dimensional and shape stability of Poly (lactic acid) (PLA) parts built by the Fused Filament Fabrication (FFF) 3D printing.

1.2.2. Specific objectives

To fulfil the general objective, the following specific objectives were determined:

- Test the effects of the thermal conductivity of the nozzle material and the heat compensation of the 3D printer bed on the bond quality between deposited filaments intra- and inter-layers;
- Print parts with new nozzles and nozzles with a long history of use, to analyze the effects of the component's lifespan;
- Build objects with different nozzles diameters, to study the meso-structure of the printed part ;
- Calibrate the FFF 3D Printing parameters to use a square profile nozzle;

- Evaluate the effects of all nozzles tested on the quality of printed parts through mechanical flexural tests and porosity measurement;
- Characterize the quality of the extruded material through free extrusion tests varying process parameters and types of nozzles;

(blank page)

2. State of the Art

2.1 Fused Filament Fabrication (FFF)

Additive Manufacturing (AM) technologies are increasingly widespread among technical users (universities, and industrialists) and non-specialists (enthusiasts). A good part of this growth is due to its great usability in the most diverse sectors, as well as the decrease in the price of equipment and printing materials. Most AM technologies stand out for producing complex shapes with good quality and mechanical strength [12]. The quality of a part produced by Additive Manufacturing can be determined by the existence of supporting structures during the printing process, the material used, the geometric precision, or the quality of the finish on the part [13].

Extrusion-based AM systems, among which the Fusion Deposition Modeling (FDM) process, also known as Fused Filament Fabrication (FFF) stands out, have the largest installed base of any additive technologies available, mainly due to the open-source movement that made this technology very accessible, as shown in Figure 1 [14]. In this master's thesis, as it is inserted in the context of the use of an open-source 3D Printing system, the acronym FFF will be adopted as standard terminology.

The *Open Source* (OS) term is typically used to describe segments such as products, services, and ideas, where the intellectual contribution of inventors is not proprietary. The term originates from the computing landscape, in which a program's source code is open for viewing and modification and there is no cost associated with downloading and using it [14].

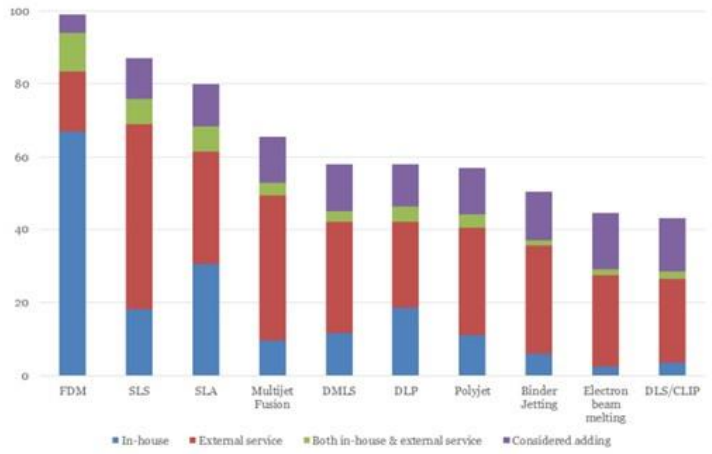

Figure 1 - Most used 3D printing technologies 2020 [15].

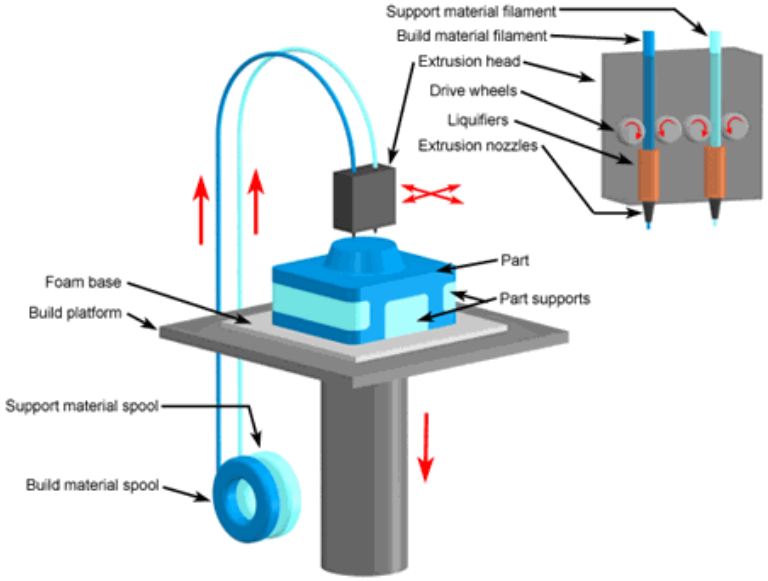

Figure 2-Fused Deposition Modeling (FDM) process [16].

In FFF printing machines (Figure 2), a source of thermal energy is generally used to transform the raw material from its initial solid state to a semi-liquid or pasty state. The building material consists, in most cases, of a cylindrical thermoplastic filament, which is pulled through the extruder head. The conduction of this material is done by a system composed of a pair of pulleys, which is responsible for pulling the filament of the coil and pushing it along a heated channel. The rigid filament itself, at the entrance of the extrusion system, acts as a plunger to generate pressure and extrude the softened polymer through a nozzle with calibrated dimensions. If this pressure remains uniform, the extruded material will flow at a constant rate and will

remain of continuous cross-sectional diameter. This diameter will remain homogeneous if the nozzle path through a deposit surface is also maintained at a constant velocity corresponding to the flow rate [17],[14].

The extruder head travels along paths while depositing extrusion material onto the build platform along the X and Y axes. The building platform moves downward in Z, equivalent to the layer thickness value. After deposition, the pasty filament solidifies by heat transfer to the previous layer and for the environment to form a solid layer.

Once the material is extruded, the FFF machine must be able to path in a horizontal plane and must also be able to start and stop the flow when pathing. When a layer is completed, the machine must index up or move the part down to proceed to the next layer [17].

Many thermoplastic materials can be used in FFF printers, including Acrylonitrile Butadiene Styrene (ABS), Polyphenylsulfone (PPSF), Polycarbonate (PC), PC-ABS mixtures, Acrylonitrile Styrene Acrylate (ASA), FDM Nylon 12, among others [14].

According to Bellini e Güçeri [18], the internal architecture of parts manufactured by FFF is similar to a composite structure of reinforced fibers, in which the individual filaments are stronger structures in the axial direction, like the fibers of a composite. On the other hand, the pieces show a weaker behavior in the adhesion region between filament-filament or between layers [14]. With FFF printing, defects, inaccuracies, or other problems related to the final quality of the produced parts often occur. Both surface roughness, dimensional accuracy, and mechanical properties of 3D printed parts do not match the quality of parts using material subtraction or injection molding [19] .

2.1.1 Extrusion head

The extrusion head of an FFF equipment is one of the central elements in the 3D printing process, precisely because it performs the functions of state transformation and material deposition. This printer device is composed of four fundamental subsystems: (i) filament traction module, (ii) wire feed channel (integrated into the heat dissipation element), (iii) a heating block, and (iv) the calibrated nozzle [20].

Some of the components mentioned above are illustrated in Figure 3.

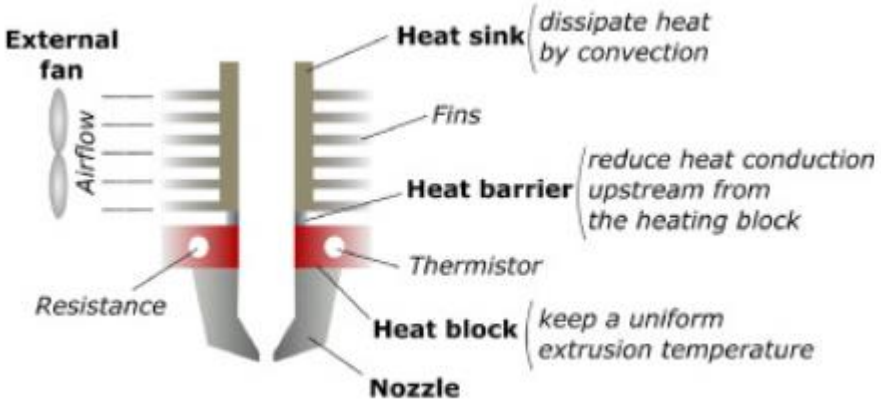

Figure 3- Schematic image of some part of the hothand [4].

(i) Traction module: in a conventional FFF 3D printer, a stepper motor is used, with or without a reduction gear system, to generate the movement and torque necessary for the feeding and retraction of the filament. A drive pulley (hobbed pulley) is connected to the motor shaft, which has grooves responsible for gripping the filament and thus generating the friction necessary to move it. The filament is positioned between the mentioned pair of pulleys. The pressure caused by this setting on the material filament to be processed must be adjusted correctly. Excessive pressure, and combined with high extrusion speeds, can damage the filament in the process causing the filament to buckle. On the other hand, insufficient pressure can lead to slipping between the filament and the drive pulleys, which will result in inconsistent material flow [21].

(ii) Feeding channel: once pulled from the spool, the filament to be processed is led to the heating zone, material is then fed into a barrel through a feed channel. This structure, which normally works as a barrier between the hot and cold parts of the extrusion system, is composed of two elements: (1) the heat break and (2) the heat sink. The first element is connected directly to the heating block, that is, in the region with the highest temperatures of the device. In this sense, this part must perform a more abrupt reduction of the generated heat, preventing it from being conducted to the upper parts of the head. For this, the heat break is made of a low thermal conductivity material, usually stainless steel. The second part, on the other hand, consists of a set of fins (conventionally in aluminum), which, integrated with the previous

component, helps to reduce the temperature in the head body through a process of heat dissipation by convection [4], [22]. Often, the dissipation system is even accompanied by a cooler fan. The design of these elements is very important to prevent heat from escaping from the hot section to the cold section. This thermal protection is important to prevent the polymeric filament from precociously softening in the initial parts of the extrusion system. Problems such as swelling of the material, or precociously softening (loss of stiffness), act directly on the continuity and stability of the extrusion flow and, therefore, on the dimensional and geometric quality of the deposited filaments. The flow of material through the nozzle is responsible for controlling the width of the deposited filaments. Filament dimensions, along with nozzle speed, determine the deposition rate of the material to be extruded, as shown in Figure 4 [21].

In addition to layer width and thickness, print speed, and filling strategy, other construction parameters require optimization for a defect-free process. Most parameters are related to material flow and head movement. A wrong adjustment of these two factors can result in defects to the structural properties of the parts.

Controlling the material flow in the extruder head is extremely important for the quality of the parts. An extruder system with precise plastic flow control must have a flow rate at the exit of the system equal to that commanded, however, this condition is not met [21].

(iii) Heating block: responsible for the transformation of the rigid material to the semi-liquid or pasty state. Thermoplastics, polymers common in the FFF process, exhibit a change in their physical state, softening when heated above their glass transition temperature. This process is completely reversible as no chemical bonding takes place during the process. The significantly reduced viscosity after heating facilitates extrusion through the nozzle. It should be noted that thermoplastics have very low heat transfer properties, so the heating block design must ensure sufficient heating of the material to allow the required degree of transformation to be achieved. This can be achieved by increasing the length of the heating block to increase the material's holding time during extrusion [23].

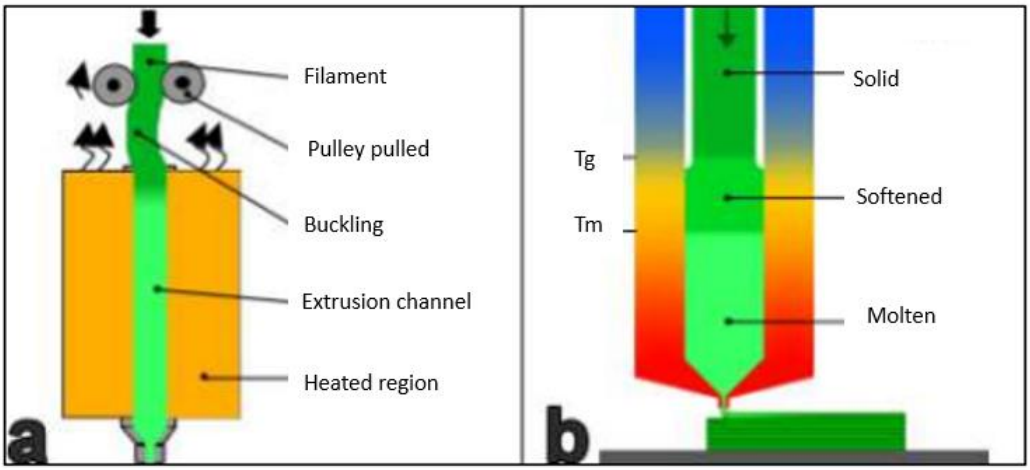

Figure 4- FDM process. a) Filament buckling (adapted from Venkataraman [24]; b) Filament melting in the channel [25].

(iv) Calibrated nozzle: the final part of the extrusion system is the nozzle, in which the cross-sectional area of the filament is changed to the dimensions established for printing the layers. This component is directly connected to the heating block. In this part, the cross-sectional area of the material is reduced. Typically, in FFF printers, the feed material is in the form of filaments with diameters of 1.75 or 2.85 mm. The nozzle inlet must have an opening compatible with the diameter of the material to be processed. Its output, however, can vary in diameters 0.1 and 1.20 mm. The nozzle diameter directly affects the dimensional accuracy, surface finish, mechanical properties, porosity, density of the part being produced. The smaller the die dimension, the greater the fine details and resolution of the objects produced. In addition, the size of the nozzle diameter has a large effect on the extrusion pressure required for a continuous flow of material. The smaller the diameter, the greater the pressure and vice versa. To decide the maximum pressure that can be supplied by the extrusion mechanism, the processing temperature and extrusion speed must be taken into account as the main success factors in this part of the process [20].

2.1.2 FFF 3D printing parameters

A correct configuration of constructive parameters is the main key to the success of Additive Manufacturing processes, which includes FFF technology. These variables will have different effects on a given product, as they affect aspects such as

material consumption, building time, mechanical properties, dimensional accuracy, and surface quality of the printed parts [26].

The following parameters are the most important for determining the technical and economic criteria associated with 3D FFF Printing:

(i) Layer thickness (*Layer height*) [1]**:** parameter that defines the height in Z of each deposited layer. This variable is related to the geometric resolution, mechanical strength and rigidity of the printed parts [14], [21].

Conventionally, the adjustment of this parameter with values equal to or less than 80% of the nozzle diameter was adopted as a reference. However, this value is merely theoretical, as filament swelling effects can be observed when it is extruded. In this sense, it is recommended that a layer height strictly equal to 80% is not used, but rather slightly lower, taking into account the rheological phenomena associated with the processing of the material [27], [11].

The thinner the layer thickness, the finer the resolution that can be achieved in printing. A lower layer height provides a smoother-looking surface but increases printing time. The adhesion between layers is also superior since the neck growth between deposited filaments increases and with that increases the contact area that allows a better adhesion. On the other hand, a higher layer thickness reduces fabrication time and the print will present more noticeable horizontal lines in each of the deposited layers [14], [11].

[1] The nomenclature inside the parentheses corresponds to the parameter name in the PrusaSlicer software (version 2.3.0) [28], used as the default slicer for this master's research. For more information, consult the website: https://help.prusa3d.com/en/category/print-settings_212 (acessed in 24/01/2022).

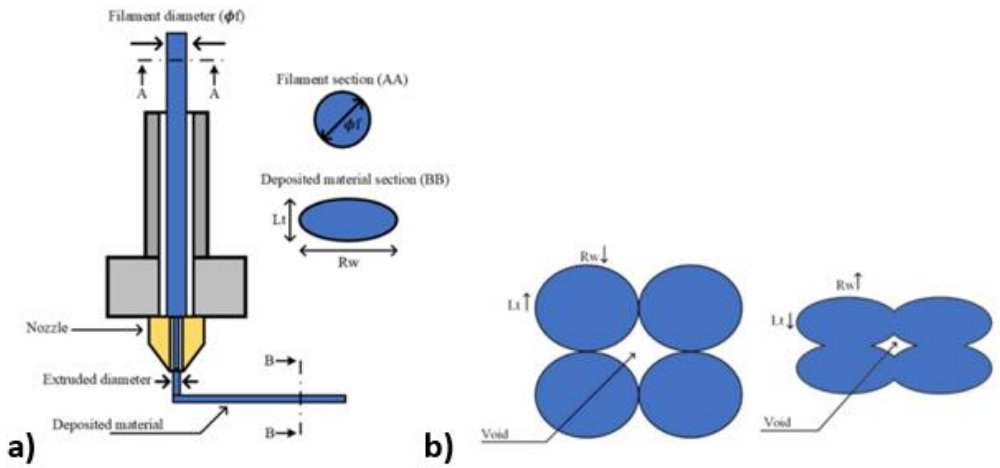

Figure 5- a) Relationship between extruded diameter with Lt and Rw; b) Relationship between the size of voids with Lt and Rw, Source: The Author.

(ii) Road width (*Extrusion width*): the road with corresponds to the width of the deposited layers. The road width has a strong relationship with the diameter of the calibrated nozzle (Figure 5), being generally set at values between 1.2 and 1.5 times greater than the exit dimension of the extrusion dies [28]. It should be noted that the layer thickness adjustment also influences the determination of the width of the deposited filaments. The width of the road has an influence on the solidification time of the material, the greater the width the longer it takes to cool down, in this way when the next layer is deposited the previous layer is still hot allowing a stronger bond between layers. On the other hand, with an increase in width, an increase in residual stresses is observed, which decreases the mechanical strength of the part, and also increases a greater dimensional distortion of the part [14], [11]. To understand how the extrusion width is calculated we must first look at the perimeter cross-section. PrusaSlicer assumes that the cross-section of extrusion is a rectangle with semicircular ends. It is observed by Figure 6 that the extrusion width includes the two semicircular ends [29].

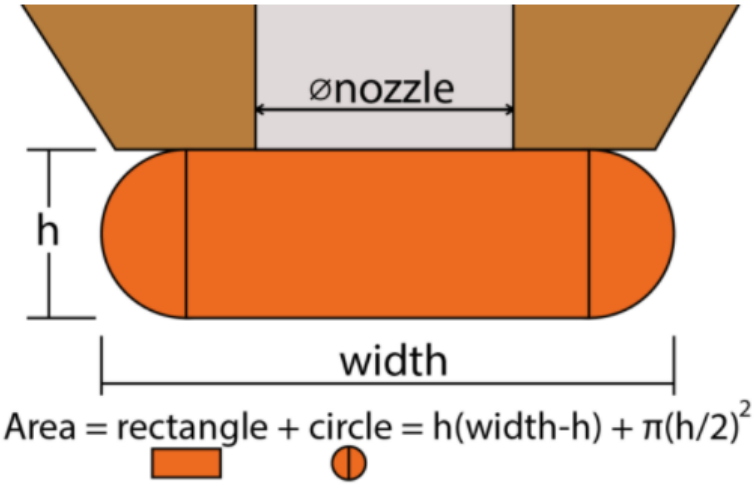

Figure 6- Schematic image of extrusion width as a function of nozzle diameter [29].

With higher extrusion widths, the pressure inside the nozzle also needs to be greater to squeeze material to the sides after exiting the nozzle. This added pression not only squeezes material to the side but also puts more pressure on individual layers [30].

The width represents the average distance between one line and the next. Increasing the width, according to the Figure 7, the total volume of defects can be reduced. The lower limit for the value of the width is usually equal to the diameter of the nozzle, and there is the possibility of reducing the value a little (for example in the need to make thin walls), in all other cases, it is advantageous to increase the width. The maximum achievable value is limited by two factors: the diameter of the nozzle flat area; and by the density of the extruded material, Figure 8 and Figure 9. For the first point, it is essential that all extruded material is contained below the nozzle, otherwise, defects may occur on the printing surface. The density of the extruded material is essential as the material is not simply deposited but also subjected to shear stress against pressure within the nozzle which increases as the extrusion temperature decreases. It should be considered that increasing the width increases the volumetric flow, as it increases the amount of material deposited per unit of time. The risk of using very low temperatures is to generate filament peeling or loss of steps [31].

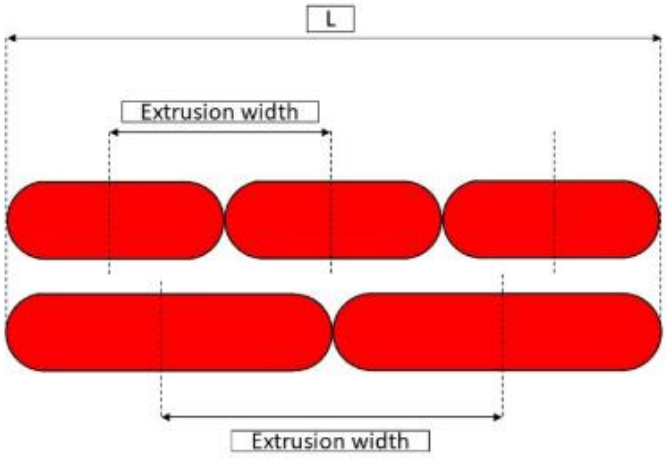

Figure 7 -Lower extrusion width (on top) and higher extrusion width (on bottom) compared for a given dimension L [31].

Nozzles Diameter	Smallest Extrusion Width (60%)	Largest Extrusion Width (200%)
0.1 mm	0.06 mm	0.20 mm
0.2 mm	0.12 mm	0.40 mm
0.3 mm	0.18 mm	0.60 mm
0.4 mm	0.24 mm	0.80 mm
0.5 mm	0.30 mm	1.00 mm
0.6 mm	0.36 mm	1.20 mm
0.7 mm	0.42 mm	1.40 mm
0.8 mm	0.48 mm	1.60 mm
0.9 mm	0.54 mm	1.80 mm
1.0 mm	0.60 mm	2.00 mm

Figure 8- Comparing nozzles diameter with smallest extrusion width and largest width [32].

Percent	Extrusion Width	Print Time
60%	0.24 mm	00:44
70%	0.28 mm	00:38
80%	0.32 mm	00:34
90%	0.36 mm	00:30
100%	0.40 mm	00:28
110%	0.44 mm	00:26
120%	0.48 mm	00:25
140%	0.56 mm	00:21
160%	0.64 mm	00:19
180%	0.72 mm	00:18
200%	0.80 mm	00:15

Figure 9- Comparing filling percentage with extrusion width and printing time [32].

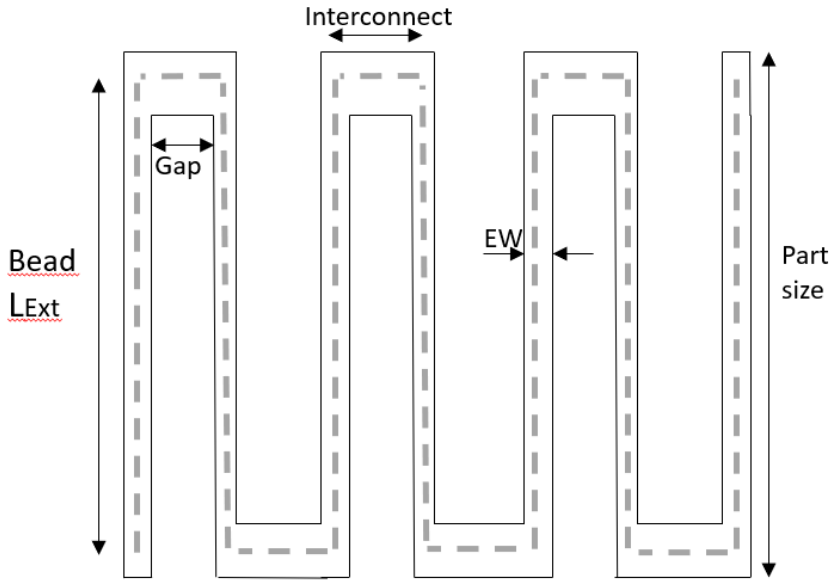

Figure 10- Schematic image showing bead length, gap, interconnect, part size, external width, Source: The Author .

(iii) Number of perimeters (*Perimeters*): it is characterized by the number of manufactured perimeters, internal and external around the part, as shown in Figure 11. The number of parameters plays an important role in determining the mechanical strength of printed parts, since the more perimeters there are, the more the beads will be aligned with the direction of loading [14],[11]. The greater the number of perimeters, the stronger and denser the structure of the part. Although the configuration of a greater

number of perimeters makes the part more functional with better mechanical performances, it also affects the aesthetics of the manufactured product, making it better. The percentage difference in part length can be improved by increasing the number of perimeters. This is because the number of perimeters is built parallel along the length of the part. This larger number of perimeters reduces the number of rasters. Therefore, a smoother and more stable surface can be obtained, resulting in minimal variation in precision along the length of the part. However, the percentage difference in part diameter can be significantly increased by reducing the number of perimeters. This is because the number of perimeters is constructed perpendicular (in the case of building a part with minimum Z height) to the diameter of the printed part. This can cause overfilling between rasters, resulting in a wide variation in part diameter accuracy [33].

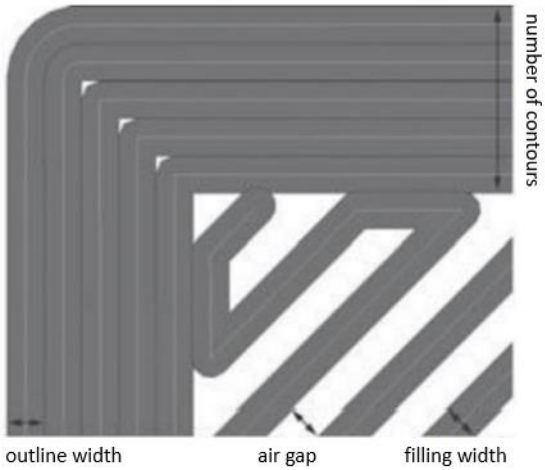

Figure 11- Exemple of number of perimeters [11].

(iv) Raster angle (Fill angle): the raster angle consists of the angle formed between the filaments deposited within the layers and the X-axis of the building platform, as shown in Figure 12. Filler orientation has a great impact on mechanical properties and is therefore much studied and analyzed. The fill angle is an influential factor in mechanical anisotropy of the printed parts. In the studies of Zohdi and Yang [34] it was found that for PLA, the highest mechanical strength was recorded for 45º. With a raster angle of 0° it showed an improvement of about 9.37% and 15.6% improvement

compared to 90°. The reason the 90° raster angle is less favorable and causes lower mechanical properties is that the mechanical loading is being carried out only by the bond between the layers and not by the fibers themselves [34].

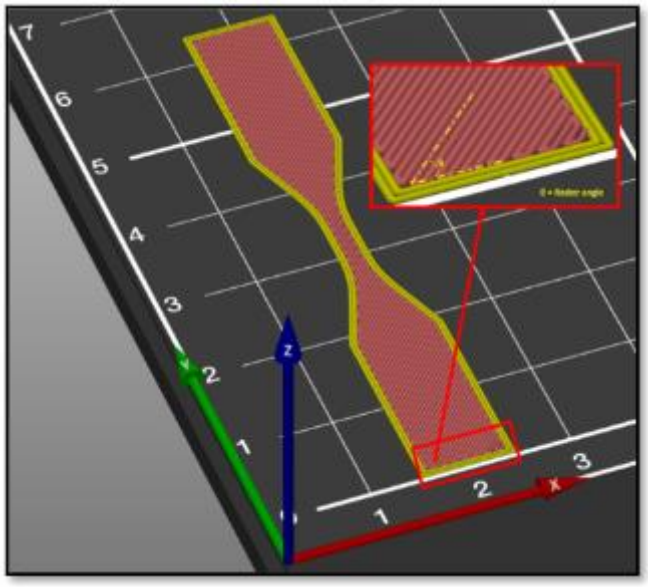

Figure 12- Schematic of raster angle in a 3D printed part [34].

(v) **Deposition strategy and filling patterns (Fill pattern):** this parameter represents how the deposition procedure is performed [35]. In Fused Filament Fabrication, each layer starts with the construction of a perimeter, which corresponds to the cross-section of the part. Each profile is a closed contour, where the start and end points coincide. After completing the printing of the perimeter, we proceed to the filling of the part, which can be done in 3 different ways [14], [36], [28], [37]:

- Raster: the material is deposited in a zig-zag pattern, with the filaments parallel to each other;
- Contour: the internal filling is based on several equidistant cycles, according to the perimeter of the part;
- Contour and raster: consists of combining the two strategies in each layer.

The first strategy seen earlier allows the use of higher speeds, in addition to having the ability to change the direction of motion of toolpath on adjacent layers. Typically, the raster direction is alternated at 90º from one layer to

the other, in order to guarantee greater mechanical resistance to the pieces [14], [11].

The fill pattern affects strength by arranging the rasters in a way that influences heat transfer. The consequence is that the bond formation between rasters and layers will be affected. The fill pattern will also determine the orientation of the raster.

Maximum strength is achieved when rasters and loading are in the same direction, so the “fill pattern line” should produce the highest tensile strength [35]. Rectilinear, gyroidal, cubic, star fill, and these are just some of the available fills. These different configurations will have a great influence on the printing times and will allow a varied filling of the pieces and consequently a saving of material.

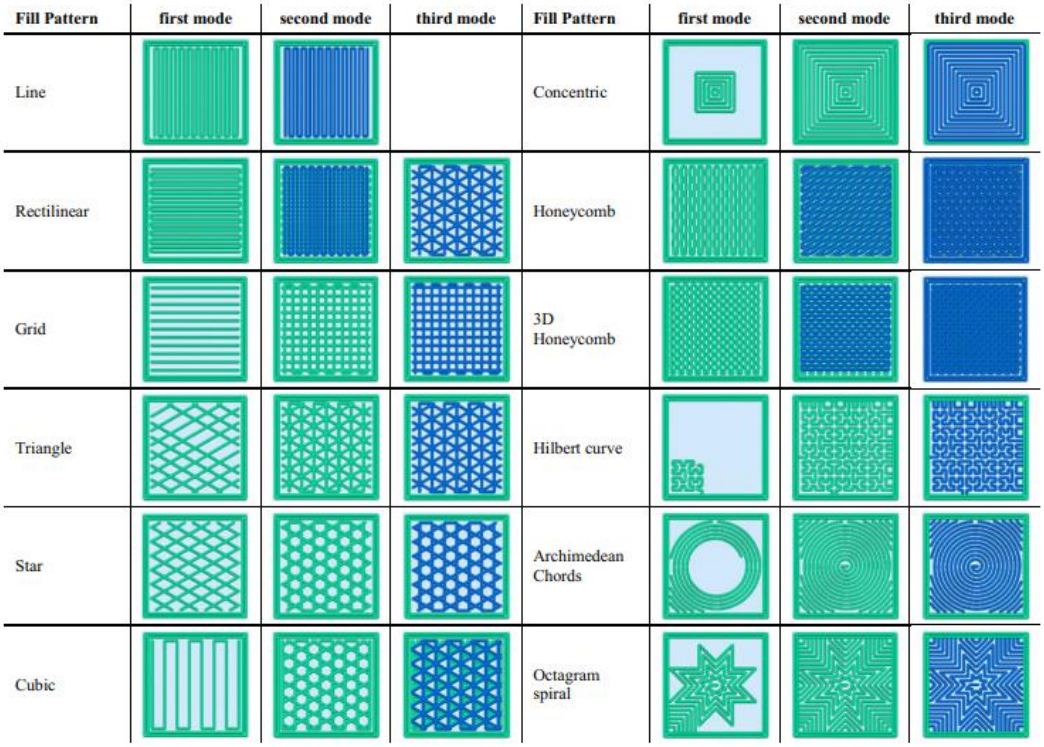

Figure 13- Different fills available [35].

Processing temperatures: This parameter can be divided into 2 main topics: the nozzle extrusion temperature and the platform temperature.

- **Extrusion temperature (Nozzle temperature):** corresponds to the temperature in the heated zone of the extruder head. It directly affects the viscous behavior of the processed material. A very low extrusion temperature does not allow a correct flow of the polymeric mass along with

the calibrated nozzle and, therefore, the deposited layers do not bond correctly, which may cause delamination or layer separation effects. On the other hand, if the temperature is too high, the material does not cool properly between layers, harming the printing, in addition to favoring the emergence of a process of thermal degradation of the polymer, generating a burnt appearance [14],[11]. According to Bellini [18], the extrusion temperature of the material must be adjusted based on the compromise between three conditions: (i) reducing the viscosity of the material in the heated region to favor the extrusion process; (ii) providing energy to trigger mobility (thermal softening) of the previously deposited layer and thus ensure good adhesion between layers and (iii) allow the material to increase its viscosity after extrusion and deposition to form filament that supports and with good adhesion properties [14].

When the semi-liquid filament flows under shear stress, entangled chains of polymer molecules are elastically deformed (viscoelastic characteristic) and become parallel to the flow direction. At the outlet of the nozzle, the polymer is released from any restriction upon contact with the free surface. The remaining elastic energy stored by the material causes the chains of molecules to regain tension, resulting in a sweeling extrudate. The extrusion irregularities that lead to variations can be directly correlated with the complexity of the flow dynamics in the liquefied due to different parameters such as flow rate, temperature, viscosity, pressure drop, or extrusion force [38].

- **Heated platform or base temperature (Bed temperature):** FFF printers extrude plastic at a temperature high enough to allow it to flow, but low enough to cool and resolidify predictably. However, if the cooling happens too fast or the extruded filament reaches too low a temperature, it contracts too much, accumulating internal stresses and causing adhesion problems and can lead to deformation, especially at the interface with the printing surface. The benefit of a heated print bed means that virtually all modern 3D printers come standard, using various types of heating elements including PCB heating traces and silicon pads with resistive power elements [39]. The main function of this temperature is to guarantee a better adhesion of the first layers deposited and with that to favor the stability in the impression. It

is possible to define different temperatures for both the first layer and the remaining layers to be built. As with the extrusion temperature, the base temperature depends on the material to be printed [11].

To date, no study has revealed strategies to identify an optimal base temperature fix for various materials and its effect on the adhesion of samples systematically produced by FFF [40]. Printing on a cold base reduces current mobility, increases residual stress leading to higher transformation performance. However, if the base temperature is too low, warping and even the first layer of the printing table may come off. It has been reported that optimal adhesion of printed objects is achieved when the print bed is heated slightly above the glass transition temperature (Tg) of the polymeric material [41].

(vi) **Print speed (Speed for print moves):** in the program used, PrusaSlicer, the speed is configured by regions of the part, therefore, the parameter has several names, the one referred to above as the general name. The print speed corresponds to linear speed with which the extruder head moves in the X and Y axes of the 3D printer [42]. High speeds tend to lead to poor print quality and shorter manufacturing time, while low speeds increase print quality and time. This parameter must be configured correctly depending on the material flow, shown in Table 1. High travel speeds must be combined with a high material flow to compensate for "lean print" effects due to elongation of the deposited filament. However, if the speed is too low, the print area will be overloaded [14].

Normally, the extruder when decelerating tends to extrude a significant amounts of material and when accelerating it tends to extrude very little, as shown in Figure 14 [43].

Power consumption can be reduced by increasing print speed while maintaining good surface quality. In a study of Elkaseer *et al*. [19] dimension and accuracy were found to be negatively influenced by high layer thickness values and high print speeds, as layers of printed material tend to spread out and high print speeds make it difficult to accurately deposition printed material. Power consumption and productivity are primarily affected by layer print speed, due to its high correlation with build time [19].

Galantucci *et al*. [44] studied the effect of layer thickness, printing speed and the resulting shrinkage problem, especially in the Z direction.

To optimize dimensional accuracy in the Z direction, a dense filling must be done together with a high printing temperature. Thin layers and high print speeds reduce percent error [19].

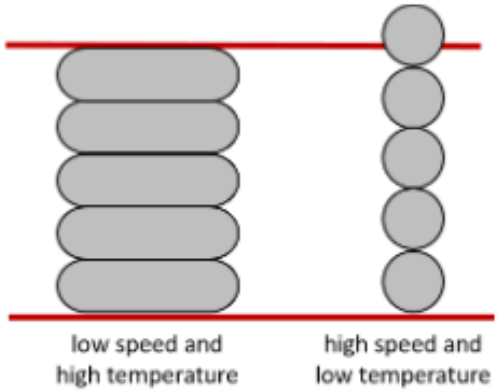

Figure 14- Effect of printing temperature and printing speed on the dimensional accuracy in the Z direction [17].

Table 1- Recommended extrusion speeds for different materials [45].

Filament	Speed (mm/s)
ASA	20-50
ABS	40-80
PETG	40-90
PLA	30-90
NYLON	40-60
HIPS	25-55
TPU	10-30

(vii) **Extrusion speed:** speed at which the filament is fed into the extrusion system. The fluidity intended for the thermoplastic, at the time of extrusion, is the point of greatest influence on this parameter. If the speed is high, more material will be extruded, causing the filament width to increase. Inside the extruder, a certain amount of heat is transferred to the filament that will cause the material to change to a viscous state. For this phenomenon to occur, there is a certain speed at which the filament must be extruded, defining the time the filament is exposed to the heat in question. If the diameter of the extrudate is high, the volume of material is greater, therefore, for the same temperature, more time will be required; therefore,

a lower extrusion speed. The opposite is also verified: for smaller diameters, the extrusion speed can be higher [11].

Since the extrusion speed and extrusion temperature will define the viscous state of the filament during deposition, it will also influence the adhesion between layers, affecting the final quality of the part and its mechanical properties.

As it is such an important parameter, it cannot be configured, being entirely calculated and defined by the Software so that the speed is compatible with the other defined parameters [11].

(viii) **Max volumetric speed (*Max volumetric speed* – MVS):** The hotend installed in a 3D printer can only melt and process a finite amount of filament in a certain period. The hotend's maximum volumetric rate is the fast limit of printer resources. This production capacity is measured in cubic millimeters per second (mm^3/s). This capacity is affected by filament type and nozzle size among other factors. When printing, the effective MVS is calculated as (Eq.1):

$$Max.VolumetricRate = LayerHeight \times ExtrusionWidth \times Speed \qquad \text{Eq. (1)}$$

This means that as we increase the extrusion width or layer height, the velocities must be reduced to stay below the desired MVS value. This does not necessarily mean that prints will be slower, but the linear nozzle speed should be kept low enough to maintain a secure MVS [46].

Most slicing software allows to configure only linear speeds, which determine the amount of time required for the extruder to move from point A to point B in the 3D printer's coordinate system. However, this parameter only allows controlling the speed of movement of the extruder head. The maximum volumetric speed, in turn, defines the volumetric transfer rate, that is, the amount of material deposited per second during the movement of the extruder [46].

The key to successful larger print is understanding the limitations of the printer hardware that wem, are working with. The printer's hot end is what effectively heats up and causes the filament to change its physical state. Each hot end has a limited capacity which is expressed as the “maximum volumetric speed” or rate it can handle.

If someone tries to push more filament than the hot end can handle, may be encountered some problems:

- uneven layer extrusion;
- click and skip extruder;
- nozzle and hot end jams;
- increased extruder motor heat.

PrusaSlicer, unlike other print planning software, allows the user to configure the maximum volumetric speed. This automatic adjustment allows the program to determine the best linear speeds to allow an adequate material output in relation to the other parameters that would already be configured [11].

Since the materials have different rheological characteristics, they will present adequate maximum volumetric velocity values, as shown in Table 2, [11].

Table 2-Maximum volumetric velocity values for each material (adapted from the Prusa website, [47]).

Filament	Max volumetric speed (mm3/s)
PLA	15
ASA/ABS	11
PETG	8
BVO/PVA	4
FLEX (TPU/TPE)	1-2.5

(ix) **Infill density (infill density):** this parameter, also known as fill density, defines the amount of material inside the part. A value of 0 corresponds to a hollow part, while a value of 100% corresponds to a maximum material density within the component, as shown in Figure 15. The fill percentage must be adjusted according to the application that the manufactured part will have. Parts with less fill print much faster than denser parts, but strength tends to decrease [14].

Nunez *et al*. [48] studied the dimensional accuracy, flatness, and surface texture of ABS in printed structures. They found that layer thickness and fill density influence the surface finish and dimensional accuracy of parts. The results showed that low layer thicknesses and high fill density were favorable for a better surface finish. Meanwhile, high layer thickness, density, and fill values tend to improve accuracy [49].

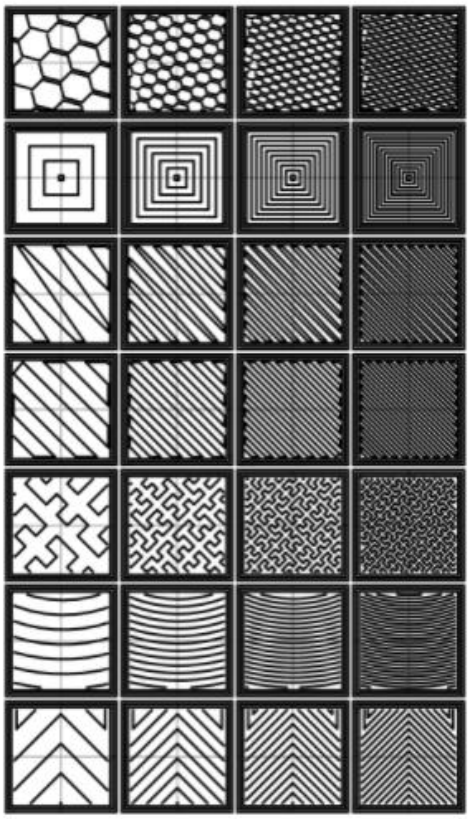

Figure 15- Different densities for different fills [34].

(x) **Spacing between filaments and between filament and perimeters (air gap):** the spacing between the deposited filaments (air gap) refers to the gap between them within the same layer (Figure 16). Normally, by default, a value equal to zero is assigned to this parameter, to guarantee that the deposited filaments only touch each other. By applying a positive value, the scans will be farther apart. On the other hand, with a negative value, a negative value indicates that the deposited filaments will overlap, thus resulting in a denser structure with a longer construction time [14],[50].

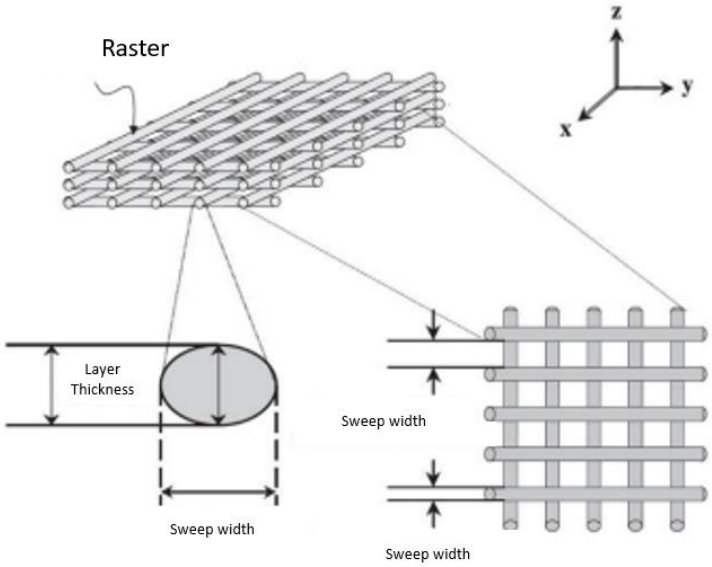

Figure 16- Representation of FDM process parameters [14].

(xi) **Build orientation:** is the definition of how the part is positioned when manufactured. This positioning is determined in relation to the X, Y, and Z axes of the construction platform, with X and Y being the axes parallel to the platform and Z being the axis oriented in the direction of the construction of the parts [21], [51].

This parameter is important to consider for the printing time and the properties of the printed parts. The direction the part is oriented changes the way the machine prints the part, as well as the supporting materials, as shown in Figure 17, [14], [52]

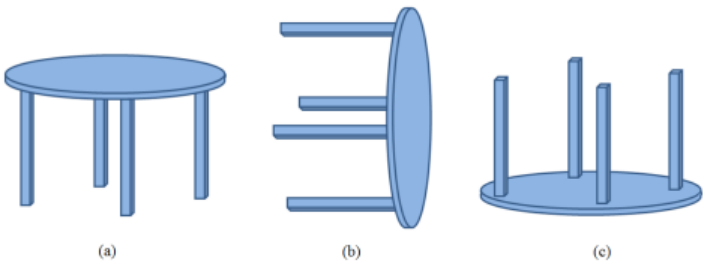

Figure 17 – Example of different building orientations [14].

(xii) **Extrusion multiplier:** the adjustment of this level affects, for example, the dimensional quality, surfaces, mechanics, and the porosity of the printed parts. It is also responsible for controlling the material flow according to the extruded volume management, per unit of time and distance traveled,

through the printhead. By default, it is set to 1. Values above those mentioned generate denser parts, however, if these values are too high, they can cause excess material deposition, impacting dimensional distortions. Settings less than 1 may result in parts printed with less material than needed to obtain good mechanical properties [53],[14].

2.1.3 Bonding between layers

The correlation between printing temperature and mechanical performance can be studied starting from the analysis of the arrangement of the filaments generated during the layer stacking process. Cohesion between and within layers can be adversely affected by material flow discontinuities. The lack of cohesion limits the mechanical load transfer by combining two main mechanisms: the stress concentration that develops around the porosities generated by the process and the lack of cohesion of the filaments that occurs at the interface. A high printing temperature tends to decrease the void density and makes the structure more homogeneous, especially when combined with the best adjustment of other printing parameters, such as part orientation, layer thickness, printing speed, among others [54].

Interlayer contact in material extrusion was originally modeled as a wetting process where the two layers combine due to surface tension forces and are impeded by viscous resistance. More recent work has shown that the typical material extrusion process results in layers and roads that cool so fast that very little wetting occurs. Many authors have shown that the lack of diffusion limits the strength of the final parts and that diffusion is a critical factor for modeling the material extrusion process [55].

The pattern and percentage of fill have a strong relationship with defining the mechanical properties of printed models [56].

Semi-fusion between layers results in anisotropic properties with the highest strength in the longitudinal direction (parallel to the deposition direction) and the lowest strength in the z-axis direction between layers. Low interlayer strength is caused by insufficient contact between layers and lack of polymer diffusion between layers [55]. Although wetting improves contact between layers long enough at elevated temperatures, pressure can force layers together much faster than wetting [57].

Semi-fusion between thermoplastic polymers during the FFF process occurs when the processing temperature is above the glass transition point of the printed

polymers. Like the polymer healing process, the bond formation of two pieces of fused polymers can be observed in the Figure 18, described in two steps: (a) contacting surfaces followed by (b) intermolecular diffusion of the polymer chain across the wetted interface. Thus, the strength of fusion bonds is determined by the formation of wet interface and degree of intermolecular diffusion between two layers of the same polymers [58].

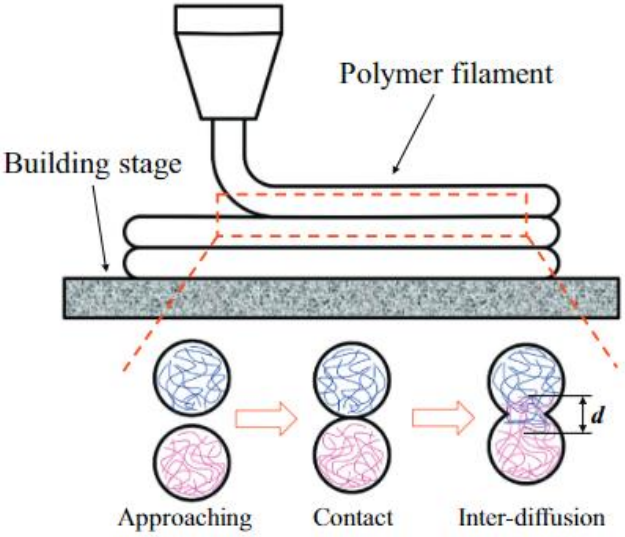

Figure 18- Schematic of layer contact and intermolecular diffusion of the polymer layer [57].

2.1.4 Rheology in the process FFF

Rheology meets the requirements of the industry's need for knowledge to develop new materials for FFF, as it responds to processes that occur during printing such as viscous flow at the nozzle and viscoelastic behavior during bonding between layers. In this sense, rheology is a quick and effective screening tool to predict the success or failure of new materials throughout the 3D printing process [59].

Viscosity is the resistance to flow that the plastic faces when it is melted, that is, if the plastic is very viscous, it has difficulty flowing through the nozzle of the injector or extruder die, unlike a low viscosity plastic that flows easily [60].

Ideal material for FFF 3D printing must have high rigidity to ensure stable feeding into the extrusion system. It must also show rapid changes in its viscosity with heating and throughout its extrusion, to minimize the required feed pressure. Lastly, this material must show a rapid increase in its viscosity after extrusion to ensure the preservation of the 3D printed structure geometry [20].

In this context, thermoplastic polymers are widely used and act as a sheer material with good viscoelastic behavior on heating and cooling. Shear roughing describes a material with the inverse relationship between viscosity and shear rate. Viscoelasticity includes two main parameters: the storage modulus and the loss modulus. When the first has a higher value than the second, the material behaves more like a solid. On the other hand, when the opposite happens, the material acts more like a fluid. After melting, the viscosity of the material drops dramatically. Furthermore, during extrusion, the material is exposed to a high shear rate due to the decrease in nozzle diameter which causes an even greater decrease in the viscosity of the material. After extrusion, this high shear disappears at the nozzle exit. This energy is all accumulated and when the filament comes out of the nozzle, it swells. In addition, the material undergoes very rapid cooling caused by the ambient temperature which is normally much lower than the nozzle temperature. For this reason, the material retains a high viscosity and solid-like behavior. However, it is very important to have sufficient time for diffusion between the deposited material and the previously printed layer. During printing, the high temperature of the material to be deposited acts as a heater that partially reheats the previous layer for a fraction of the time. The described mechanism is very important in order to reach a temperature above the Tg [20].

The crystallization behavior in a semicrystalline polymer has a great effect on the deformation of the layers during printing and this is because of the crystallization process that induces dimensional variations. A possible solution to reduce this effect is by adding filler materials that slow down the crystallization process [62].

During FFF printing, both the shear flow within the nozzle and the velocity gradients induced by the deposition process (where material leaves the nozzle and is deposited on a build plate) can significantly deform the polymer microstructure.

After deposition, the filament bonds with the adjacent material that remain hot, the melt cools and solidifies so that the final object structure consists of several partially welded filaments. Takeoffs governed by shear stresses along weld lines are known to be a key failure mechanism.

Non-isotherm ability introduces extra complexity to polymer dynamics. With non-crystalline melts approaching a glass transition after cooling to Tg, while semi-crystalline melts will nucleate and crystallize below the melting temperature TM before transitioning to a glassy state at Tg<TM; in the diffusion of Tg, and therefore

crystallization is stopped. It is suggested that interdiffusion should precede crystallization and glass transition to ensure good adhesion and welding strength [62].

All aspects analyzed above play a crucial role in improving the mechanical properties of 3D printed objects [20].

In FFF there are several obstacles to the development of new materials, among them the diameter and the mechanical properties required for the filament. By refining filament manufacturing methods, a suitable diameter can be achieved. A filament to be used in the FFF process must be rigid enough to withstand the force applied by the pulling mechanism and to act as a piston in the extrusion process without buckling failure. As already mentioned, the materials used have a glass transition temperature (Tg) above room temperature, or a sufficient degree of crystallinity, to impart substantial mechanical strength to the filament to prevent buckling. The glass transition temperature is uniquely associated with the amorphous phase of the polymers. This is the temperature at which the transition occurs from a glassy state, in which the molecules of the amorphous phase do not have mobility, to a “rubbery” state, in which the molecules of the amorphous phase become mobile [59].

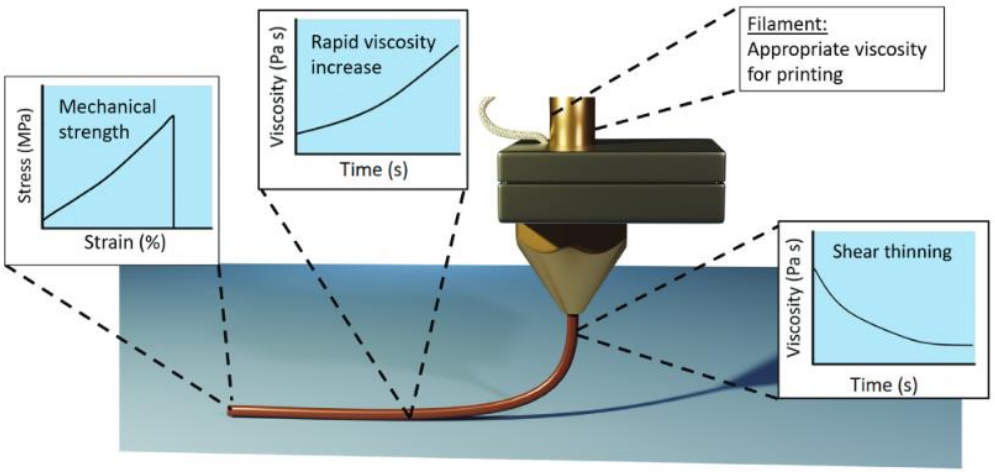

Figure 19- Key properties required for 3D extrusion printing of polymers [23].

Gaining a complete understanding of the semi-melt rheology behavior of polymers in FFF will benefit processing control as well as product quality [63]. Rheology is the most critical material property for most polymers, Figure 19. Rheology influences melt temperature through viscous dissipation, determines material output and flow rate, determines shear rate and velocity profiles along the material flow path.

Creates the pressure profiles that determine process force and moment requirements and can influence the final shape and strength of the material [64].

Heat transfer seems like a topic that is not influenced by rheological behavior, but this is not true. Research carried out by Schowalter *et al*, [65] focused on the use of hot-film anemometry to determine the presence of slip in polymer solutions and melts. The anemometer was used to find a Nusselt number[2] as a function of the shear rate to reveal that slipping occurred when there was extrusion distortion. These studies show that heat transfer in non-Newtonian fluids is a function of shear rate.

Saadat *et al*, [66] investigated the viscoelastic melting behavior and matrix expansion of ABS and their experimental results showed a significant reduction in matrix expansion of nanocomposite samples. Agrawal [67] also examined the effect of changing nozzle geometry on pressure drop distribution for PCL scaffolding material in the FDM process. Their results showed that reducing the nozzle diameter and angle can lead to increased pressure, which results in better manufacturing resolution. Heller *et al*. [68] investigated the effects of matrix expansion and nozzle geometry on the FDM extrusion process for a carbon fiber polymer composite using a computational approach. The results indicated that the matrix has a major effect on fiber orientation and the resulting mechanical properties. It seems necessary to conduct research on the flow behavior of molten polymer throughout the FDM extrusion to determine how the process conditions of the FDM process affect die swelling, which has a significant effect on the mechanical properties and dimensional accuracy of manufactured components [69].

Another important property is the melt flow index (MFI). The MFI is an important parameter to determine the polymer's property of flowing at the melting point under the application of the standard weight (2.16 kg). This MFI provides the required data on polymer mass flow rate for 10 min [70].

Table 3- MFI value for different materials adapted from[71]–[75].

Materials	MFI values (g /10min)
HIPS	7.5 ± 0.20
ABS	8.76 ± 0.16
PLA	13.52 ± 0.11
Natural PLA	2.24 ± 2.22
PLA 850	7-9

continues

[2] The Nusselt number is the ratio of convective to conductive heat transfer across a boundary

PLA d2003	32
PLA D 3052	14
PLA D 4032	7
Blue PLA	14.95 ± 0.55
PETG	14.70 ± 1.29
PP	5.9 ± 0.10
PVA	5.14 ± 0.12
TPU	14–28

2.1.5 Materials for FFF

Among the raw materials available and in FFF printing, polymers are the most used material, Figure 21.

Parameter optimization in the FFF process can only be improved until a certain point by determining an optimal combination of process parameters through process parameter analysis. This happens because the pure thermoplastic materials used for the FFF process also have material property limits that cannot be exceeded [76].

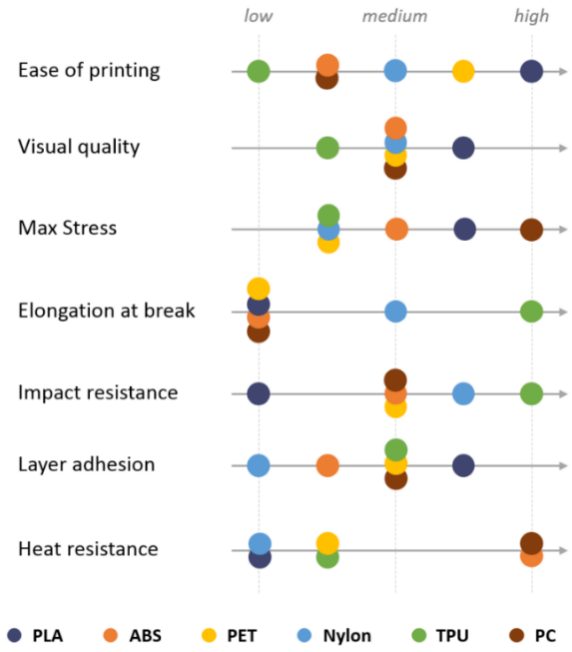

Figure 20- Comparison of different properties for different materials [77].

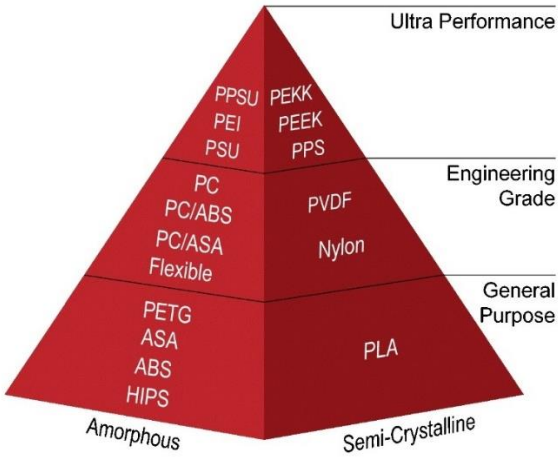

Figure 21- Organization of thermoplastics according to type of use and their crystallinity [78].

Despite the wide range of thermoplastic materials available (Figure 21), the most used are Polylactic Acid (PLA), Polyethylene Glycol Terephthalate (PETG) and Acrylonitrile Butadiene Styrene (ABS), and their properties are described and compared in Figure 20, [79]. In the following topic, a description about PLA will be presented, which was the material used in this research.

2.1.5.1 Poly (acid lactic)

PLA consists of a biopolymer that belongs to the family of aliphatic polyesters, of the poly (α - hydroxy-acid) type, produced from the chemical synthesis of lactic acid obtained from renewable sources such as wheat, corn, rice, among others [14].

This is a material that is of interest in the biomedical field due to its good mechanical properties and the ability to be highly hydrolysable in the human body.

Regarding its mechanical properties, it exhibits a behavior similar to polyethylene terephthalate (PET) and polyethylene (PE), however, PLA has high fragility, with less than 10% elongation at break, which limits its application in some cases [14].

PLA has low heat resistance, high brittleness, it is brittle, and has low toughness and impact resistance.

This is a known material due to its sensitivity to moisture above 60°C. Parts constructed of PLA typically exhibit low distortion during printing compared to other materials such as ABS but have low thermal conductivity and toughness [76].

Properties	Values	Reference
Melting temperature (Tm)(°C)	170 to 180	PEREZ *et al.*, 2014; MENG *et al.*, 2012; AHMED, 2017
Glass transition temperature (Tg) (°C)	55 to 65	
30-50ºC	0.110	JI *et al.*, 2013
60-80ºC	0.227	
Mechanical		
Modulus of elasticity (GPa)	2.02-4.00	
Tensile strength (yield) (%)	9.8-10	GARLOTTA, 2001;
tensile strength (break) (%)	0.50-9.2	LANZOTTI *et al.*, 2015a;
Flexural modulus (GPa)	2.392-4.930	PROSPECTOR, [2016]; WANG
Flexural resistance (MPa)	48-110	*et al.*, 2017.
Density (g/cm³)	1.25	HENTON *et al.*, 2005, SANTANA *et al.*, 2016
Coefficient of friction	0.16±0.02	BEHALEK *et al.*,2012

Figure 22- PLA properties according to the literature [14], [80]–[88].

2.3 Calibrated nozzle

One of the main components of 3D printing in the FFF process is the calibrated nozzle, responsible to produce thermal energy for processing the construction material and for controlling the extrusion volume and resolution of the printing process, as it affects the dimensions and geometries of the filaments. extruded. In this sense, the nozzle plays a very important role in the technological properties of printed parts, and in the economic aspects of the importance of these components. Scientific studies are dedicated to evaluating the effect of the nozzle diameter in terms of porosity, surface, roughness, dimensional quality, and density. of printed parts [10].

2.3.1 Material

To create a small part, the nozzle has a huge impact on the quality of the final print, the time it takes to print the model, and how often the filament clogs causing errors. The two main factors that people vary for using 3D printers are the size of the nozzles (their diameter) and the material of the nozzle itself [89].

When choosing the nozzle material, some important considerations must be considered when printing, such as: (i) efficiently transferring heat from the heating block; (ii) must resist wear from abrasive and unusual materials; (iii) must retaining shape when heated, as some materials tend to expand when heated, distorting nozzle size, and (iv) must provide a smooth, frictionless surface for thermoplastic flow [90].

The main problem with designing an effective 3D printer nozzle is trying to balance all these factors [90].

It has been reported that extrusion nozzle wear is a significant problem when using hard plastic filaments [86].

Nowadays numerous materials can be used for the nozzles of 3D printers. In Figure 23 and Figure 24 it shows the main properties for some nozzle materials.

- **Brass nozzle:** it is the most used material for extruder nozzles, since it has high thermal conductivity and stability, in addition to being easy to machine and offering an economical price. The main disadvantage is the rapid wear induced by abrasive materials [91].
- **Hardened steel nozzle:** to solve the rapid wear of brass nozzles, hardened steel nozzles appeared, which can be up to ten times more resistant than brass to wear and maintain the same qualities. As disadvantages, these nozzles have less heat transmission and, since they contain lead in their composition, they are not recommended for making parts that are in contact with the skin or food [91].
- **Stainless steel nozzle:** nozzles made of this material have a higher hardness than brass and have the advantage of not containing lead. For this reason, stainless steel nozzles are suitable for 3D printing with filaments approved for these applications that would be contraindicated in the nozzles [91].
- **Ruby Nipples:** This is a special nib made from a brass nib with a recessed ruby tip. This combination allows a stable temperature, an almost infinite durability and a very high dimensional accuracy of printing [91].
- **Tungsten carbide nozzle**: with simple plastics, most used nozzle metals can easily resist flow. Unfortunately, once we start using plastic filaments with hard reinforcing fibers like carbon and glass, it can make printing difficult. These reinforcing materials will scratch the inside wall of the nozzle orifice as they pass due to flow and pressure. Both glass and carbon are known to be very hard. Resulting in abrasion inside the nozzle. Tungsten carbide nozzles are the best choice when it comes to materials that provide wear and abrasion resistance. Tungsten carbide is hard enough that the size and height of the nozzle always remain the same regardless of how long the nozzle is used and the abrasiveness of the filament material in use [92].

Figure 23- Different properties for different nozzle materials [93].

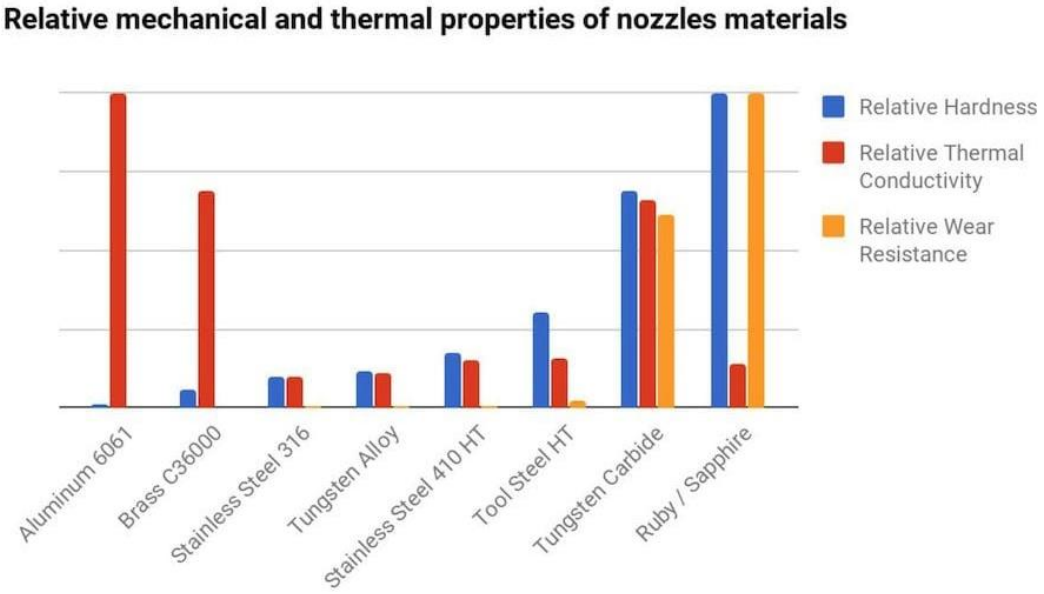

Figure 24- Chart of materials properties for 3D printing hot end nozzles [90].

The nozzle presents wear with its use due to the friction generated with material, which varies according to the nozzle material and the type of filament used. Nozzles are the most common 3D printer replacement parts. They affect the quality and speed of your printers [94], [95]. To detect when the nozzle is worn, two techniques are used:

- **Visual method:** when the wear is very accentuated, it is easily detectable with the naked eye at the tip of the nozzle, as can be seen in Figure 25. It may

happen that even with all the correct printing parameters, the 3D model without imperfections and the nozzle in good condition to the naked eye, is internally worn and causes malformations and poor surface finish on printed parts due to turbulent flow of plastic inside [95].

Figure 25- Comparison between nozzles [95].

- **Theoretical method:** to be able to apply this method it is necessary to have the technical drawing of the nozzle of the 3D printer that is being used. In this case we will use Figure 26 as an example.

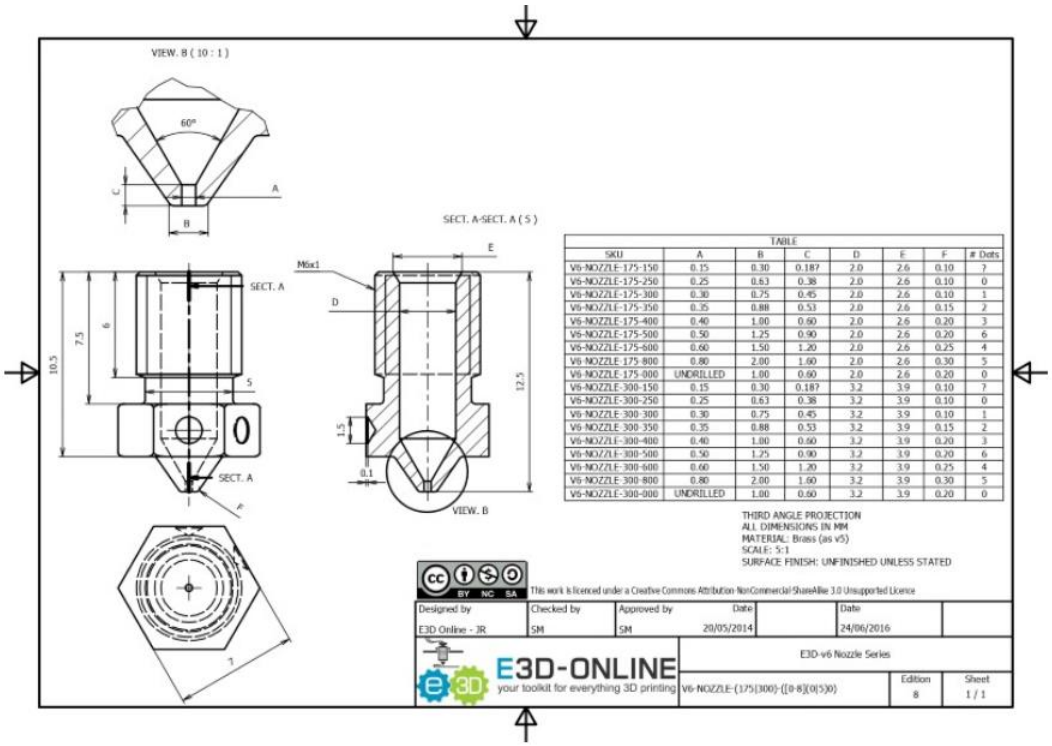

TABLE

SKU	A	B	C	D	E	F	# Dots
V6-NOZZLE-175-150	0.15	0.30	0.187	2.0	2.6	0.10	7
V6-NOZZLE-175-250	0.25	0.63	0.38	2.0	2.6	0.10	0
V6-NOZZLE-175-300	0.30	0.75	0.45	2.0	2.6	0.10	1
V6-NOZZLE-175-350	0.35	0.88	0.53	2.0	2.6	0.15	2
V6-NOZZLE-175-400	0.40	1.00	0.60	2.0	2.6	0.20	3
V6-NOZZLE-175-500	0.50	1.25	0.90	2.0	2.6	0.20	6
V6-NOZZLE-175-600	0.60	1.50	1.20	2.0	2.6	0.25	4
V6-NOZZLE-175-800	0.80	2.00	1.60	2.0	2.6	0.30	5
V6-NOZZLE-175-000	UNDRILLED	1.00	0.60	2.0	2.6	0.20	0
V6-NOZZLE-300-150	0.15	0.30	0.187	3.2	3.9	0.10	7
V6-NOZZLE-300-250	0.25	0.63	0.38	3.2	3.9	0.10	0
V6-NOZZLE-300-300	0.30	0.75	0.45	3.2	3.9	0.10	1
V6-NOZZLE-300-350	0.35	0.88	0.53	3.2	3.9	0.15	2
V6-NOZZLE-300-400	0.40	1.00	0.60	3.2	3.9	0.20	3
V6-NOZZLE-300-500	0.50	1.25	0.90	3.2	3.9	0.20	6
V6-NOZZLE-300-600	0.60	1.50	1.20	3.2	3.9	0.25	4
V6-NOZZLE-300-800	0.80	2.00	1.60	3.2	3.9	0.30	5
V6-NOZZLE-300-000	UNDRILLED	1.00	0.60	3.2	3.9	0.20	0

Figure 26 E3D-Online nozzle V6 technical design [96].

The measure of interest is the “C” which represents the length of the filament exit perforation after the extrusion cone. The wear should never be more than 80% of

the total length of the “C” because if the wear is closer to the inner cone, the impressions will be of poor quality, or even impossible to make. To check this value, we must remove the nozzle from the hot end, measure the total length, and apply the following Eq. (2):

$$= \frac{\boldsymbol{Original\ total\ length - Real\ total\ length}}{\boldsymbol{C}} \times \mathbf{100} \qquad \text{Eq. (2)}$$

As shown, the total length is 12.5 mm, and “C” is 0.60 mm. In this case, the total length of the nozzle is 12 mm and then applying the formula above we obtain that the percentage of wear is 83%, which indicates that it is necessary to replace the nozzle with a new one [95].

$$\frac{12.5mm - 12mm}{0.60mm} \times 100 = 83.33\%$$

2.3.2 Diameters

The nozzle diameter must be chosen considering the user's objective to adapt according to the desired characteristics. Hole diameter will play an important role in maximum strength, surface finish, porosity, and dimensional quality [11].

The standard 3D printer nozzle diameter is 0.4mm. Smaller nozzles start at around 0.1mm and size 1.4mm can also be found, however diameters between 0.2mm and 0.8mm are most used [89].

The use of both smaller and larger nozzles has its advantages and disadvantages. With a larger nozzle, you can extrude more filament at once, having a shorter printing time, on the other hand, with a smaller nozzle it is possible to print more precise details [89].

This parameter can be studied to understand what consequences the use of larger or smaller diameter nozzles may have, always bearing in mind that the remaining parameters must be decided and maintained for all diameters.

The geometric structure of the nozzle also has significant effects on the qualities and properties of parts created by 3D printing [5], [11].

Triyono *et al.* [5] concluded that increasing the nozzle orifice diameter of the 3D printing process tends to increase product density and tensile strength.

With an increase in the diameter of the nozzle, a greater deposition of material volume is allowed, thus ensuring a better filling of voids inside the part, making the samples more solid, this also causes an increase in the volumetric mass [11].

2.3.3 Geometries

Buswell *et al*. [97], in a study related with cement and concret, mentioned that the different shapes of extrusion nozzles used in previous works (circular, ovular or rectangular) did not show much difference in the results between the different nozzle geometries. Bos et al. [98] argued that for the required shape it is necessary to have an appropriate mouthpiece for such. In this study, it was mentioned that the nozzle orientation and its various geometries (ellipse, circular, quadrangular, and rectangular) were used and it was concluded that the circular nozzle provided more freedom and ease to change the nozzle angle for the printed part [98]. The study of Kwon [99] concluded that square hole has better surface finish than ellipse type.

Papon *et al*. [100] studied the star geometry in nozzles and he studied that, in addition to the viscous behavior, the melt flow is also affected by the liquefied geometry.

Nozzle orifice geometric attributes are known to affect the quality of printed parts, a typical FFF printer only uses a single nozzle with a constant orifice area. Thus, part fabrication may take longer and may result in poor surface properties. On the other hand, nozzles that can extrude different layer widths can overcome the problems mentioned above, since the cross-section of the hole can be continuously varied according to the geometric characteristics associated with the layers. That is, larger bead widths can be employed to fill interior regions in less time, while thinner features (such as exterior surfaces, edges, corners, etc.) can be printed in more detail using smaller bead widths [8].

The flow rate and cross-section of the molten polymer exiting the nozzle vary according to the geometry of the nozzle. In addition to increasing the interlocking force between the layers, the surface area of the molten polymer must be expanded by modifying the cross-sectional shape while maintaining the unit volume of each layer [5].

2.3.4 Design parameters

For the low-cost 3D printer to have a wide variety of applications in manufacturing 3D models, the technology requires more analysis and development to meet the requirement in terms of consistency and stability of extruded parts. Recent research only focuses on process parameters to improve finish. However, the hardware system is also an important element that contributes to the best extrusion process, thus providing good products. So this brings an opportunity to add even more to this technology. One of the main elements of a 3D printer is the extrusion head, as the main component of the printer, it is essential to have a nozzle that meets different requirements, depending on feed, consumption, time, materials and final quality finish. The constant improvement of technology in 3D printing is causing the increasing use of composite properties of carbon fiber in industrial manufacturing. Thus, in proportion to carbon fiber reinforced plastics (CFRP), the mouthpiece must also evolve to adequately handle the advancement of the composite material. To produce the ideal nozzle geometry and material recommendation, some parameters were analyzed, thus improving the nozzle capacity. The nozzle design also influences the flow and thermal behavior of the filament passing through it [101].

The phenomenon of nozzle clogging in FFF is still poorly studied. Other studies focus on clogging Newtonian fluids filled with particles in microchannels. Different fouling mechanisms appear during continuous flow, which are caused by hydrodynamic forces and DLVO forces (it is the explanation of the stability of colloidal suspension which describes the balance between two forces, electrostatic repulsion and van der Waals attraction). The deposition of particles on the wall decreases the effective cross section of the channel. If the adhesive particles collide, they can bond together by normal stresses and act as a nucleus for other particles. Particle clumps develop in the stream, which can connect with particles deposited on the channel surface by friction or surface interaction. Particle collisions, a changing flow field or influences can cause particles to fragment, breaking up agglomerates and releasing them into the flow. It is observed that dendrites develop on the surface of the channel, growing in most of the flow and creating an asymmetry of the flow field. If the geometric shape of the channel changes, arch configuration occurs at the restriction. Standard printer nozzles have a restriction on transition from fusing zone to nozzle ground [102].

Common 3D printer nozzles are all very similar to each other. There is a hole bigger than the diameter of the filament that goes almost to the tip, where the small

hole that defines the diameter of the nozzle begins. There is a slight variation on the cheaper nozzles as they are only drilled with a standard 118° drill bit. The E3D company tried to improve this aspect many years ago with a staggered hole probably to improve the internal flow, but now they use like many other high-quality manufacturers a special drill with a pointed tip for better flow characteristics. The nozzle shown in Figure 27 is Bondtech's new CHT nozzle which has a special core that divides its filament into three separate channels. CHT stands for “Core Heating Technology” which means the material is not only melted from the outside in, but also the inside out, promising higher melting rates [103].

Figure 27- Schematic of the new Bondtech CHT nozzle [103].

2.4 Printing defects

Visual inspection analysis, Figure 53, sought to identify the effects of over and under-extrusion, warping, delamination between layers, lateral detachment, overheating, “elephant foot”, ghosting and the presence of thermally degraded (“burnt”) material on the surfaces of the model.

Under-extrusion is a very common problem in 3D printing that occurs when too little filament is extruded. This usually leads to voids, gaps, missing layers, or spots where the deposited filament is missing. Increasing the flow to compensate for the lack of material is not a good idea, as there is no point in increasing the flow when the filament passage is limited. The faster the print, the less time the filament has to warm up before being pushed through the extrusion nozzle, causing it to clog [104]. The under-extrusion problem did not happen during calibration.

Over-extrusion is primarily the result of poor extrusion calibration. As the name implies, it occurs when the 3D printer outputs a lot of material and can, therefore, ruin

the quality of the prints. Dimensional inaccuracy, layer drop, leakage, bubbles and even clogging can all result from an over-extruded printer. Some tips to solve this problem are as follows: change the extrusion multiplier to a lower value and lower the printing temperature [105]. The over-extrusion problem happened during calibration, Figure 53.

The lack of adhesion between the deposited material and the build platform (printer bed) can occur due to mechanical adjustments — incorrect distance between the bed and the nozzle, or platform leveling — but also due to the lack of affinity of the extrudate with the printing surface — temperatures base, presence of dirt, lack of adhesives, among others [106]. When 3D prints do not stay in place on the build plate, disastrous results can be obtained, typically manufacturers use various types of 3D printing surfaces to help different materials adhere to the board during printing. Most commonly 3D printers use aluminum, stainless steel, glass, BuildTak, Kapton tape, PET tape, masking tape or PEI film; but there is no single type of bed that works best for the adhesion of all types of filaments [107].

Layers delamination and lateral detachment (between infill and perimeters) can occur due to polymer shrinkage or lack of binding energy between deposited structures. Layers shifting can happen due to excessive temperature in stepper motors or drivers, lack of power in motors, or mechanical failure. Overheating of the parts occurs mainly due to working with an excessive extrusion temperature. The “elephant foot” consists of the expansion in the horizontal plane of the first layers of the pieces, the main causes may be due to the nozzle being too close to the layer or the temperature of the table being too high. To try to solve this problem, you can start by leveling the printing table and adjusting the nozzle, sometimes this defect is simply the result of an uneven building platform or an incorrect nozzle height. These problems cause the first layer to be crushed, forcing the already printed material to swell. One way to solve it is to lower the bed temperature: reduce the bed temperature incrementally by 5ºC until it prints successfully [108]. The elephant foot problem happened during calibration most likely because the nozzle clogged during printing, as shown in Figure 53.

Finally, ghosting is a 3D print quality issue that can detract from the visual appearance of a model. You can usually identify it visually by noticing that the outside walls of a part look wavy or just not smooth. This print quality issue occurs in 3D printing when the nozzle is prevented from depositing material in a controlled manner,

creating an ever-changing print environment. The ripple effect on the sides of the prints is a result of vibrations in the layers, very high print speed, and displacement in the print area. The solutions to this problem are presented below: tighten the printer's belts; print at a slower speed, however, it is important to mention that you should not decrease the standard print speed (about 60mm/s for PLA) by more than 25%, finally, one of the best ways to reduce vibrations is to print on a solid base and stable [109]. The ghosting problem did not happen during calibration, as shown in Figure 53.

3. Materials and methods

In this section, the methodological procedures, equipment, and materials used to carry out the master's research will be presented. There were used three different case studies that are outlined in the Figure 28.

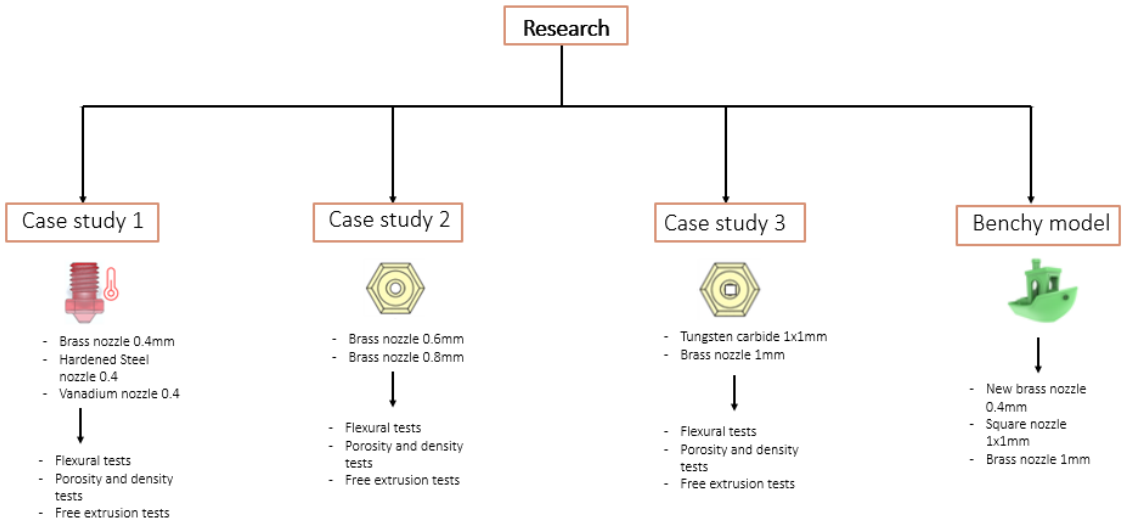

Figure 28- Scheme of the applied methodology.

3.1 3D printing equipment

In this work, an Original Prusa i3 MK3s 3D printer from the Prusa Research™ brand, previously mounted on the LDPS/FEUP, was used. The technical specifications of the equipment, according to the manufacturer [47], are presented in Table 4.

Table 4-Technical Parameters of Prusa MK3s [47].

Technical Parameters	
Build Volume	250×210×210 mm
Layer height	0.05 - 0.35 mm
Nozzle diameter	0.4 mm default, wide range of other diameters/nozzles supported
Filament diameter	1.75 mm
Supported materials	Wide range of thermoplastics, including PLA, PETG, ASA, ABS, PC (Polycarbonate), CPE, PVA/BVOH, PVB, HIPS, PP (Polypropylene), Flex, nGen, Nylon, Carbon filled, Woodfill and other filled materials.
Max travel speed	200+ mm/s
Max nozzle temperature	300 °C
Max heat bed temperature	120 °C
Extruder	Direct Drive, Bondtech™ gears, E3D V6 hot end

continues

Print surface	Removable magnetic steel sheets (*) with different surface finishes, heat bed with cold corners compensation
Printer dimensions (without spool)	7 kg, 50×55×40 cm; 19.6×21.6×15.7 in (X×Y×Z)
Power consumption	PLA settings: 80 W / ABS settings: 120 W

3.1.1 Equipment calibration procedure/printing process

Considering that the 3D printer used was already assembled and with its drive, control, motion, and extrusion systems calibrated, the first procedure performed was to confirm its stability through a simple printing test. For this, five cubic samples of (15x15x15) mm were built, based on a fixed parametric configuration, Table 5, developed during the studies of Santana *et al*. [1], [2], [110], [111] and refined in the study of Castro [112]. The works mentioned above were carried out at LDPS/FEUP, based on Polylactic Acid (PLA) polymer. These were adopted as a reference model, because, like the present dissertation, they are part of the laboratory's research line in the context of low-cost extrusion-based 3D printers.

The planning of the 3D Printing process of the calibration elements, as well as of all the samples produced in this investigation, was carried out in the PrusaSlicer software (version 2.3.3). A white PLA filament, 1.75 mm in diameter from the Filament PM™ brand, was used as a pattern for the construction of the cubes and other main parts of this project. Further details on material properties will be presented in section 3.3. It is important to highlight that in the calibration step, a brass nozzle (0.4 mm diameter) was used to make the models.

Table 5 – 3D Printing parameters configuration [112].

Print settings	**Values**
Layer height and First layer height	0.2 mm
Infill density	100 %
Infill pattern	Concentric
Perimeter's speed	20 mm/s
Infill speed	40 mm/s
Overlap	27 %
Seam position	Aligned
Filament settings	**Values**
Nozzle temperature (first layer/ other layers)	215 ºC/ 210 ºC
Bed temperature (first layer and other layers)	60 ºC
Extrusion multiplier	1 d.u.
Printer settings	**Values**

continues

Nozzle diameter	0.4 mm
Retraction speed	30 mm/s
Retraction length	1 mm

The cubic calibration samples were dimensionally analyzed using a Mitutoyo™ digital caliper with a resolution of ±0.02 mm —Figure 29(a) —, by mass measurement (HLD300 scale, Scale House™ resolution ±0.05 g) — Figure 29(b) — and visual inspection.

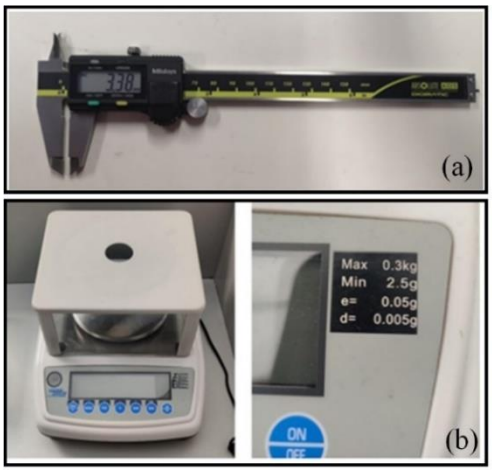

Figure 29- Measuring equipment used in the calibration study: (a) caliper and (b) scale.

Changing nozzles was a constant task in the experimental stages, requiring, therefore, a calibration system to adjust the nozzle/table distance and analysis of the deposition quality (deposited filament continuity, material adhesion on the building platform, and between filaments). The tuning of these parameters is essential for 3D printing to occur safely and with the least possible occurrence of failures.

When changing the nozzle, also because not all nozzles were all Prusa originals, it was necessary to calibrate the distance of the nozzle and the leveling sensor to the table (building platform). Initially, the magnetic part of the table was removed. With the help of a plastic clamp, adopted as a standard distance of 2.5 mm, the height of the sensor to the base was adjusted, Figure 30. To calibrate the distance from the nozzle to the table, its value was manually calibrated in the printer using a rotary knob.

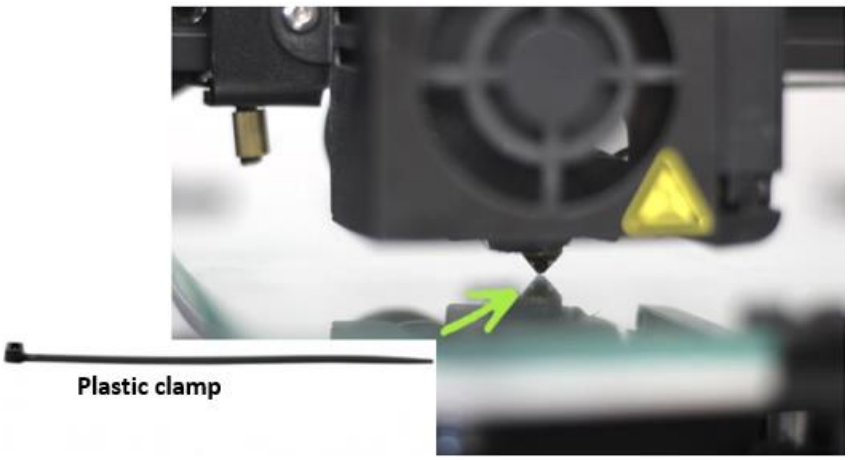

Figure 30- Illustration to exemplify the calibration of the distance between sensor and table with the aid of a plastic clamp, adapted from [113].

To obtain a good adhesion of the extruded filament to the construction platform, the first layer deposition (*First Layer Calibration*) must be calibrated, as well as the flow with which the material is deposited. Although it is a quick test, it needs to be carried out several times, as the values are manually changed and results observed until the desired quality are reached, Figure 31, being important to reduce the over-extrusion of the material.

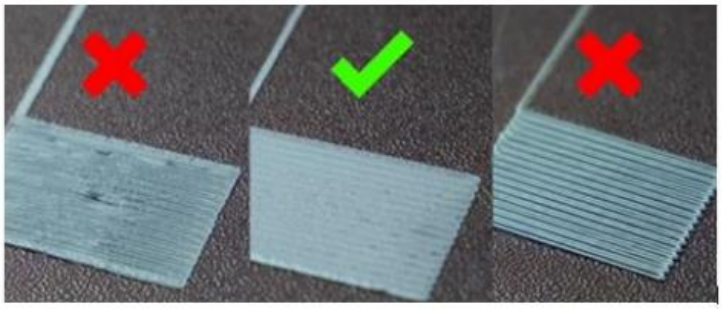

Figure 31- Demonstration of results of calibration of first layer (a) under extrusion, (b) calibrated extrusion, (c) over extrusion [114].

3.2 Calibrated nozzles

3.2.1 Commercial nozzles

Throughout the experiments, seven commercial nozzles were used (Figure 32). These nozzles were distinguished from each other according to the material they were made of the nozzle diameter and the time of use.

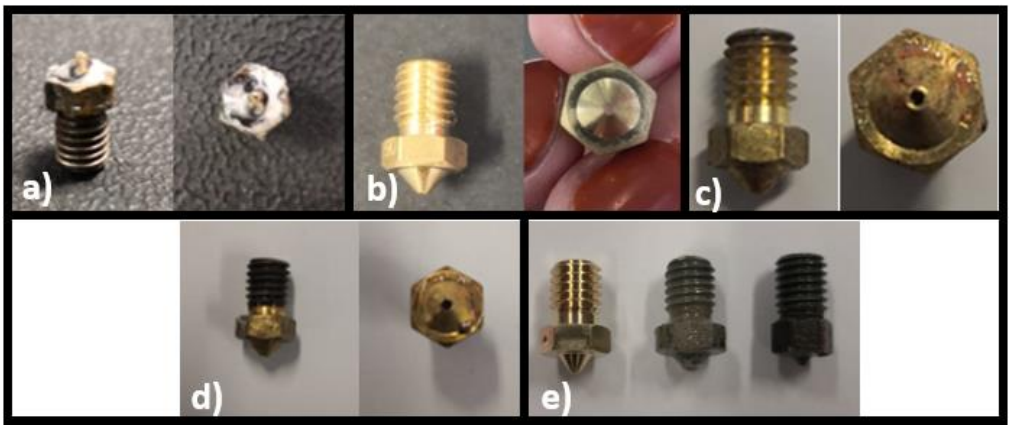

Figure 32- a) 0.4mm brass nozzle; b) 0.6mm brass nozzle; c) 0.8mm brass nozzle; d) 1mm brass nozzle; e) side comparison of brass, hardened steel, and vanadium nozzle, respectively.

Although the nozzles were all distinct from each other, in general they resembled the scheme of the Figure 33.

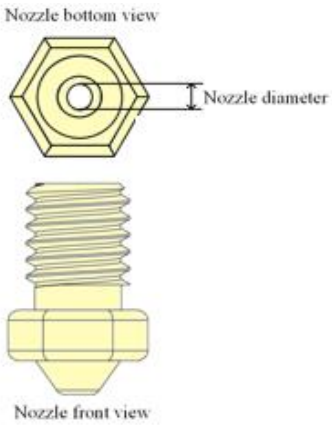

Figure 33- Schematic nozzle structure.

The description of the components used is presented in Table 6.

Table 6 – Description of the nozzles used in the study.

ϕ (mm)	**Material**	**Supplier**	**Model**	**Price (€)- consulted in 18/01/2022**	**T.C. (W/m.k)**
*0.4	Brass	E3D™	V6	7-12 [115]	105 [116]
0.4	Hardened steel	E3D™	V6	4-45 [117]	18-22 [116]

continues

0.4	Vanadium	Bondtech™	V6	45 [118]	31-37 [119], [120]
0.6	Brass	E3D™	V6	7 [121, p. 6]	105 [116]
0.8	Brass	E3D™	V6	7 [122]	105 [116]
1.0	Brass	Aimsoar™	V6	1-10 [123]	105 [116]

* In the case of the 0.4 mm brass nozzle, two components were used: one with a long history of use (1 year) and another new. Nozzle diameter (ϕ), T.C. (thermal conductivity).

3.2.2 Square profile nozzle

The square profile nozzle design (1x1 mm) with a depth of 0.80 mm, Figure 34 and Figure 35, was developed by Diogo Vieira da Silva during his curricular internship at LDPS/FEUP in 2021. The component was manufactured in partnership with Palbit™[3], a leading company in the production of carbide tools, with over 100 years of experience in the area. To make the die for the extruder head, a tungsten carbide (WC) alloy with 7% (wt.) of cobalt (Co) was used. The material has a hardness of 1730 ± 50 HV10 with a transverse breaking strength (TRS) of 2850 N/mm^2. The microscopy image of the material is presented in Figure 35

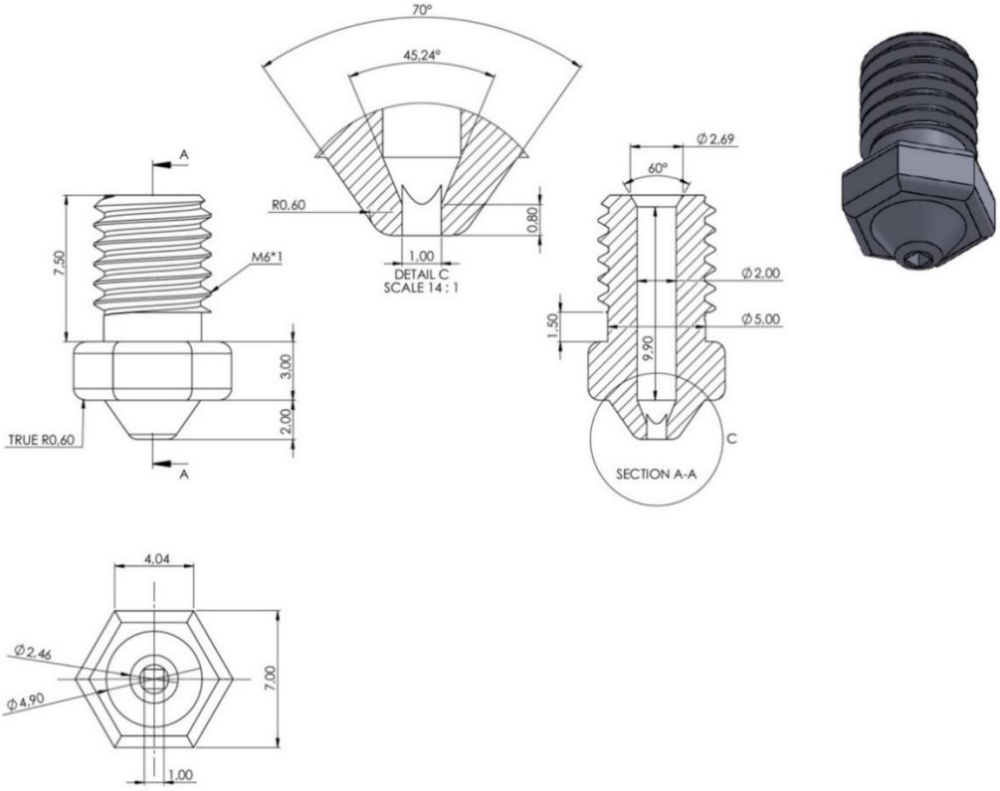

Figure 34 – Technical drawing of 1x1mm square nozzle (designed by Diogo Vieira da Silva) (all dimensions in mm).

[3] More information about Palbit™: https://www.palbit.pt/ (accessed on 01/24/2022).

Regarding the manufacturing processes used to obtain the part, the following are highlighted: (i) uniaxial pressing with cylindrical geometry; (ii) green machining to give the desired geometry; (iii) sintering, in a Sinter-HIP furnace, with a temperature of 1455°C and a pressure of 30 bar; (iv) grinding; (v) sharpening; (vi) Electrical discharge machining (EDM) and (vii) polishing.

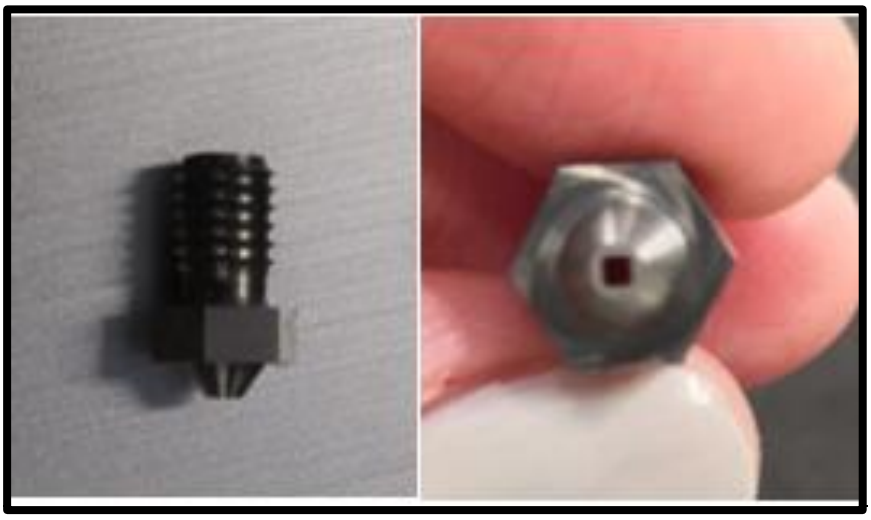

Figure 35 – Nozzle with square cavity.

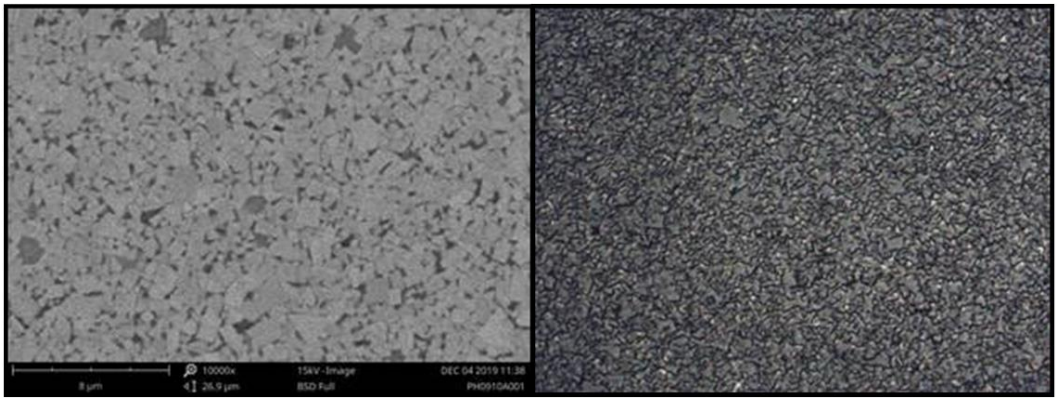

Figure 36 – Microstructure of square nozzle material (Courtesy, Palbit™).

Thermal conductivity is an extremely important property for tungsten carbide since most of its applications involve exposing the material to high temperatures. This property is crucial in predicting the behavior and durability of machining tools. It is used to study and determine the maximum working temperatures, the temperature gradients generated along the tool, and the possible resulting thermal stresses [124]. The thermal conductivity will be useful for this study as it will be used to evaluate if the results obtained in the bending tests are following the expected, since the thermal

conductivity is related to the energy supplied to the material, in this case. Therefore, if more heat is supplied to the material, it will have a better adhesion between the layers.

The influence of the cobalt content on the thermal conductivity of WC-Co is not very clear, and there are several works in the literature that report contrary trends. Williams *et al*. [125] report that the total thermal conductivity decreases with increasing cobalt content. The thermal conductivity of tungsten carbide is around 85W/m.K [126].

An image of the nozzle cavity was captured with a *Zeiss Axiophot* microscope. The result present in Figure 37 shows a geometry that approximates a square. However, due to the characteristics of the tools and the machining process, added to the manufacturing difficulties imposed by the small dimensions of the part, the corners of the square are slightly rounded, that is, they are not sharp corners with 90°.

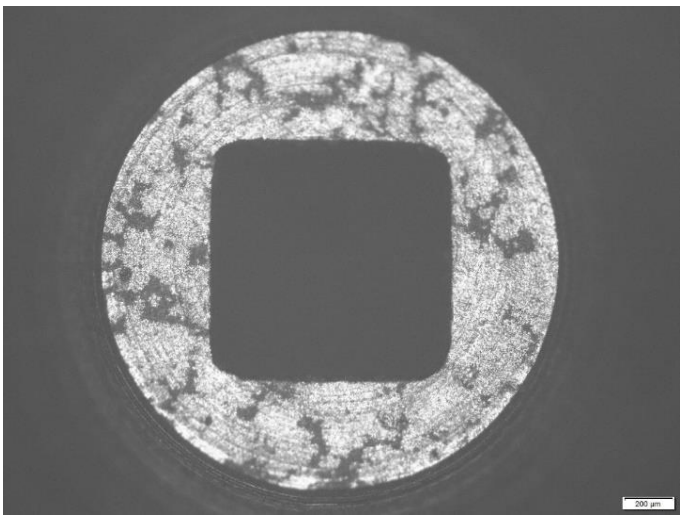

Figure 37- Microstructure of the square nozzle seen under a microscope.

In this sense, the nozzle outlet geometry is more like the super-ellipse concept. A super-ellipse is a closed curve like an ellipse, retaining the geometric characteristics of the semi-major and semi-minor axes, and symmetry about them, but a different overall shape, Figure 38. In the Cartesian coordinate system, the set of all points (x,y) on the curve satisfies the Eq. (3) [127].

$$\left|\frac{x}{a}\right|^n + \left|\frac{y}{b}\right|^n = 1 \qquad \text{Eq. (3)}$$

Where n, a and b are positive numbers and the vertical bars around a number indicate the absolute value of the number [127].

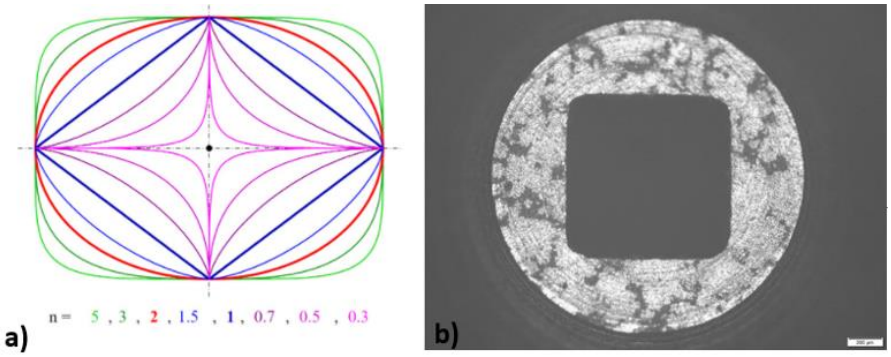

Figure 38- a) Possible values of n [127], b) Microscopic image of the 1x1 mm square nozzle.

3.3 Material

The standard material used for the study was white PLA filament from Filament PM™, whose properties are shown in the Table 7. White PLA was used because in a mass study of Castro's dissertation [112] and it was the filament that gave the best mechanical properties.

Three auxiliary materials were also used. These were applied in the study stage with the square nozzle to validate the parametric configuration found for this component in the printing of parts with PLA:

- Transparent and red PLA by the Filament PM brand, whose characteristics are the same as those presented in the first part of the Table 7*;*
- Fil3D brand red PLA whose characteristics are described in Table 8;

Table 7- Characteristics of the PLA filaments used in the study.

Filament PM™(adaptado de [14])	
Filament diameter (mm)	1.75 ± 0.05
Extrusion temperature (°C)	200-230
Bed temperature (°C)	20-60
Thermal properties	
Vicat softening temp. (°C)	55
Heat deflection temp. (°C)	55
Mechanical properties	
Impact strength (kJ/m²)	16
Flexural modulus (MPa)	3500
Physical properties	
Density (g/cm³)	1.24
Melt flow index (g/10 min)	
Filament PM™ (PLA white) – Castro [112]	
*Maximum flexural strength (MSF) (MPa)	100.10 ± 0.336
Flexural modulus (FM) (GPa)	3.25 ± 0.024

continues

Density (g/cm³)	1.27± 0.03

Note: * MSF and FM values obtained from parts printed with the print configuration described in Table 5. In this case, a lateral build orientation was used.

Table 8- Properties of red filament by Fil3D™.

Fil3D™ datasheet [128]	
PLA grade	3D850
Density (g/cm³)	1.24
Melt flow index (g/10 min)	7-9
Filament diameter (mm)	1.75 (1.67 to 1.83)
Printing temperature (ºC)	210 ± 20
Bed temperature (ºC)	60 ± 10ºC
Ingeo™ 3D850 [129]	
Melt temperature (°C)	165-180
Glass transition temp. (°C)	55-60
Feed throat (°C)	45
Feed temperature (°C)	190
Print bed temperature	None needed (or 50-70 (°C) if aplicable)
Tensile Elongation, %	3.31

3.4 Case Study 1: nozzle material

Case study 1 aimed to evaluate the effects of the material in which the nozzle is built, in terms of service life and thermal conductivity, on the quality aspects of FFF printed parts.

The analysis of the lifespan and the thermal conductivity of the materials of the nozzles was carried out indirectly from the evaluation of the quality of the printed parts, in terms of mechanical properties and porosity levels. Nozzles with 0.4 mm, in brass, hardened steel and vanadium were selected. Brass nozzles are the most frequently available on 3D printers (are easily machinable and cheap and have good thermal performance) (Carolo [130]). [126]). However, they are susceptible to working wear. This is the reason why were selected for the study of the lifespan, considering the following criteria: (i) brass nozzle with a long history of use (one year), (ii) compare the parts manufactured with this nozzle, with ones produced with nozzles with low thermal conductivity (hardened steel and vanadium) and the results were also compared with a brand new 0.4 mm brass nozzle, and (iii) use a thermoplastic with good printability; PLA filament (white, 1.75 mm diameter) from PM™ supplier, previously presented in section 3.3.

To study the effects of heat conduction from the nozzle on the formation of printed layers parallelepiped samples (127x12.7x3.2 mm) were manufactured for flexural testing, based on the ASTM D790 [131] standard, varying only two process parameters, raster angle and build orientation, under two experimental conditions: lateral and in-plane aligned (45°/-45°). The other process parameters were kept fixed, according to the configuration presented in Table 5 of section 3.1.1. The printing conditions are detailed below:

(1) Lateral orientation (unidirectional deposited filaments) (Figure 39)**:** the first combination consisted of deposition of unidirectional filaments combining the use of a concentric deposition strategy with lateral part orientation. This configuration, by having all the filaments aligned between and within the layers, provides better mechanical properties. However, in the lateral position, one of the largest dimensions of the specimen (12.7 mm) is in the Z-stacking direction, causing a portion of the sample layers to move away from the heated bed of the 3D printer and have its formation energy dependent, mostly, the temperature of the nozzle. Six specimens were printed, simultaneously, for this condition.

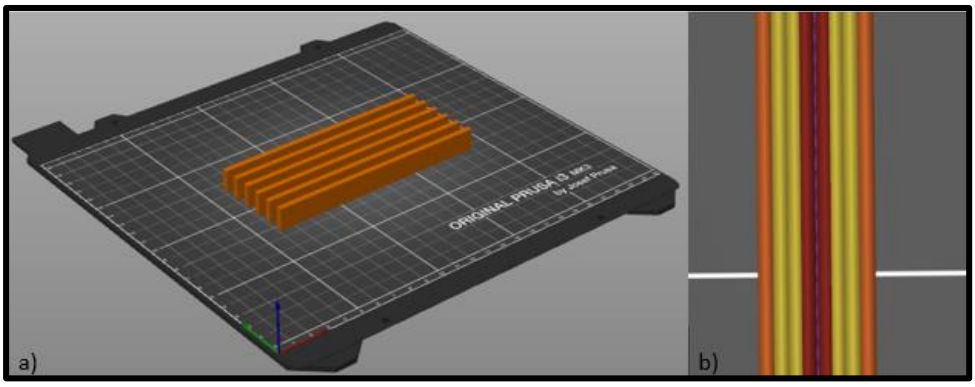

Figure 39 – (a) lateral orientation and (b) unidirectional filaments.

(2) On the plane (Figure 40): in the second case, an “on the plane” build orientation was used, with the smallest part dimension (3.2 mm) in Z, together with a raster angle of 45°/-45°. In this situation, we sought to compensate for the thermal conductivity limitations of the nozzles through the thermal energy of the heated bed and the deposition of filaments with

smaller vector lengths. As in the previous case, six specimens were also printed at the same time.

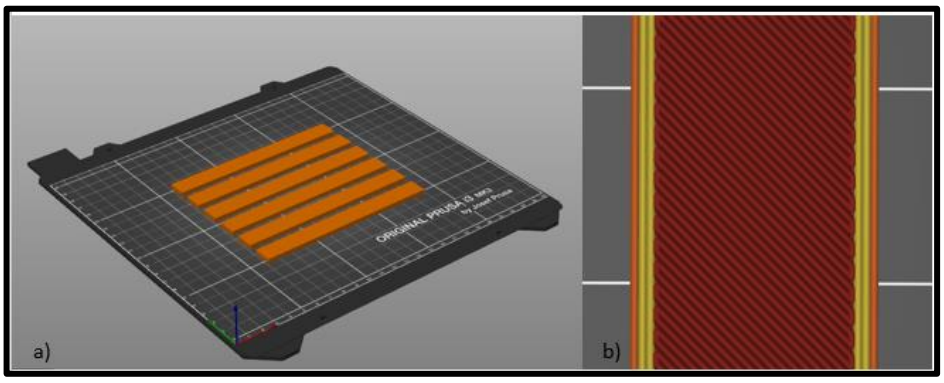

Figure 40- (a) “in-plane” orientation and (b) filaments deposited at 45°/-45°.

Another important parameter related to the calibrated nozzle is the extrusion width. In the case of configurations (1) and (2), the width values were automatically calculated by PrusaSlicer, to guarantee compatibility with the matrix dimensions. The width measurements, by regions of the part, are shown in the Table 9.

Table 9 – Extrusion width values for the different parts of the printed part.

Part region	**Road width values (mm)**
External perimeters extrusion width	0.45
Perimeters extrusion width	0.45
Solid infill extrusion width	0.45
Top infill extrusion width	0.40
Infill extrusion width	0.45

Immediately after printing, all 12 specimens were subjected to dimensional analysis and mass measurement. For these procedures, the same caliper and scale described in topic 3.1.1 were used. The dimensions of the samples were acquired at (5) points along their length, width, and thickness (Figure 41). The average of the thickness values and the average of the width were applied in the calculations for the determination of the mechanical properties in the bending of the samples: maximum stress and modulus.

The flexural tests, in the three-point mode, were performed in an equipment composed of a dynamometer with a load cell of 2.5 kN — AFG (Advanced Force Gauge) 2500 N — coupled to a displacement column model Multitest 2.5 – dV

(resolution of displacement of 0.001 mm) of the Mecmesin brand. The tests were carried out at a speed of 5 mm/s.

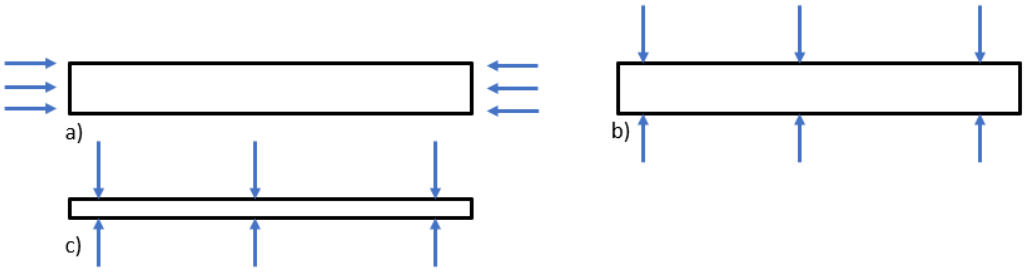

Figure 41 - Measuring points for length (a), width (b) and thickness (c).

For the porosity and density measurement tests, three cubes with dimensions 15x15x15 mm were printed. The configurations used to manufacture these parts were described in section 3.1.1 and based on Castro dissertation [112].

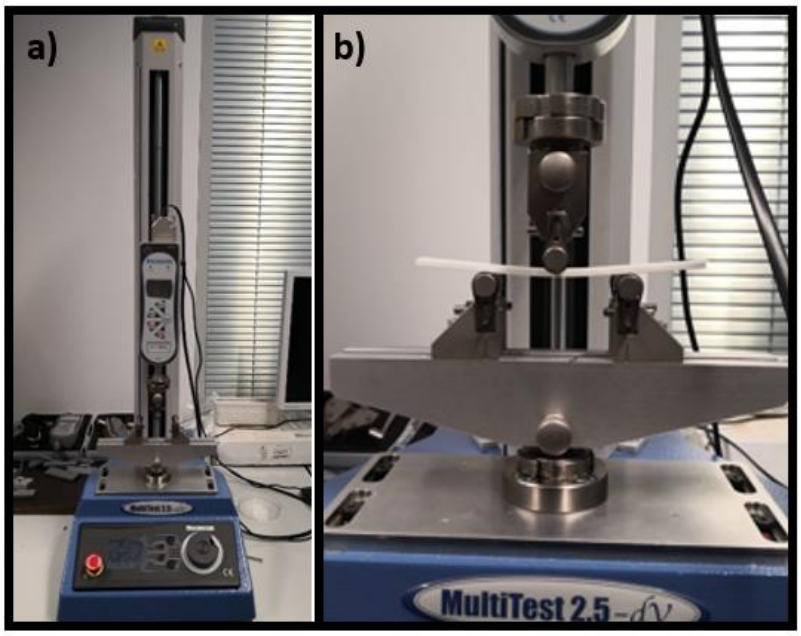

Figure 42 – a) Testing machine used; b) position of the specimen for the bending test.

The porosity study was applied in all the case studies of part manufacturing carried out in this dissertation. It should be noted, however, that in some situations the print settings were adjusted according to the nozzles used, which will be detailed in the following topics.

The first step of density and porosity test consisted of measuring the density of the white PLA filament (standard material for this master's degree), since this parameter is an input for determining the percentage of porosity of the printed parts. For this procedure, a Mettler Toledo XS205 Dual Range scale (d=0.01 mg/0.1 mg) provided by LabMat UFSC (Brazil) was used —Figure 43 (a). The equipment has a special setup for density measurement Figure 43 (b) —, based on Archimedes' method, as well as a function in your software capable of automatically calculating the values of this property. For this, the user just enters the system with the following parameters: (i) standard liquid and its temperature, (ii) mass of the dry material, (iii) mass of the material submerged in the liquid. In this study, five filament samples, 1.75 mm in diameter and 3 cm in length, were measured in distilled water at 22°C. The average measurement result was 1.26±0.01 g/cm³.

Figure 43 – Scale for density measurement (a) and setup (b).

With the filament density established, the next step consisted in determining the level of porosity of the printed cubes, obtained from the mathematical equation (Eq.4) described in the study of Al-Maharma *et al*. [132]:

$$Porosity\ (\%) = \left(1 - \frac{W_s/V_s}{\rho_m}\right) \qquad \text{Eq. (4)}$$

- W_s is the mass of the sample;
- V_s is the volume of the sample;
- ρ_m is the density of the material.

To measure the mass of the cubes (Ws) a Mettler H31AR balance with a resolution of ±0.1 mg was used, which was available at the Metallography Laboratory of FEUP. The cube volume (Vs) was calculated from the average of measurements of its dimensions in XYZ, obtained with the aid of a Mitutoyo™ IP65 micrometer with ±0.001 mm resolution.

Figure 44- Micrometer used for dimensional analysis.

Five measurements were made in the three main directions (x, y and z) of the cubes. In Figure 45 it is showed an example of measurements taken along the z-axis is shown, the same procedure was carried out for the other two axes.

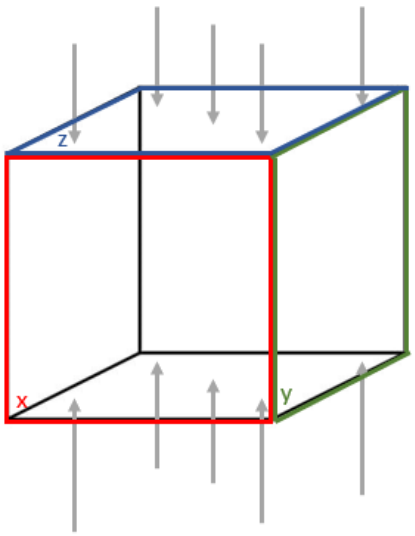

Figure 45- Points used for dimensional analysis of cubes.

Finally, the density of the cubes was measured. As in the case of filaments, the Archimedes method was also used, Figure 46. The Mettler H31AR balance was used as a measuring instrument. First, the mass of the dry cubes was measured, the wire was used to tie the cubes and the cubes were weighed with the wire. The last procedure was the measurement of the mass of the cubes suspended by the wire but immersed in distilled water (22°C). To calculate the density of the cubes, the following equation was used (Eq.5):

$$\rho c\ (\frac{g}{cm^3}) = \frac{(Ws + WD) - Ws}{(Ws + WD) - (Ws + Wi)} * \frac{\rho_w}{1000} \qquad \text{Eq. (5)}$$

W_D – Dry sample mass for density measurement;

W_i – Sample mass immersed in distilled water for density measurement;

W_S – Mass of the wire used to measure the density.

Figure 46- a,b) Scale used for porosity tests.

3.5 Case study 2: nozzle diameter

In case study 2, the same nozzle material was always kept, in this case, brass, varying the diameter of the dies by 0.6 mm and 0.8 mm and the results were compared with the 0.4 mm brass nozzles. The two diameters were selected because they balance the scalability of the production process — increasing the volume of material deposited (larger road widths and layer thicknesses) and reducing printing time — with

certain levels of resolution. However, this balance is especially effective in the manufacture of large parts, making it an interesting challenge in meso-structure formation when the physical limits of the printed object are reduced.

This study focuses on cases such as the latter, of small parts, such as specimens for flexural tests and cubes for porosity measurement. The effects of the dimensional variation of the nozzle on the material flow control (extrusion and deposition in the layers) and, consequently, on the determination of the quality of the unions between filaments within and between layers and on the growth of the void density were evaluated.

To modify the meso-structure of the parts manufactured by each nozzle diameter, two parameters were varied for the construction of the bending specimens and the hubs: road width (Rw) and layer thickness (Lt) (Table 10). In the case of the extrusion width, two situations were tested: (i) deposition of a width smaller than the nominal diameter of the 0.6 mm and 0.8 mm nozzles, with values calculated by the slicer compatible with the 0.4 mm nozzle diameter — “Rw (0.4)”[4]; and (ii) deposition of filaments with widths calculated by the slicer compatible with a 0.6 mm nozzle — “Rw (0.6)” — and a 0.8 mm nozzle — “Rw (0.8)”. The layer thickness under conditions (i) and (ii) remained fixed at 0.2 mm — Lt (0.2). A third condition was tested for each nozzle, varying the layer thickness: 0.6 mm — Lt (0.6) — for the 0.8 mm nozzle and 0.45 mm — Lt (0.45) — for the 0.6 mm nozzle. The other process parameters were kept fixed according to the configuration of the calibration step (Table 5). In Figure 47 shows a schematic of how Rw and Lt vary as a function of nozzle diameter.

[4] The RW code (0.4) corresponds to the extrusion width (road width) calculated for the 0.4 mm diameter nozzle. The same interpretation must be performed for the code Rw (0.6) (nozzle 0.6 mm) and Rw (0.8) (nozzle 0.8 mm).

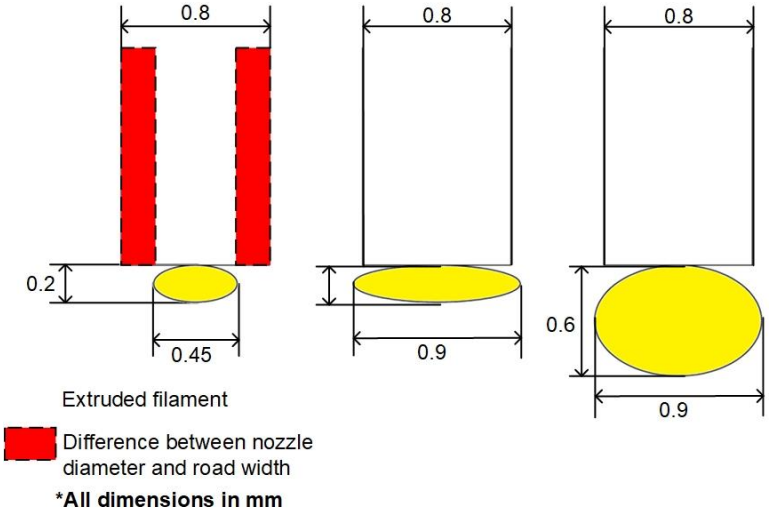

Figure 47- Representation of differences between nozzle diameter (example for 0.8mm nozzle) and extrusion width.

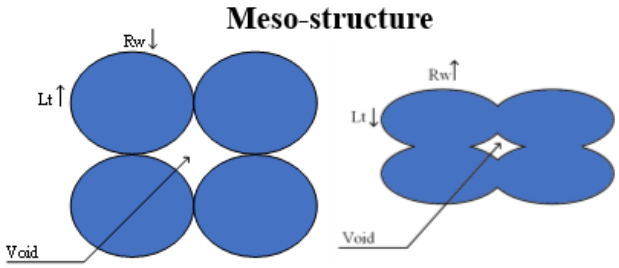

Figure 48- Schematic about the meso-structure of the extrudate in relation to the layer thickness and to the layer height.

They were printed, for each condition of the Table 10, six specimens for flexural tests and three cubes for porosity/density. It should also be noted that the flexural test specimens were printed with the lateral aligned orientation. Dimensional analysis, mass measurement and bending tests with ASTM D790 specimens [131], as well as the measurement of porosity/density of the cubes, follow the methodology described in topic 3.4.

Table 10 – Parameters used for the 0.6 mm nozzle and for the 0.8 mm nozzle.

Nozzle 0.6 mm			
Parameter	**Conditions**		
	Rw (0.4)	*Rw (0.6)*	*Lt (0.45)*
Layer thickness (Lt) (mm)	0.2	0.2	0.45
Road width per part region (mm)			
External perimeters	0.45	0.65	0.65
Perimeter	0.45	0.65	0.65

continues

Solid infill	0.45	0.65	0.65
Top infill	0.40	0.60	0.60
Infill	0.45	0.65	0.65

Nozzle 0.8 mm

Parameter	**Conditions**		
	Rw (0.4)	*Rw (0.8)*	*Lt (0.6)*
Layer thickness (Lt) (mm)	0.2	0.2	0.6
Road width per part region (mm)			
External perimeters	0.45	0,9	0,9
Perimeter	0.45	0,9	0,9
Solid infill	0.45	0,9	0,9
Top infill	0.40	0,8	0,8
Infill	0.45	0,9	0,9

3.6 Case study 3: square profile nozzle

The third case study was based on the application of the square geometry nozzle in the manufacture of parts by FFF in PLA. As it is a non-commercial component, that is, validated by large-scale production, and by the novelty of the geometric variation of the extrusion matrix, still little explored in the literature in the area. This stage of the research aimed to explore the calibration of the system, as well as identifying the strengths and weaknesses of the project developed by LDPS/FEUP.

All the mentioned issues led to the application of a design of experiments (DOE) for the systematic analysis of key parameters for the functional characterization of the nozzle in the printing process of the layers. Therefore, variables related to print resolution (layer thickness), energy supply for the thermoplastic state transformation (extrusion temperature) and material flow control (volumetric velocity) were selected.

The last parameter mentioned causes the slicer to calculate the best linear printing speeds to stabilize the volume of material to be deposited; this volume, which also takes the layer thickness and width values as input. The volumetric speed, in turn, is related to the rheological properties of the material, as described by the PrusaSlicer manual. [133]. In this study, only PLA was used, which, due to its good printability, was considered the best candidate for the initial analysis of square nozzle performance. In the future, other materials will have to be tested for the complete validation of the component.

Returning to the DOE, for each of the three studied printing parameters, four levels were assigned, as shown in

Table 11.

Table 11- Parameters and levels: study of the square nozzle.

Parameters	Levels			
	1	*2*	*3*	*4*
Layer thickness (mm) (L_t)	0.2	0.4	0.6	0.8
Extrusion temperature (°C) (E_t)	215	225	235	245
Max. Volumetric Speed (mm^3/s) (MVS)	3	8	15	25

Based on the number of variables and levels, an orthogonal array L16 of Taguchi was applied, in which 16 combinations between parameters and configuration values were established, Table 12. For each of the conditions, sets of three ASTM D790 specimens were printed [131] for flexural test, using the white PLA, generating a total of 48 samples. It is important to highlight that, as in previous studies, all other printing parameters were kept fixed according to the Table 5 of the calibration step. The specimens were also printed in the lateral aligned orientation.

Table 12 – Taguchi L16 orthogonal arrangement: study of the square beak.

Conditions	Lt (mm)	Et (°C)	MVS (mm^3/s)
1	0.2	215	3
2	0.2	225	8
3	0.2	235	15
4	0.2	245	25
5	0.4	245	8
6	0.4	215	3
7	0.4	225	25
8	0.4	235	15
9	0.6	245	15
10	0.6	215	25
11	0.6	225	3
12	0.6	235	8
13	0.8	215	25
14	0.8	225	15
15	0.8	235	8
16	0.8	245	3

Each test piece manufactured (Table 12) was subjected to dimensional analysis, mass measurement and bending tests, following the protocols described in case study 1 (section 3.4). The extrusion width and print speed values automatically calculated by PrusaSlicer for conditions 1 to 16 are shown in the Anexo 1.

Obtained the results of the mechanical properties in bending, from the parts manufactured in the experiment of Table 12, a statistical analysis was performed, based on the combination of Analysis of Variance (ANOVA) with Post-hoc tests. The best levels were obtained for each of the evaluated process parameters. With the levels established, a new print configuration was created, called the “verification model” (Table 13), which was used to build a block of six samples for flexural test.

Table 13 – Verification model.

Verification model	
Parameters	**Level selected**
Layer thickness (mm)	0.2
Extrusion temperature (°C)	215
Max. Volumetric speed (mm³/s)	15
Road width (mm)	
External perimeters	1,12
Perimeter	1,12
Solid infill	1,12
Top infill	1,00
Infill	1,12

To validate the quality of the verification model, the following tests were also performed:

(1) Printing of three cubes in white PLA, with a square nozzle, for measuring porosity, whose procedure is described in section 3.1.1;

(2) Printing of three porosity cubes and six bending specimens on different PLA filaments: natural and red by Filament PM™ and red PLA by Fil3D. All prints with the square nozzle, whose procedure is described in section 3.1.1;

Finally, the square nozzle (1x1 mm) was compared with a 1 mm diameter brass nozzle. With the latter, porosity cubes (3 pieces) and bending specimens (6 samples) were also printed based on white PLA.

3.7 Free extrusion test

Free extrusion test was performed for each nozzle used in previous studies. It is an analysis process that only involves the extruder head and its mechanisms: traction, plunger effect, heating, state transformation, and dimensional calibration of the processed material. There is no movement of the extruder, nor the deposition of the material in controlled paths. The main objective of this analysis was to evaluate the effects of the constructive parameters of the nozzles, as well as the extrusion variables, on the quality of the extruded material — diameter and mass compliance.

Initially, it was necessary to verify that the material feed control system was supplying the extruder with the correct amount of filament. As we wanted to make a free extrusion based on a thread of 50 mm in length, this distance was marked on the filament, with the aid of a pen, from the entrance of the traction module, as seen in Figure 49 (a).

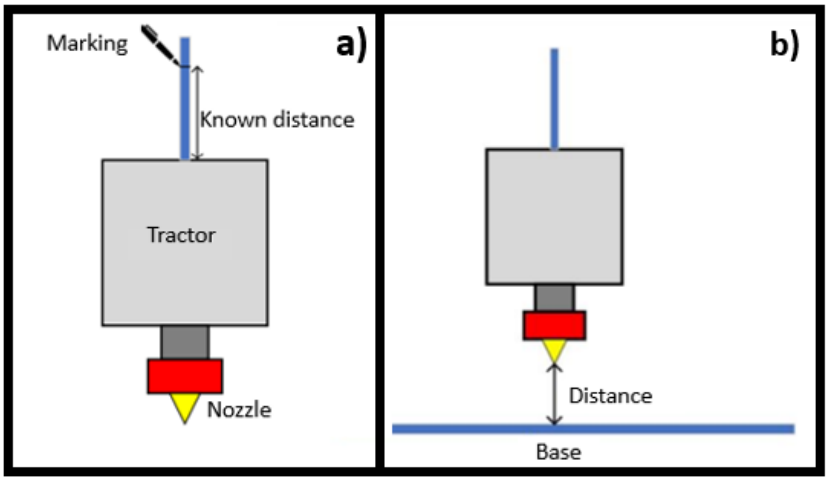

Figure 49- a) Marking scheme for free extrusion; b) schematic representation of the distance from the nozzle to the base of the 3D printer.

For the study of free extrusion, the full factorial DOE was followed, as shown in Table 14. The variables that changed were the extrusion temperature and the filament feed speed. For each parameter, four levels were assigned, generating a total of 16 extrusion conditions.

Table 14 – Factorial DOE, free extrusion study.

Conditions	Et (°C)	FFS (mm/s)
1	190	20
2	190	40
3	190	60
4	190	80
5	210	20
6	210	40
7	210	60
8	210	80
9	220	20
10	220	40
11	220	60
12	220	80
13	235	20
14	235	40
15	235	60
16	235	80

After defining the test conditions, the extruder head was positioned in the center of the construction platform (X and Y) and a fixed distance of 50 cm was added between the nozzle and the base (in Z), as exemplified in Figure 49 (b). Five tests were performed for each condition presented in Table 14. The extrusion commands, with parametric variation, were sent to the 3D printer through the software host *Pronterface,* Figure 50*.* The extrusion commands, with parametric variation, were sent to the 3D printer through the host software:

- G92 E0, this code was used to inform the origin of the extruder, resetting the system to each new free extrusion;
- Ex: G1 E50 F40, this sequence of commands was used for the test itself.

In this example, the equipment is being informed to execute a linear movement (G1), displacing 50 mm of filament at a speed of 40 mm/s. The temperature is set on the printer whenever it needs to be changed.

Immediately after the motor stopped feeding material, the material was cut from the nozzle tip. Then, the diameter of each piece of filament was measured in three different places with a micrometer and its mass was measured. The instruments used were the Mettler H31AR micrometer and balance described in section 3.4.

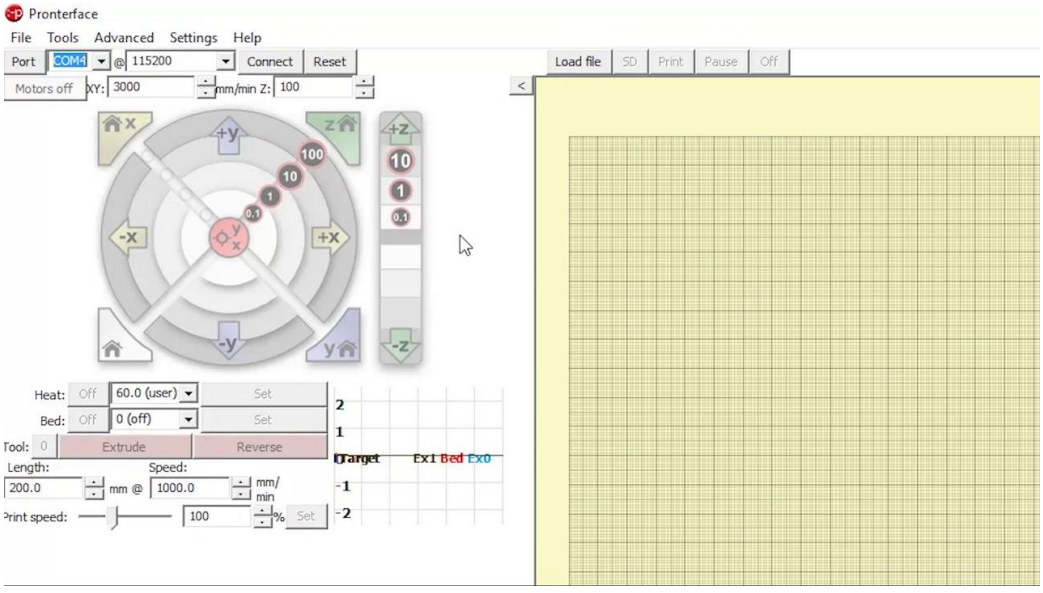

Figure 50- Pronterface interface, software used to send the necessary commands to the printer.

3.8 Benchy impression

The 3D Benchy (Figure 51) is one of the leading models for calibration testing on FFF 3D printers. The part is designed to be printed without the need for support material. The different surfaces of the model reveal typical problems regarding surface finish, model accuracy, deformation, among others. [134].

Figure 51- Benchy exemple [134].

The main features (Figure 51 e Figure 52) that make the Benchy model an excellent FFF 3D Printing analysis and learning platform are presented below [135]:

- The hull: is a large, smooth curved surface that is challenging for 3D printing and reveals any surface deviations;
- Symmetry: this calibration model is perfectly symmetrical, which facilitates the detection of any distortion;
- Flat horizontal faces: the upper surfaces of the deck, box, and chimney are flat, horizontal, and parallel to the lower plane;
- Cylindrical shapes: the chimney is designed to define concentric cylindrical shapes with inside and outside diameters. Such elements show deviations in circularity;
- Protruding Surfaces: Problems associated with protrusions are often at the forefront of 3D printing. The Benchy model offers several challenging areas, such as inside the hard-to-reach bridge;
- Low Slope Surfaces: Clearly show the layered structure of 3D printing. If printed horizontally, the roof of the bridge will reveal the stair effect formation;

- Large Horizontal Holes: The rear window offers a large circular horizontal hole. The boat wheel offers a hard-to-reach, insulated, round feature;
- Small Slanted Holes: The fishing rod holder provides a very small, slightly angled blind hole;
- First Layer Details: The shallow lettering on the underside of the boat reveals the typical first layer crush.

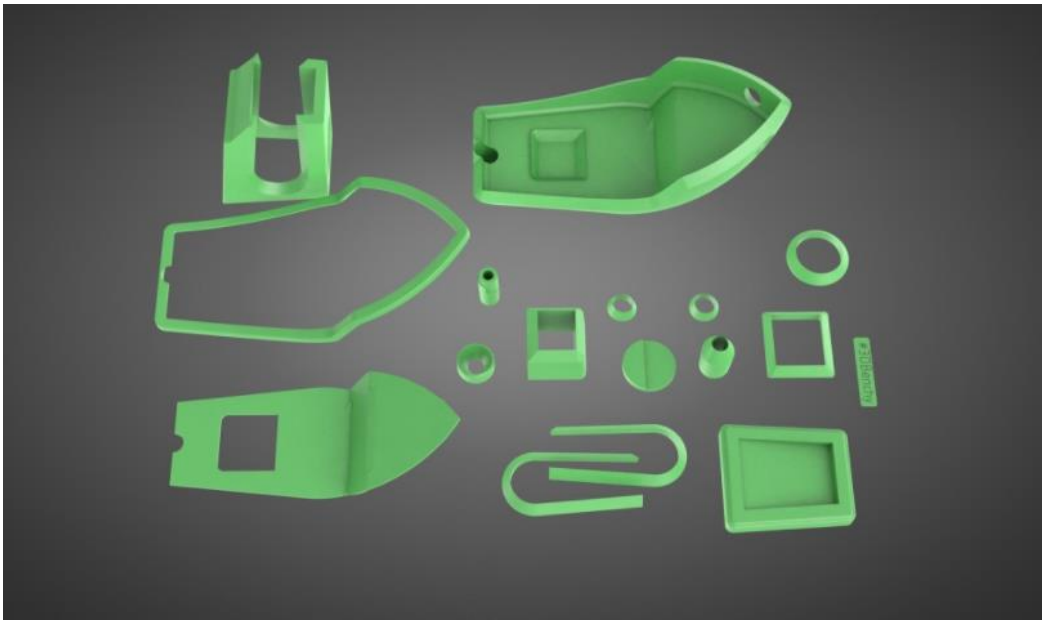

Figure 52- Main components of the Benchy calibration model [136].

The STL model used was obtained from the developers' profile on the Thingiverse platform [136]. A sample was constructed for the square nozzle, for the 1 mm brass nozzle and for the new 0.4 mm brass nozzle. For the first two nozzles mentioned above, the print configuration of the verification model was used (section 3.6) and for the 0.4 mm brass nozzle, the configurations presented in the calibration step, in section 3.1.1 were used for white PLA.

An Atos Triple Scan (Gom) 3D scanner (16-megapixel camera resolution) was used to survey the shapes of the pieces. The digitized models were overlaid with the CAD model to assess shape and dimensional differences.

(blank page)

4. Results and discussion

Analysis of the results of the calibration cubes:

Case study 1 addressed the influence of thermal conductivity, nozzle service life and analyzed the mechanical properties and porosity of the parts produced. The analysis of the structural issue was measured through the mechanical responses to flexural test, the level of porosity (φcube), and density (ρcube) of elements manufactured under different parametric conditions, materials, and lifespan.

The synthesis of results of dimensional analysis and of measurement of the mass of the cubes is presented in Table 15.

Table 15 – Results of dimensional analysis and cube mass measurement.

	Dimensional analysis		**Mass measurement**	
Direction	*Avg. dimension (mm)*	*CV (%)*	*Avg. Mass (g)*	**CV (%)**
X	14.88 ± 0.03	0.10		
Y	14.91 ± 0.01	0.10	3.95 ± 0.01	0.00
Z	15.09 ± 0.03	0.11		

Note: coefficient of variation (CV), average (Avg.)

After dimensional analysis, mass, and visual analysis, it was found that the five cubes were sufficient for correct calibration of the process, verifying a low variation in the three main dimensions (XYZ) of the cubes, as well as in the mass. As previously mentioned, the parameters described in Castro's thesis were used. [112], as there was good repeatability, it was not necessary to change or adjust the parameters.

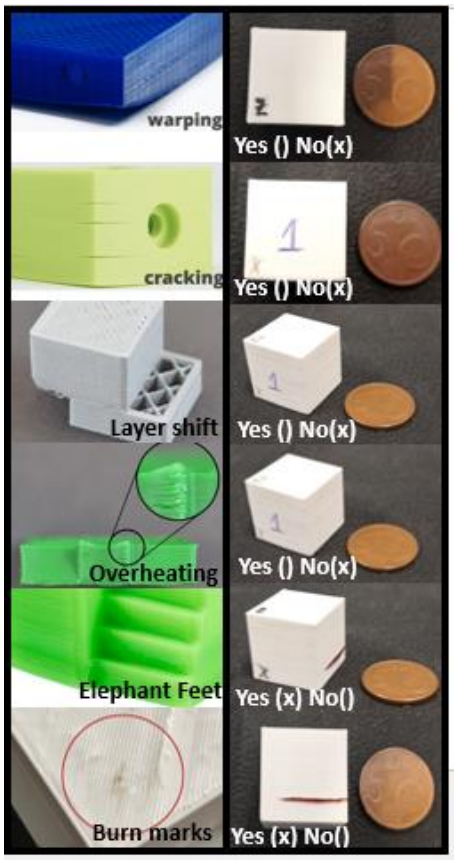

Figure 53- Comparison between printed cubes and possible defects likely to exist, adapted from [106], [137].

4.1 Case study 1

Through Analysis of Variance (ANOVA, α=95%), it was found that in the “on the plane” condition, the use of different nozzles — in this case, brass (with a long printing history), hardened steel and vanadium — significantly affected the maximum flexural strength (MFS) ($F(2,14) = 190.02$, $p = 0.00$) and flexural modulus (FM) ($F(2,14) = 62.52$, $p = 0.00$). A Tukey test was performed to identify the differences between the means of the three levels of the “nozzle type” factor in the variation of MFS and FM — Figure 54 (a) and (b), respectively. Different letters in the yellow bars, Figure 54, indicate different means.

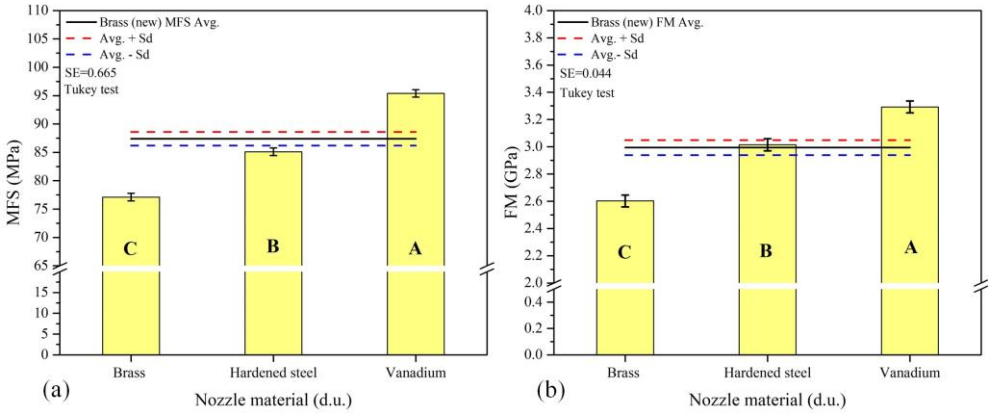

Figure 54- Average maximum flexural strength (a) and flexural modulus (b) for “on the plane” build orientation. Bars with the same letters correspond to equal means by Tukey’s test.

The basic principle of FFF structures formation is based on the supply of thermal energy for the extrusion of the building material and for the extruded filament to provide bonding to the previous layers. The higher and more stable this energy level, the more efficient the mechanisms responsible for the neck growth between the deposited filaments intra- and inter-layers and, consequently, the greater the mechanical strength of the printed parts. According to Ferretti et al. [31], the heat transfer from the hot zone of the extrusion system to the material to be processed depends on the thermal resistance of the nozzle. Therefore, a nozzle with lower thermal resistance, or higher thermal conductivity, provides more energy for processing the thermoplastic.

Based on the concept described above, it would be more logical for the brass nozzle to promote the best results for MSF and FM, since it has a higher thermal conductivity —120 W/mK (Tichý et al.,[138]) — than steel — 23 W/mK (Ferretti et al.,[31]) — and vanadium steels — 28 W/mK, reference value for an AISI M2 steel with 1.75-2.20 (wt%) vanadium (Wilson, [139]). However, the scenario observed in Figure 54 shows that the MFS (77.11 ± 1.47 MPa) and FM (2.60 ± 0.10 GPa) results obtained with the long-used brass nozzle are approximately 19% and 20% lower than those obtained with the Vanadium™ nozzle.

The performance loss verified in the brass nozzle may be related to the natural wear of the component, which may have caused damage to its geometry and initial dimensions (diameter and output channel size) from the previous printing runs. Such damage can be caused by the loss of material due to friction with the print bed or by

pressures generated by the polymer mass inside the nozzle or in the contact between layers.

Structural changes in the nozzle can affect the material flow and the mechanisms of polymer deformation in the extrusion die, thus having consequences on the dimensional and shape continuity of the deposited filaments. Variations in the morphology of the deposited filaments lead to the formation of random voids in the union zones, as well as the formation of weak bonds between neighboring filaments.

In addition, a considerable concentration of residual material adhered to the external walls of the nozzle was observed, a behavior that, most likely, should occur on the internal surfaces of the extrusion channel over time, Figure 55. These residues, in the printing cycles, undergo a process of thermal degradation. The degraded material can be transferred to the parts during printing, promoting the formation of failure points in the joints between deposited filaments.

Figure 55- Old brass nozzle 0.4 mm.

The Vanadium™ nozzle, according to its manufacturer, has a repellent surface coating that prevents the accumulation of plastic residue, leaving the nozzle cleaner (Slice Engineering, [140]). This differential factor may have contributed to the better mechanical properties of the parts printed with this nozzle in the “on the plane” condition, compared to those obtained with the hardened steel nozzle (MSF= 85.10 ± 2.05 MPa; FM= 3.01 ± 0.14 GPa) and, including a new brass nozzle (MSF= 87.39 ± 1.23 MPa; FM= 2.98 ± 0.07 GPa) —Figure 54 (a) and (b), black line (average values) and blue and red lines (positive and negative standard deviation, respectively).

The “on the plane” condition also allows the heat conducted by the printer bed to act for a longer time on the manufactured layers, guaranteeing energy and mobility for the polymer in the sintering process of the bonding lines between filaments and for the PLA crystallization process to occur more slowly and effectively. Bed temperature has been proven to help overcome the thermal limitations of hardened steel and

Vanadium™ nozzles. In addition, the use of a raster angle of 45°/-45° leads to the deposition of small vectors, that is, filaments with shorter path lengths within the layers due to the dimensions of the flexural samples. Such strategy decreases time between depositions and increases the thermal energy use by the extruded material from the nozzle and bed temperatures. In this favorable environment, the low thermal conductivity of the nozzle can be advantageous, because when printing blocks of six samples, there is less energy dissipation in the empty transitions between parts.

However, it should be noted that PLA is a polymer with low melting (when semi-crystalline) and glass transition temperatures (thermal reference in which the layers must be for adhesion formation between them). Additionally, the PLA used may still have good fluidity at low extrusion temperatures. This set of good thermal and rheological properties may have contributed to the good performance of the hardened steel and Vanadium™ nozzles in the “on the plane” condition.

The lateral building orientation requires a greater influence of the nozzle temperature to drive the bonds between and within the layers. This happens because of the distance, as the parts “grow” in Z axis, from the layers closest to the top of the printed model to the heat source generated by the heated bed. In this situation, due to the higher thermal conductivity, the brass nozzle should be more efficient than the hardened steel and Vanadium™ nozzles. This behavior is confirmed when analyzing the results of MFS and FM, Figure 56 (a) and (b), obtained with the new brass nozzle.

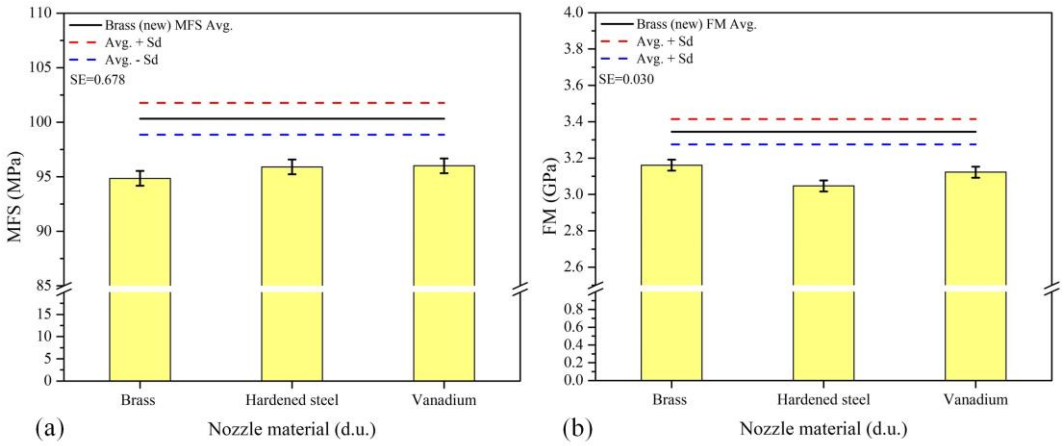

Figure 56- Average maximum flexural strength (a) and flexural modulus (b) for lateral building orientation.

The maximum flexural strength (100.32± 1.45 MPa) of the parts built with the new brass nozzle was about 4% and 5% higher than the values generated by the samples in the Vanadium™ nozzles (96.01± 1.07 MPa) and hardened steel (95.91 ±

2.19 MPa). In the modulus (3.35±0.07 GPa), the percentage differences were 10% and 7% higher than the response of parts manufactured with hardened steel dies (3.05 ± 0.08 GPa) and Vanadium™ (3.12 ± 0.07 GPa).

Considering that the mechanical strength of FFF printed parts is related to meso-structural quality, any increase in the resistance to applied efforts and in the rigidity of the parts is the result of an improvement in the quality of the bonding between filaments, a reduction in the voids density and the proper processing of building material. As this is a study in which the printing parameters were kept fixed and the nozzle material was varied, it is possible to infer that in this condition the thermal conductivity of brass benefited the formation of the internal structure of the manufactured components.

The study with lateral building orientation also confirmed the functional wear of the brass nozzle with a long printing history. The analysis of variance (ANOVA, α=95%) show that the maximum flexural strength (F (2.14) =0.88, p=0.44) and flexural modulus (F (2.14) =3.67, p=0.06) were not affected by the nozzle material —Figure 56 (a) and (b) (yellow bars), respectively. There is statistical equality of the values of MFS (94.86±0.98 MPa) and FM (3.16 ± 0.05 GPa) between the parts made with the worn brass nozzle, the Vanadium™ nozzle, and the hardened steel nozzle ones. This situation opposes the scenario discussed in the previous comparison with the new brass nozzle responses, which were all superior than the ones found for the low thermal conductivity nozzles. Therefore, it is understood that functional wear can also affect the thermal energy deliver to the extruded/deposited.

The cubes for porosity measurement were built with 100% infill, that is, depositing as much material as possible to complete the volume of the part. It should be noted, however, that the parts in this filling configuration will not be massive, as natural voids of the layered structure will be present.

Parts made with a brass nozzle are even more porous (8.26 ± 0.22%) and less dense (1.17 ± 0.01 g/cm³) that those made with hardened steel (φcube = 6.32 ± 0.50% and ρcube= 1.17 ± 0.01 g/cm³) and vanadium (φcube = 5.43± 0.22% and ρcube= 1.21 ± 0.01 g/cm³) nozzles — Figure 57 (a). Through this analysis, lower conductivity materials showed greater stability in the flow of deposited material, which allowed better-connected filaments and smaller voids between and within layers. With the new

brass nozzle, Figure 57 (b), the porosity (5.59 ± 0.10%) and density (1.21± 0.01 g/cm³) values were very close to those verified in the cubes produced with the Vanadium™ nozzle, indicating what may be the natural limit of void density for the porous structures constructed in this study. Therefore, the higher porosity and lower density verified in the parts produced with the long-use brass nozzle confirms the loss of its functional properties.

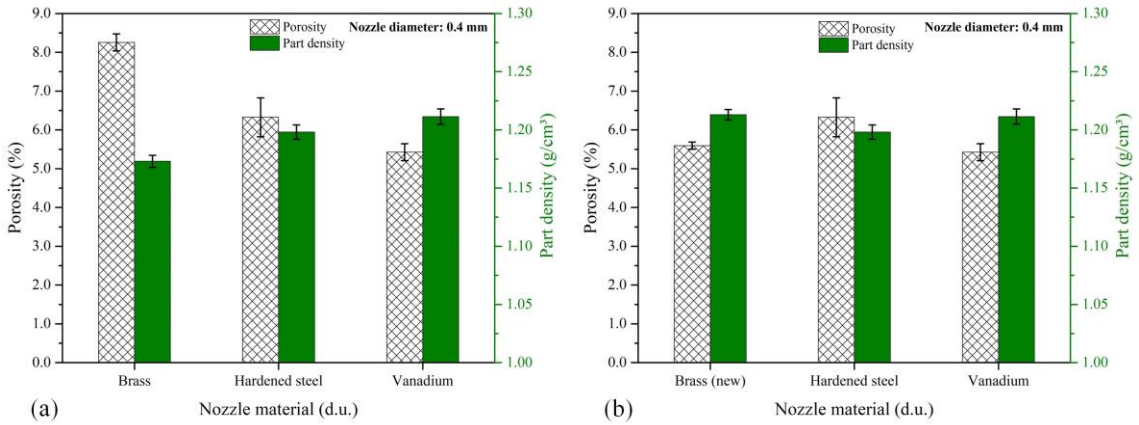

Figure 57 - Porosity and density of cubes as a function of nozzle material: (a) worn brass nozzle and (b) new brass nozzle comparisons.

Analysis for free extrusion with 0.4 mm nozzles in different materials:

With the free extrusion tests comparing the different materials, it is verified that the diameters that are in greater conformity with the original nozzle diameter are brass. If we have a lower temperature and higher speed, we increase the diameter of the extrudate. If we increase the temperature, the diameter of the extrudate decreases.

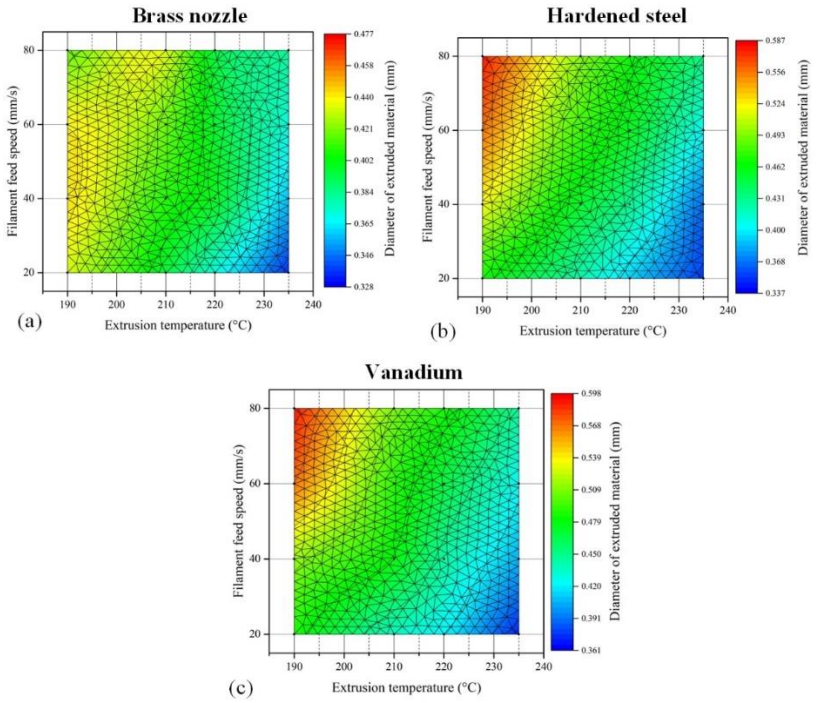

Figure 58- Free extrusion test for: (a) 0,4mm diameter brass nozzle; (b) 0,4mm diameter hardened steel nozzle; (c) 0,4mm diameter vanadium nozzle.

The filaments with the old brass nozzle had a smaller diameter reduction compared to the other nozzles, Figure 58. There is evidence that the thermal conductivity of the material may have been affected. Because nozzles with lower thermal conductivity have greater thinning at high temperatures than brass, which theoretically has higher conductivity.

It will be analyzed, based in Table 16, a comparison between speeds and temperatures, relative to free extrusion tests, based on Scott-Knott tests. The Scott-Knott method uses the likelihood ratio to attest to the significance that treatments can be divided into groups that maximize the semes of squares between groups.

Basically, columns with the same capital letters have the same averages, just as rows with the same lowercase letters also have the same averages.

Analyzing the Table 16, for the 0.4 mm brass nozzle about the temperature of 190ºC, it appears that the speed does not affect the diameter, this being the only case in which the speed does not affect the diameter. For example, in the 210ºC column, for the 0.4 mm brass nozzle, there is an increase in diameter, which may be caused by an increase in shear rates with a greater thermal expansion.

In all lines, when the temperature increases, the diameter decreases, it may be due to the issue of fluidity, which with gravity thins the filament, or the increase in

temperature softens the material too much, causing the filament to flame in the inlet stopping the extrusion flow.

Table 16- Scott-Knott test for different materials.

Scott-Knott (Diameter)				
Brass nozzle 0.4 mm	**190ºC**	**210ºC**	**220ºC**	**235ºC**
20 mm/s	0.432 a A	0.395 b A	0.372 c A	0.337 d A
40 mm/s	0.442 a A	0.408 b A	0.398 b B	0.357 c A
60 mm/s	0.439 a A	0.418 a B	0.397 b B	0.371 c B
80 mm/s	0.418 a A	0.433 a B	0.394 b B	0.381 b B
Stainless Steel nozzle 0.4 mm	**190ºC**	**210ºC**	**220ºC**	**235ºC**
20 mm/s	0.468 a A	0.421 b A	0.392 c A	0.354 d A
40 mm/s	0.520 a B	0.452 b B	0.428 c B	0.367 d A
60 mm/s	0.556 a C	0.477 b C	0.456 c C	0.404 d B
80 mm/s	0.578 a D	0.495 b D	0.467 c C	0.432 d C
Vanadium nozzle 0.4 mm	**190ºC**	**210ºC**	**220ºC**	**235ºC**
20 mm/s	0.487 a A	0.436 b A	0.421 b A	0.372 c A
40 mm/s	0.515 a B	0.478 b B	0.444 c B	0.405 d B
60 mm/s	0.568 a C	0.491 b B	0.465 c C	0.425 d C
80 mm/s	0.589 a D	0.508 b C	0.487 c D	0.446 d D

4.2 Case study 2

Case study 2 addressed the effects of varying nozzle diameter, extrusion width and layer thickness on the formation and quality of the meso-structure of printed parts. The analysis of the structural issue was measured through the mechanical responses to flexural test, the level of porosity (φcube) and density (ρcube) of elements manufactured under different parametric conditions (Table 17). It is noteworthy that the results presented here will also be used to consolidate the hypothesis of functional wear of the 0.4 mm brass nozzle of the first case study.

Table 17 – Results for the analyzes with the 0.6mm and 0.8 mm nozzles, under different conditions.

Conditions	**Nozzle 0.6 mm**			
	MFS (MPa)	*FM (GPa)*	φ_{cube} *(%)*	ρ_{cube} (g/cm³)
Rw (0.4)	105.34 ± 1.04	3.59 ± 0.06	7.44 ± 0.12	1.21 ± 0.00
Rw (0.6)	105.57 ± 0.76	3.53 ± 0.01	3.57 ± 0.16	1.24 ± 0.00
Lt (0.45)	88.44 ± 2.39	2.82 ± 0.11	5.81 ± 0.08	1.21 ± 0.00
Conditions	**Nozzle 0.8 mm**			
Rw (0.4)	89.53 ± 0.75	2.98 ± 0.09	7.34 ± 0.08	1.21 ± 0.00
Rw (0.9)	101.14 ± 1.58	3.30 ± 0.09	6.70 ± 0.12	1.24 ± 0.00
Lt (0.6)	89.61 ± 1.06	2.85 ± 0.06	9.07 ± 0.36	1.21 ± 0.00
Condition	**Nozzle 0.4 mm***			

continues

Rw (0.4)	**94.86 ± 0.98**	**3.16 ± 0.05**	**8.26 ± 0.22**	**1.17 ± 0.01**

Note: * values obtained with 0.4 mm nozzle with long print history. Results for the laterally aligned condition.

In Table 17 it is possible to see the results referring to the MFS and FM, as well as the porosity and density, for the three nozzles used in this case study.

The effects of the nozzle diameter on the printing of parts with extrusion width calculated specifically for the 0.4 mm nozzle will be analyzed. According to the analysis of variance, the maximum flexural strength (F (2.12) =373.48, p=0.000) and the flexural modulus (F (2.12) =106.01, p=0.000) — are shown in Figure 59 (a) e (b), respectively — were significantly affected by the nozzle diameter in the Rw (0.4) print condition.

Analyzing the graphs, the 0.6 mm nozzle presents the best result, followed by the 0.4 mm nozzle and finally the 0.8 mm nozzle. Although the 0.4 mm nozzle has been printed with a width specially adjusted for it, it has worse mechanical properties than the 0.6mm nozzle, most likely because it is worn out. The 0.6 mm nozzle, despite not having a width adjusted especially for it, still manages to provide sufficient levels of thermal energy to promote binding energy and mobility for the material to flow in the layers and compensate for the nozzle diameter variation. It is also interpreted that there is an acceptable limit regarding the issue of manufacturing a width smaller than the nozzle diameter. This means that up to 0.6 mm in diameter it is still possible to form a stable structure with a width of 0.4 mm, but the difference between the nozzle and the width is 50%, it already loses capacity, as can be seen from the results of the 0.8 mm nozzle.

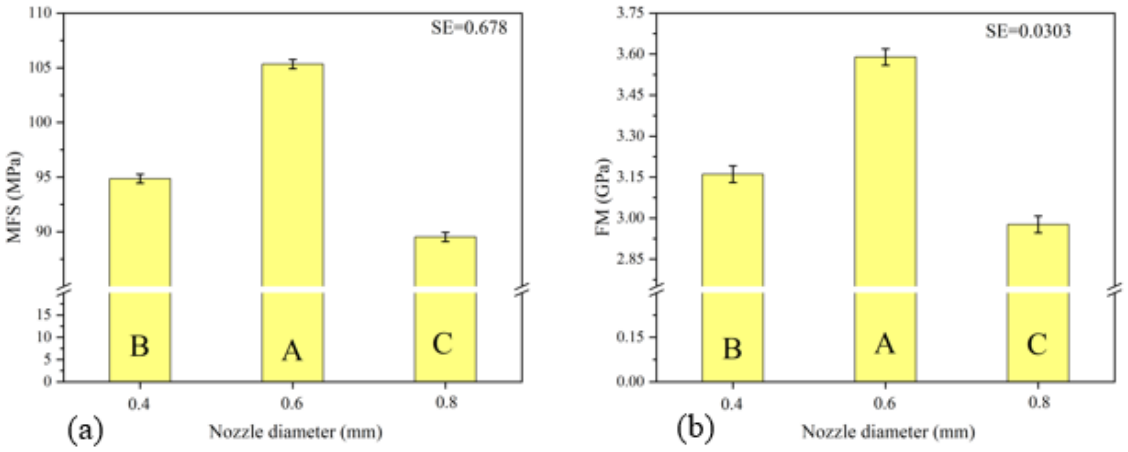

Figure 59-ANOVA results for: (a) MFS 0.4 mm; 0.6 mm; 0.8 mm nozzle and (b) FM 0.4 mm; 0.6 mm; 0.8 mm nozzle.

Comparing the 0.4 mm and 0.6 mm nozzles with respect to the MFS and FM it appears that the 0.4 mm nozzle, in theory, would be the best as it would have the benefit of building structures with higher resolution, but in this case, this is not what is happening. Using the data in the table, it is found that:

MFS (Rw(0.4), bico 0.6 mm)= 105.34

MFS (Rw (0.4), bico 0.4 mm) = 94.86

((105.34/94.86)-1)*100= 11%

The 0.6 mm nozzle allowed the construction of parts with maximum flexural strengths 11% greater than what was found in the 0.4 mm nozzle.

The fact that the 0.4 mm nozzle had a worse performance than the 0.6 mm nozzle, even in this case the 0.6 mm nozzle being forced to make a road width smaller than its diameter, is yet another indication that this nozzle has suffered damage from previous print runs. Wear can interrupt the flow and also because the nozzle has had a previous use, it could be that it was dirty, thus interfering with the conduction of temperature. The presence of residual material can lead degraded polymer to the interior of the layer, interfering and modifying the quality of the printed parts.

It was also noticed that the 0.8 mm nozzle gave the worst results as it increases the void density which worsens the mechanical properties. Mainly since we force the nozzle to make a width 50% smaller than its diameter. Flow instabilities, material thinning adhesion between and within layers may have been impaired.

The ANOVA analysis for the case of the 0.6 mm nozzle focused on studying the effects of the variation in the geometry of the deposited filaments, as a function of changes in road width and thickness on the mechanical properties.

Analysis of variance (ANOVA, α=95%) shows that the maximum flexural strength (F (2,12) =196.73, p=0,000) and the flexural module (F (2,12) =176.71, p=0,000), Figure 60, were influenced by meso-structural modification.

For the 0.6 mm nozzle the worst results were for Lt (0.45) condition, since as the layer thickness increased, the voids also increased. In addition to increasing the density of voids, it also reduces the contact between the filaments deposited between and within the layers, that influences the mechanisms of synthesis, molecular diffusion and randomization with neck growth and reducing adhesion and its mechanical properties.

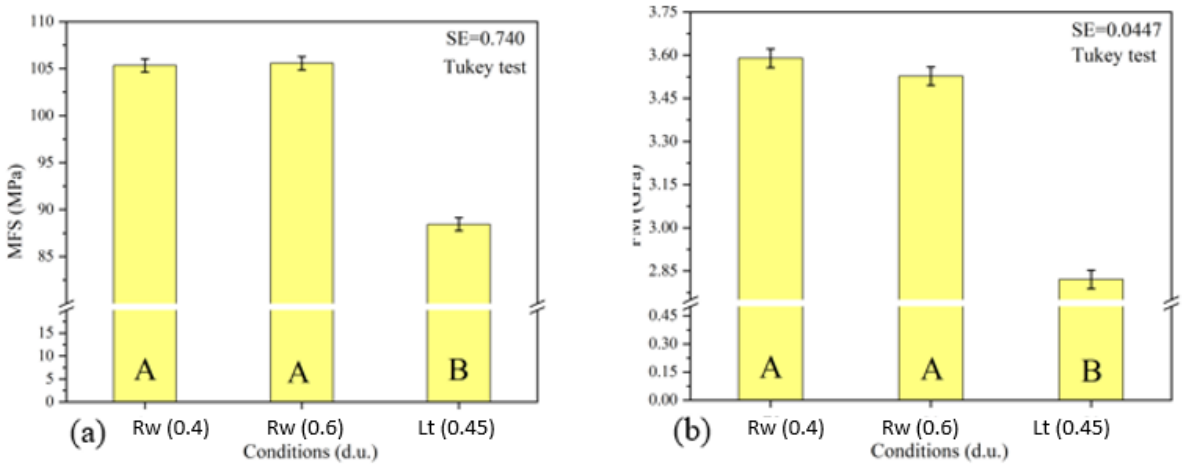

Figure 60-ANOVA results for: (a) MFS 0,6 nozzle and (b) FM 0.6 nozzle.

Analysis of variance (ANOVA, α=95%) for the 0.8 mm brass nozzle shows that the maximum flexural strength (F(2.12)=223.305, p=0.000) and the flexural modulus (F(2) ,12) =39.18, p=0.000), shown in Figure 61 a) and b) respectively, were influenced by the road width and layer thickness. It is verified that the best condition was for a road width of Rw (0.8), and both the road width of Rw (0.4) and the layer thickness Lt (0.6) had the same results, being the worst conditions. The worst conditions (Rw(0.4) and Lt(0.6)) favored the formation of voids in the printed parts, favoring the appearance of voids, thus worsening the mechanical properties.

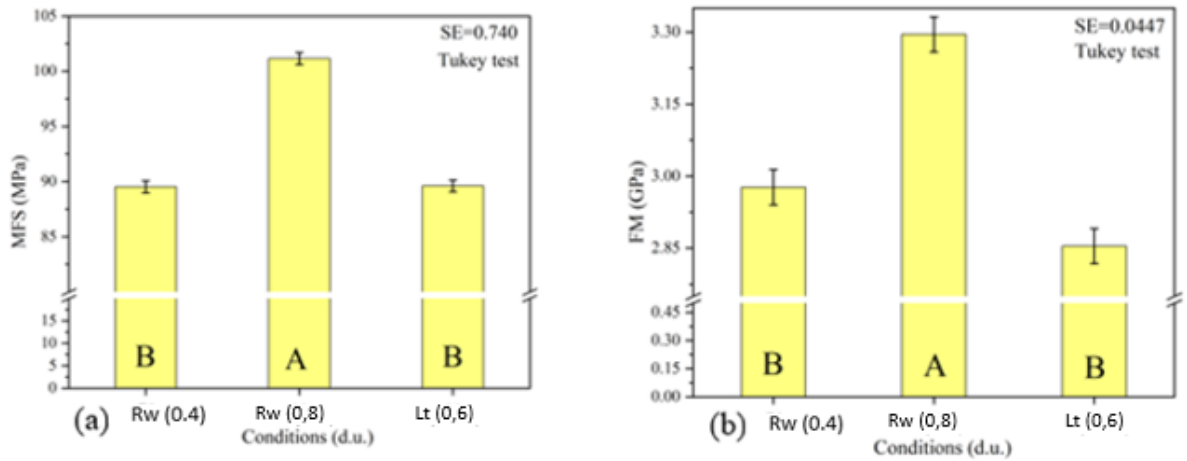

Figure 61-ANOVA results for: (a) MFS 0.8 nozzle and (b) FM 0.8 nozzle.

It will be analyzed the results of the free extrusion tests for brass nozzles with different diameters. The results are presented in Figure 62.

With the free extrusion tests (Figure 62) it is verified that the 0.4 mm nozzle is the nozzle that originates filaments closest to its nominal diameter, and the 0.8 mm brass nozzle is the one that originates values farthest from its nominal value. These results may be related to the fact that nozzles with larger diameters, will need a higher temperature so that the entire filament is at the same temperature and flows correctly.

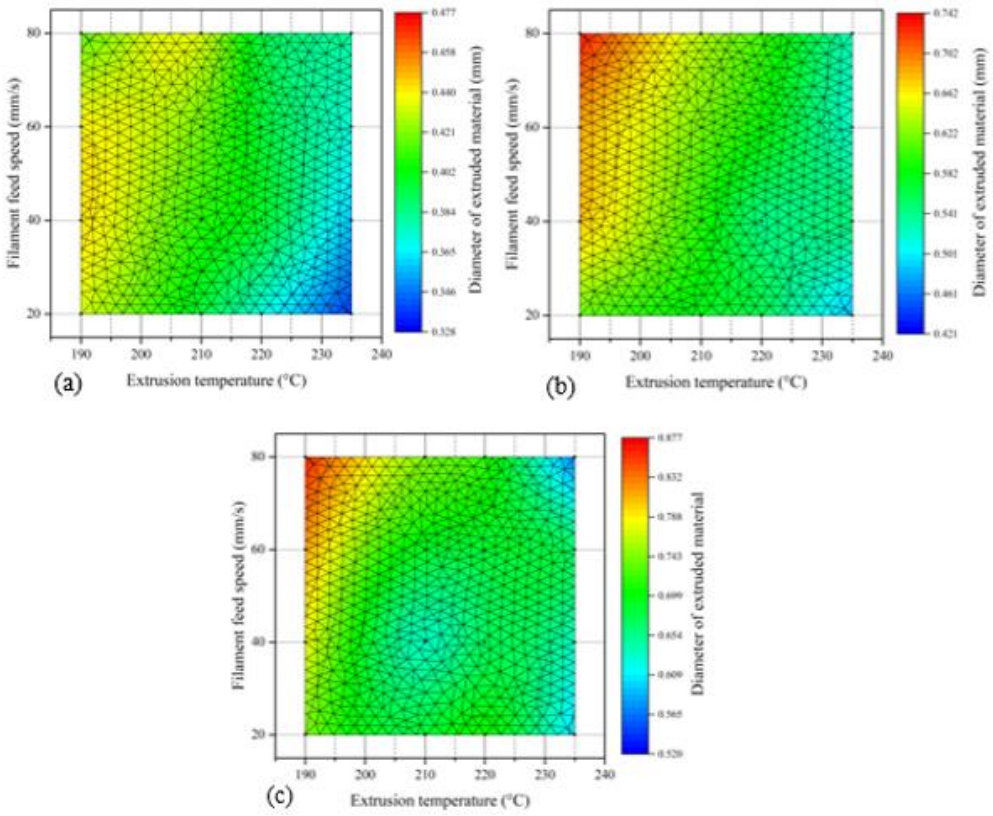

Figure 62-Free extrusion test for: (a) 0,4mm diameter brass nozzle; (b) 0,6mm diameter brass nozzle; (c) 0,8mm diameter brass nozzle.

It will be analyzed based in Table 18, a comparison of speeds and temperatures, relative to free extrusion tests, based on Scott-Knott tests for different nozzle diameters.

Based on the table, either for a temperature of 190ºC, for the 0.4 mm brass nozzle, or a temperature of 220ºC, for the 0.8 mm brass nozzle, the speeds did not affect the nozzle diameter, since, for all other columns, the same is not true. In all lines, when the speed is increased to a certain speed, a decrease in the extruded diameter is observed.

Table 18-Scott-Knott test for different diameters.

Scott-Knott (Diameter)				
Brass nozzle 0.4 mm	**190ºC**	**210ºC**	**220ºC**	**235ºC**
20 mm/s	0.432 a A	0.395 b A	0.372 c A	0.337 d A
40 mm/s	0.442 a A	0.408 b A	0.398 b B	0.357 c A
60 mm/s	0.439 a A	0.418 a B	0.397 b B	0.371 c B
80 mm/s	0.418 a A	0.433 a B	0.394 b B	0.381 b B
Brass nozzle 0.6 mm	**190ºC**	**210ºC**	**220ºC**	**235ºC**
20 mm/s	0.615 a A	0.576 b A	0.558 b A	0.480 c A
40 mm/s	0.677 a B	0.595 b A	0.545 c A	0.543 d B
60 mm/s	0.686 a B	0.618 b B	0.585 c B	0.521 d B
80 mm/s	0.731 a D	0.639 b B	0.604 b B	0.527 c B
Brass nozzle 0.8 mm	**190ºC**	**210ºC**	**220ºC**	**235ºC**
20 mm/s	0.743 a A	0.684 b A	0.708 a A	0.601 b A
40 mm/s	0.780 a A	0.636 b A	0.671 b A	0.634 b B
60 mm/s	0.818 a B	0.689 b A	0.686 b A	0.664 b B
80 mm/s	0.862 a B	0.734 b B	0.715 b A	0.567 c A

Next, the results of the porosity and density test for the different nozzle diameters will be analyzed. For the 0.6 mm nozzle it is more porous when we have a width of Rw(0.4) and the smallest porosity is achieved when the values are adjusted for the nozzle diameter, as shown in Figure 63. For the 0.8 mm nozzle it is more porous when we have a layer thickness of 0.6 mm and the smallest porosity is achieved when the road width is 0.8 mm. As expected by increasing the layer thickness we increased the porosity as the voids increase.

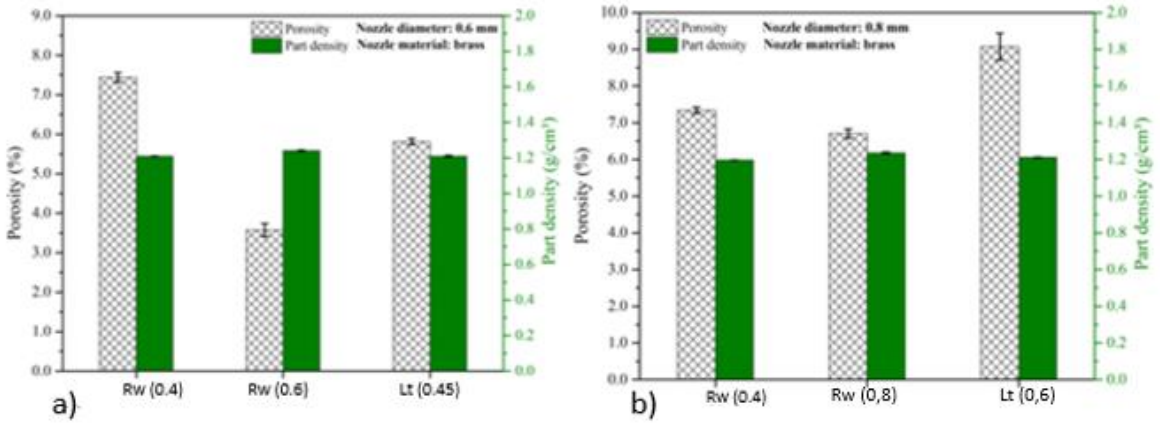

Figure 63- (a) Porosity nozzle brass 0,6 mm; (b) Porosity nozzle brass 0,8 mm.

It was proven that forcing the nozzle to make a width smaller that its diameter increases the voids, which is also seed with the increase in layer thickness, even when adjusting the width compatible with the nozzle.

The best scenario therefore is to reduce the thickness and match the width to the nozzle diameter.

4.3 Case study 3

Case study 3 addressed the effects of the variation of the nozzle geometry, in this case, square, on the formation and quality of the meso-structure of the printed parts. The analysis of the structural issue was measured through the mechanical responses to bending, the level of porosity (φcube), and density (ρcube) of elements manufactured under different parametric conditions.

Analysis of variance (ANOVA, α=95%) shows that the results for the layer thickness is MFS (F(3.38)=12.88, p=0.000). The ANOVA for temperature is MFS (F(3.38)=7.72, p=0.000). For volumetric rate the ANOVA is MFS (F(3.38)=10.40, p=0.000). All results were significant (Figure 66), that is, the maximum flexural strength value depends on these three factors: thickness, volumetric speed, and temperature.

Likewise, the results for the flexural modulus — FM (F (3.38) =9.09, p=0.000) for the layer thickness, FM (F (3.38) =7.02, p= 0.001) for temperature and FM (F (3.38) =5.84, p=0.002) for maximum volumetric speed — shown in (Figure 68), also showed significant results, so the flexural modulus is dependent of these three parameters that were modified throughout the experiments.

Analyzing the results of the flexural module (Figure 64) it was found that the best results for layer thickness were for levels 1 and 2, that is, using a thickness of 0.4 mm or 0.2 mm the answer will be the same. On the other hand, the module will also decrease if 0.6 mm or 0.8 mm thicknesses are used. In general, with smaller layer thicknesses, a better result is achieved, while with greater thicknesses, a worse result is obtained as it forces the nozzle to deliver more material than expected. This can lead to clogging of the nozzle itself, worsening mechanical properties. Although the thicknesses of 0.4 mm and 0.2 mm gave the same result, a layer thickness of 0.2 mm was chosen for the verification model since, according to the literature, smaller layer thicknesses lead to better results, as we improve the mechanical properties and the contact area between and within the layers. However, these literature studies are for circular and cylindrical nozzles, so for a square nozzle, as is the case may not be true.

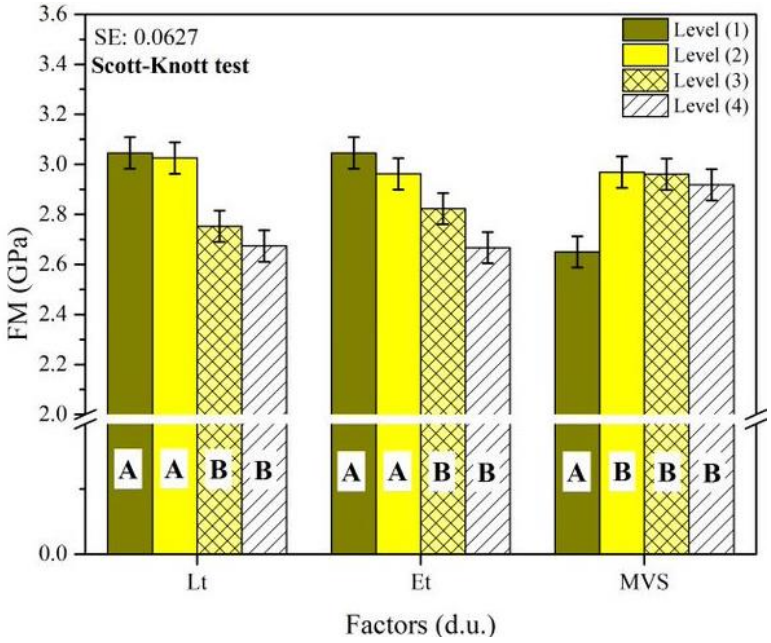

Figure 64- Average flexural modulus for differents levels.

Regarding the temperature for the flexural modulus results, level 1 and level 2 are also equal, which correspond to temperatures of 215ºC and 225ºC and present the best results. Levels 3 and 4 of extrusion temperature, corresponding to the values of 235ºC and 245ºC, generated the worst results, and their averages were also the same. It is known that by increasing the nozzle temperature too much (more than the recommended temperature), it will affect the fluidity of the material and in the case of levels 3 and 4 the material could be degrading inside the nozzle, thus not obtaining the expected mechanical properties.

The temperature of 215ºC was chosen for the verification model, as it is also the temperature recommended by the literature [14], [112], in addition to that for higher temperatures (235ºC and 245ºC) there was a tendency of degradation, therefore, if a combination with other parameters is forced, even more degradation may occur.

Speaking of the volumetric speed still for the flexural modulus, only level 1, corresponding to a volumetric speed of 3 mm^3/s, differs from the other levels. Such low volumetric speeds are only advisable for materials with very high fluidity. According to [133], the recommended volumetric velocity for the PLA is 15 mm^3/s, which is actually one of the levels that obtained a better result, and therefore this value was chosen for the verification model.

Regarding the results of the MFS (Figure 65) these were very similar to those seen previously on FM and that goes as expected. The only case that varies and

contradicts the previous results is the temperature value, but it may be related to the position of the base, which in this case may have compensated for the behavior of the material modification, thus affecting the statistics.

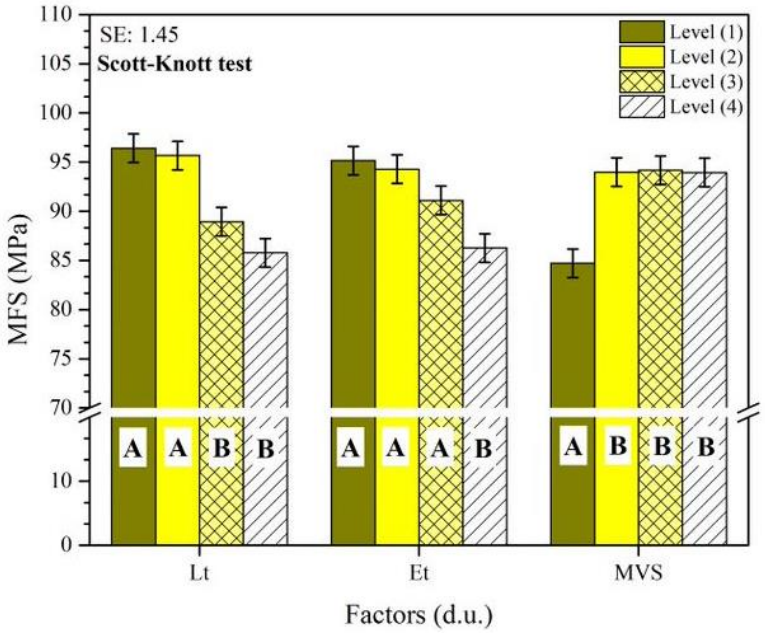

Figure 65- Average maximum flexural strength for different levels.

Based on the results of both the FM and the MFS, the parameters chosen for the verification model have already been explained previously throughout the analysis of results and are as follows:

- Layer thickness: 0.2 mm;
- Temperature: 215 ºC;
- Maximum volumetric speed: 15mm³/s.

These parameters chosen for the verification model were used to test other PLA of different colors and suppliers to verify their mechanical properties, porosity, and density.

The results will now be interpreted regarding the MFS and FM of different materials. The materials will be: red PLA from Filament PM™, red PLA from Fil3D™, and transparent PLA from Filament PM™. These PLA will be compared with the white PLA from Filament PM™.

Through analysis of variance (α = 95%), it was found that in the square nozzle the different PLAs showed a significant difference for their mechanical responses — MFS(F(3.16)=20.47, P=0.000) and FM(F(3.16)=7.414, P=0.0025), FM(F(3.16)=7.41,

P=0.002)—that is, the mechanical properties are being influenced by the media. Complementing the ANOVA, the means for each color of PLA were compared with each other, by Tukey's test, to verify the presence of differences and equality. (Figure 66).

It was found that the white PLA is the only one that gives a different result compared to the other 3 PLAs. The different PLAs were processed at the same temperature and nozzle, so the lower mechanical properties of white PLA may be related to a thermal degradation effect at low extrusion temperatures. The nozzle, due to its geometry and/or composition, may have led to a change in the thermal conditions, causing a degradation effect, or also, it may have affected the rheological behavior of different materials, affecting the shear rates. This result contradicts the study by Castro [112], that using the same materials for a 0.4 mm brass nozzle, found that the white PLA showed better results than the red PLA.

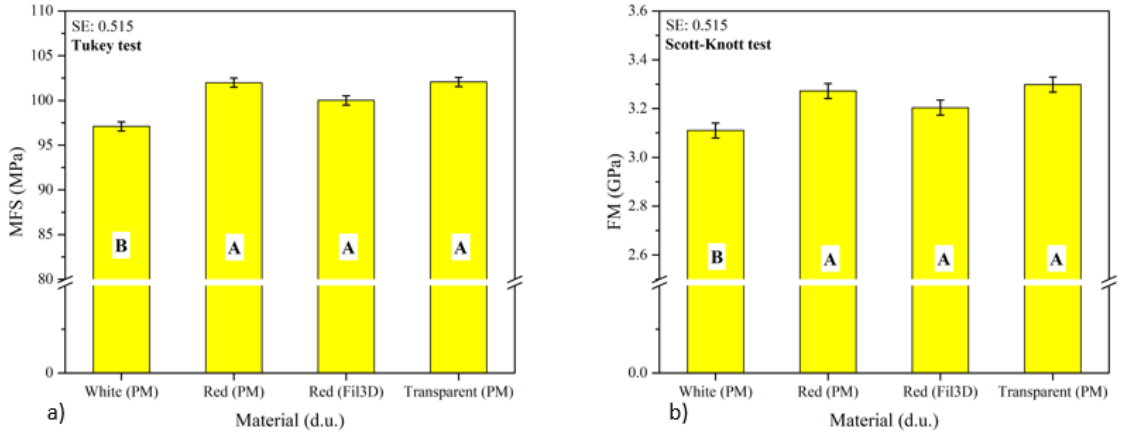

Figure 66- ANOVA results for: (a) MFS 1x1 nozzle with different material and (b) FM 1x1 nozzle with different material.

Regarding free extrusion tests (Figure 67), it appears that in the square nozzle it was able to extrude material, at higher temperatures and higher extrusion speeds, closer to its dimensions (1x1 mm).

Comparing the free extrusion results between the square nozzle and the circular nozzle, it may be that in the square nozzle, the material is coming out colder than in the cylindrical nozzle, hence the difference between the diameter of the samples.

A study by Alhijjaj et al. [141], in which they evaluate the optimization of the printing process to obtain a better precision and quality of the printed parts at a

pharmaceutical level, through the polycaprolactone material, states that the thickness of 3D printed objects tends to decrease with an increase in temperature, as verified in the results: with higher temperatures, the diameter of the filament is smaller, both for the square nozzle and for the circular nozzle.

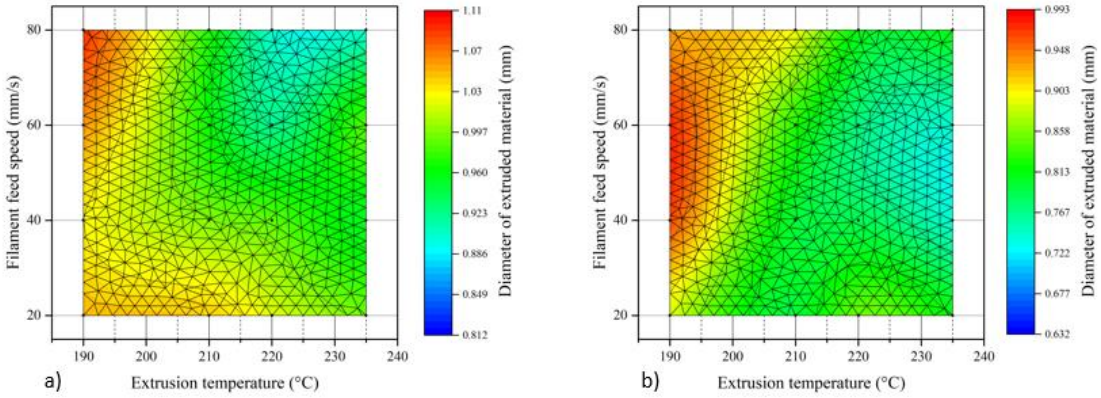

Figure 67- Free extrusion test for: (a) 1x1mm nozzle; (b) 1mm diameter brass nozzle.

To analyze the square nozzle with the 1 mm circular brass nozzle, a T-test was performed to verify if the averages of MFS and FM were different between the nozzles, as seen in Table 19.

Table 19- T-test results for different nozzles.

Nozzle	N	Mean	StDev	SE Mean
Squared nozzle (FM)	5	3.1101	0.0984	0.044
Brass nozzle (FM)	5	3.3794	0.0794	0.036
Squared nozzle (MFS)	5	97.10	1.50	0.67
Brass nozzle (MFS)	5	102.254	0.751	0.34

In the graphics, in Figure 68, shows that the standard deviations do not intersect and therefore the averages are different, with the brass nozzle being higher than the square nozzle, in terms of both MFS and FM. The p-value was less than 0.05, so the nozzle shape influenced the results. The square nozzle, being made of tungsten carbide, has a worse thermal conductivity compared to brass and it has also been verified that the PLA could be degrading due to high temperatures, so the combination of these two factors may have led to a decrease in the mechanical properties of this nozzle.

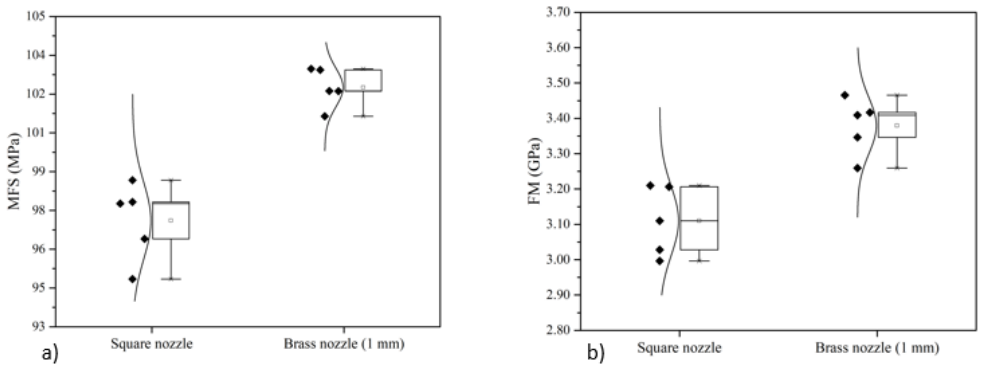

Figure 68- Results for: (a) MFS 1x1 nozzle and for Brass nozzle 1 mm and (b) FM 1x1 mm nozzle and for Brass nozzle 1 mm.

Regarding the analysis of porosity and density, Figure 69, comparing the two nozzles, it appears that there were very few differences between them. If it is compared, for example, with the, it is verified that with these nozzles, lower porosities and higher densities were obtained compared to the best nozzle of the same results. This is as expected, since the nozzle has larger dimensions, the layer width will also be greater, filling the voids better and making the part denser and less porous. According to Papon *et al.* [100], whose studies were based on nozzles with different geometries, found that by controlling the nozzle contact angle with the table, the bead spreading can be improved by reducing voids between layers which would eventually improve the mechanical properties, we can apply these conclusions both in cylindrical geometry as square as the mechanical properties are strongly related to the width of the layer as it is approached.

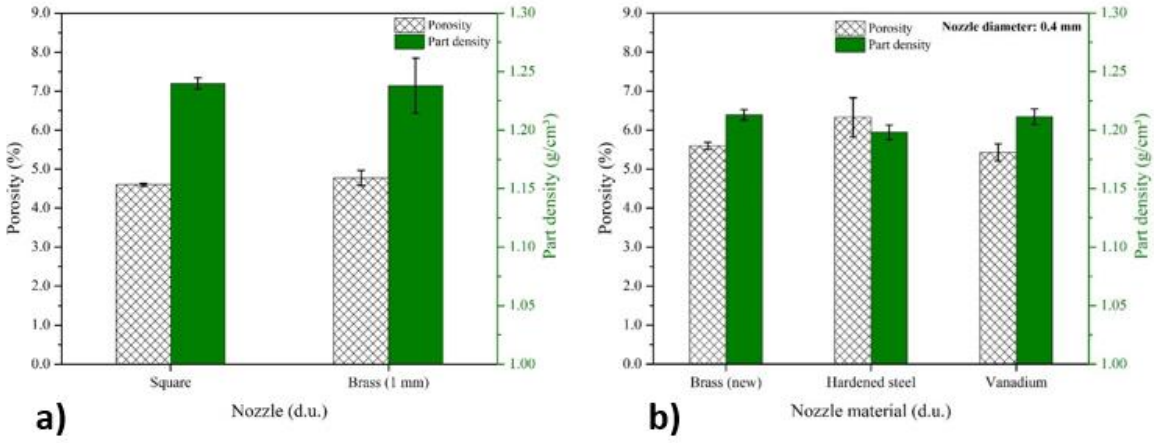

Figure 69- a) Porosity of squared nozzle and 1 mm brass nozzle; b) Porosity and density of cubes as a function of nozzle material, study with the new brass nozzle.

4.4 Scanning study of the Benchy model

4.4.1 New brass nozzle 0.4 mm

We will now analyze the results of the Benchy model, for the new 0.4mm brass nozzle, presented in Figure 70.

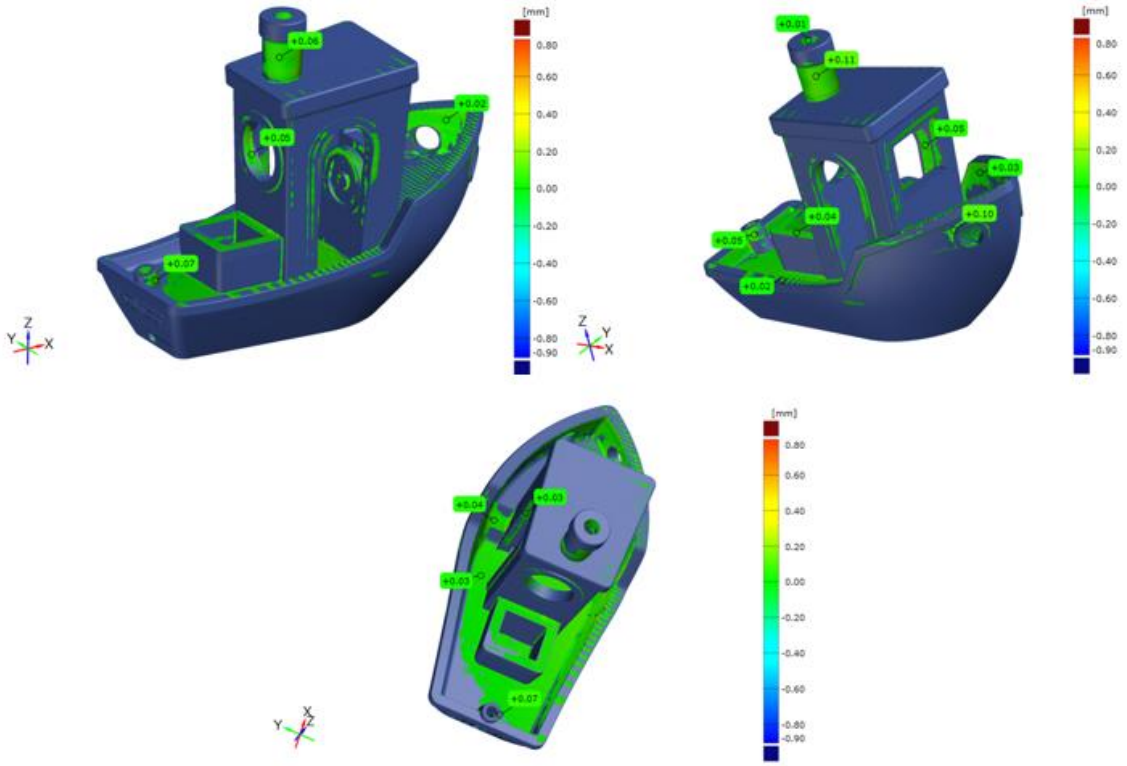

Figure 70- Results of different views of the Benchy model for the 0.4 mm brass nozzle.

The results were based on scanning the printed model with the original 3D CAD overlay (blue color). In the case of this nozzle, it appears that there were not many differences between the two models. The largest dimensional differences occurring in the chimney, which was one of the most demanding constituents, as well as on the floor of the boat, on the inside of the hull and there was still a ladder effect in the sloping areas of the edges.

The Benchy model for the 1 mm nozzles and for the square nozzle will now be analyzed.

Starting with the 1 mm nozzle (Figure 71) it appears that it has a lot of geometric and dimensional inaccuracies on the chimney, the floor of the boat, the interior of the hull, and on the walls of the deck, with irregular surfaces in some areas. The defects are like those shown in the Figure 70, but the values are higher, which means there was more discrepancy between the printed model and CAD model.

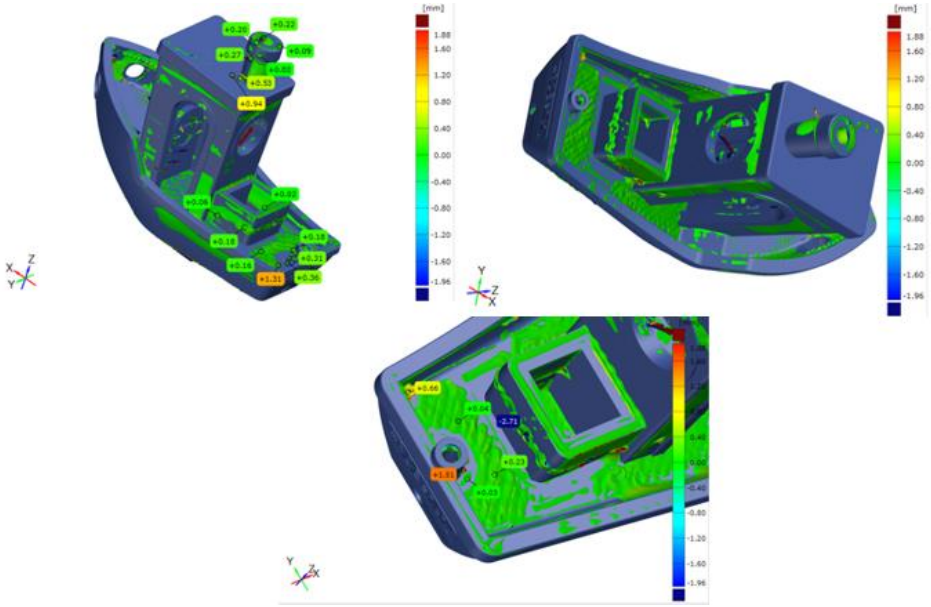

Figure 71- Calibration test results, by the Benchy method, with different perspectives for the 1 mm nozzle.

Now for the square nose (Figure 72), the defects were very similar to the 1mm nozzle, showing worse dimensional accuracy on the outside of the hull. Once again, Hsiang Loh *et al*. [142] consider that over extrusion affects both the dimensional accuracy and the aesthetics of the printed object.

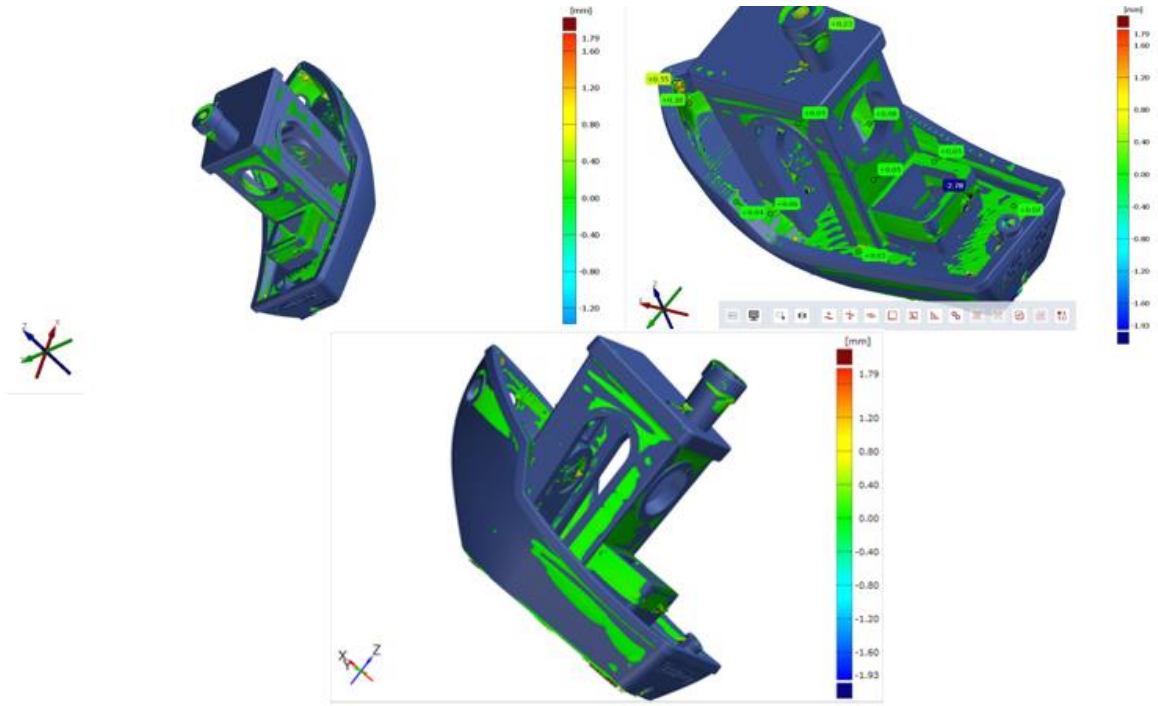

Figure 72- Results of the calibration test, by the Benchy method, with different perspectives for the square nozzle.

5. Conclusions and future work

Brass nozzles are susceptible to functional wear. A previously used 0.4 mm brass nozzle did not behave according to theoretical thinking, that is, with better thermal conductivity there would be better adhesion between and within the layers and, therefore, greater mechanical strength and less porosity. So, users should be warned about the period of good nozzle performance because we concluded that the nozzles have a service life. In addition, the printing of unidirectional filaments, even in situations where the nozzle had lower thermal conductivity, generated better mechanical properties, respecting the assumptions of the load distribution relationship on the deposited filaments and not on the adhesion lines between and inside of the layers. However, it is noteworthy that the design for 3D manufacturing must consider construction guidelines that favor as much as possible the conduction of heat from the base to the layers, including in unidirectional deposition conditions, since the steel nozzle had its response enhanced, compared to the others, in the flat condition with filaments at 45°/-45°. The PLA used in this study has good fluidity at low thermal level, which may have affected the thermal conductivity analysis of the nozzles. Future studies should test printing materials that require a higher extrusion temperature and with less fluidity at low temperatures.

The 0.6 mm hardened steel and brass nozzles were the ones that provided the best results for the response evaluated in their respective stages. However, as it is known the 0.4 mm brass nozzle may have been harmed due to its natural wear due to long printing journeys. With this study, it was concluded that when choosing a printer nozzle, the user must consider the component’s useful life, the stability of its deposition as well as its printing quality repeatability.

Concerning the squared nozzle, the results showed that the mechanical properties, modulus, and maximum flexural stress, of the samples printed with the square nozzle were slightly lower than those obtained with the cylindrical. The porosity levels were equivalent in both nozzles, indicating a similar meso-structural organization, in relation to voids. Both group of samples showed deviations of close shapes, showing, therefore, similar levels of resolution. The lower mechanical properties obtained with the square nozzle may be related to its influence on shear behavior and heat transfer to the material to be extruded. In addition, controlling the square cavity alignment with the printing platform's X and Y axes was not

straightforward, which may have affected the geometric orientation of the extrudate during deposition. The mentioned issues may have affected adhesion strength of the filaments inter- and intra-layers. New studies should be carried out to optimize the square nozzle assembly process, extrusion pressure control and thermal energy supply.

6. References

[1] L. Santana, J. Lino Alves, e A. da Costa Sabino Netto, «A study of parametric calibration for low cost 3D printing: Seeking improvement in dimensional quality», *Materials & Design*, vol. 135, pp. 159–172, dez. 2017, doi: 10.1016/j.matdes.2017.09.020.

[2] L. Santana, J. L. Alves, A. da C. Sabino Netto, e C. Merlini, «Estudo comparativo entre PETG e PLA para Impressão 3D através de caracterização térmica, química e mecânica», *Matéria (Rio J.)*, vol. 23, n. 4, dez. 2018, doi: 10.1590/s1517-707620180004.0601.

[3] C. Li, W. Cheng, e J. Hu, «Nozzle Problem Analysis and Optimization of FDM 3D Printer»:, apresentado na 2017 7th International Conference on Mechatronics, Computer and Education Informationization (MCEI 2017), Shenyang, China, 2017. doi: 10.2991/mcei-17.2017.59.

[4] R. Jerez-Mesa, G. Gomez-Gras, J. A. Travieso-Rodriguez, e V. Garcia-Plana, «A comparative study of the thermal behavior of three different 3D printer liquefiers», *Mechatronics*, vol. 56, pp. 297–305, dez. 2018, doi: 10.1016/j.mechatronics.2017.06.008.

[5] J. Triyono, H. Sukanto, R. M. Saputra, e D. F. Smaradhana, «The effect of nozzle hole diameter of 3D printing on porosity and tensile strength parts using polylactic acid material», *Open Engineering*, vol. 10, n. 1, pp. 762–768, ago. 2020, doi: 10.1515/eng-2020-0083.

[6] T. Tezel e V. Kovan, «Determination of optimum production parameters for 3D printers based on nozzle diameter», *RPJ*, vol. ahead-of-print, n. ahead-of-print, set. 2021, doi: 10.1108/RPJ-08-2020-0185.

[7] N. A. Sukindar, M. K. A. Ariffin, B. T. H. T. Baharudin, C. N. A. Jaafar, e M. I. S. Ismail, «ANALYZING THE EFFECT OF NOZZLE DIAMETER IN FUSED DEPOSITION MODELING FOR EXTRUDING POLYLACTIC ACID USING OPEN SOURCE 3D PRINTING», *Jurnal Teknologi*, vol. 78, n. 10, set. 2016, doi: 10.11113/jt.v78.6265.

[8] B. Gharehpapagh, M. Dolen, e U. Yaman, «Investigation of Variable Bead Widths in FFF Process», *Procedia Manufacturing*, vol. 38, pp. 52–59, 2019, doi: 10.1016/j.promfg.2020.01.007.

[9] Y. Tlegenov, W. F. Lu, e G. S. Hong, «A dynamic model for current-based nozzle condition monitoring in fused deposition modelling», *Prog Addit Manuf*, vol. 4, n. 3, pp. 211–223, set. 2019, doi: 10.1007/s40964-019-00089-3.

[10] P. Pitayachaval e K. Masnok, «Feed rate and volume of material effects in fused deposition modeling nozzle wear», em *2017 4th International Conference on Industrial Engineering and Applications (ICIEA)*, Nagoya, Japan, abr. 2017, pp. 39–44. doi: 10.1109/IEA.2017.7939175.

[11] Diogo Vieira da Silva, «Efeitos da variação do diâmetro do bico de extrusão nas propriedades mecânicas de peças impressas por FFF em PLA», ISEP, Porto, Relatório de estágio curricular, 2021.

[12] G. Ćwikła, C. Grabowik, K. Kalinowski, I. Paprocka, e P. Ociepka, «The influence of printing parameters on selected mechanical properties of FDM/FFF 3D-printed parts», *IOP Conf. Ser.: Mater. Sci. Eng.*, vol. 227, p. 012033, ago. 2017, doi: 10.1088/1757-899X/227/1/012033.

[13] Silvina Luísa, Rodrigues Félix, e da Silva, «Design para fabrico aditivo Contributos de uma mudança de paradigma construtivo para a prática do designer», Universidade de Aveiro, Aveiro, 2019.

[14] L. Santana, «Avaliação das capacidades da impressão 3D de baixo custo na fabricação de snap-fits: uma relação de reconhecimento usuário-sistema de impressão», Doutorado, Universidade do Porto, Porto, 2019. Acedido: 4 de janeiro de 2022. [Em linha]. Disponível em: https://hdl.handle.net/10216/121051

[15] Sophian Beyerlein e M. Aboushama, «Evaluation of Continuous Fiber Reinforcement Desktop 3D Printers Desktop 3D Printers Overview», 2020, doi: 10.13140/RG.2.2.16640.87040.

[16] «Fused Deposition Modeling (FDM)», *custompart.net*. https://www.custompartnet.com/wu/fused-deposition-modeling

[17] I. Gibson, D. Rosen, B. Stucker, e M. Khorasani, *Additive Manufacturing Technologies*. Cham: Springer International Publishing, 2021. doi: 10.1007/978-3-030-56127-7.

[18] A. Bellini e S. Güçeri, «Mechanical characterization of parts fabricated using fused deposition modeling», *Rapid Prototyping Journal*, vol. 9, n. 4, pp. 252–264, out. 2003, doi: 10.1108/13552540310489631.

[19] A. Elkaseer, S. Schneider, e S. G. Scholz, «Experiment-Based Process Modeling and Optimization for High-Quality and Resource-Efficient FFF 3D Printing», *Applied Sciences*, vol. 10, n. 8, p. 2899, abr. 2020, doi: 10.3390/app10082899.

[20] B. Shaqour *et al.*, «Gaining a better understanding of the extrusion process in fused filament fabrication 3D printing: a review», *Int J Adv Manuf Technol*, vol. 114, n. 5–6, pp. 1279–1291, mai. 2021, doi: 10.1007/s00170-021-06918-6.

[21] Leonardo Santana, «Avaliação de uma impressora 3D baseada em projeto de código aberto na fabricação de peças em PLA», Mestrado, Universidade Federal de Santa Catarina, Florianópolis, 2015. Acedido: 4 de janeiro de 2022. [Em linha]. Disponível em: https://repositorio.ufsc.br/xmlui/handle/123456789/160786

[22] R. Jerez-Mesa, J. A. Travieso-Rodriguez, X. Corbella, R. Busqué, e G. Gomez-Gras, «Finite element analysis of the thermal behavior of a RepRap 3D printer liquefier», *Mechatronics*, vol. 36, pp. 119–126, jun. 2016, doi: 10.1016/j.mechatronics.2016.04.007.

[23] Z. Jiang, B. Diggle, M. L. Tan, J. Viktorova, C. W. Bennett, e L. A. Connal, «Extrusion 3D Printing of Polymeric Materials with Advanced Properties», *Adv. Sci.*, vol. 7, n. 17, p. 2001379, set. 2020, doi: 10.1002/advs.202001379.

[24] N. Venkataraman, S. Rangarajan,B. Harper, M. John Matthewson, Ahmad Safari, S.C. Danforth, *Process-Property-Performance Relationship for Fused Deposition of Ceramics (FDC) Feedstock Materials*. 2000.

[25] F. David Alencar de Sena Pereira, «Desenvolvimento de um cabeçote para extrusão de filamento fundido aplicado a manufatura aditiva», Mestre em Engenharia Mecânica, Universidade Estadual de Campinas, Campinas, 2014. doi: 10.47749/T/UNICAMP.2014.931397.

[26] D. Moreno Nieto e D. Moreno Sánchez, «Design for Additive Manufacturing: Tool Review and a Case Study», *Applied Sciences*, vol. 11, n. 4, p. 1571, fev. 2021, doi: 10.3390/app11041571.

[27] O.S. Carneiro, A.F.Silva, R.Gomes, «Fused deposition modeling with polypropylene», *Materials & Design*, vol. 83, n. 15, pp. 768–776, 15 de outubro de 2015.

[28] Agarwala, M. K.; Jamalabad, V. R.; Langrana, N. A.; Safari, A.; Whalen, P. J.; Danforth, «Structural quality of parts processed by fused deposition.», vol. Rapid Prototyping Journal, p. 2(4), 4–19, 1996.

[29] «Layers and perimeters». https://help.prusa3d.com/en/article/layers-and-perimeters_1748 (acedido 16 de janeiro de 2022).

[30] «The effect of extrusion width on strength and quality of 3D prints», *CNC kitchen*, 19 de outubro de 2019. https://www.cnckitchen.com/blog/the-effect-of-extrusion-width-on-strength-and-quality-of-3d-prints (acedido 16 de junho de 2020).

[31] P. Ferretti *et al.*, «Relationship between FDM 3D Printing Parameters Study: Parameter Optimization for Lower Defects», *Polymers*, vol. 13, n. 13, p. 2190, jun. 2021, doi: 10.3390/polym13132190.

[32] Martin, «3D Printer Line/Extrusion Width | Best Settings & Examples», *The 3D printer Bee*. https://the3dprinterbee.com/3d-printer-line-extrusion-width/ (acedido 16 de janeiro de 2020).

[33] O. A. Mohamed, S. H. Masood, e J. L. Bhowmik, «Modeling, analysis, and optimization of dimensional accuracy of FDM-fabricated parts using definitive screening design and deep learning feedforward artificial neural network», *Adv. Manuf.*, vol. 9, n. 1, pp. 115–129, mar. 2021, doi: 10.1007/s40436-020-00336-9.

[34] N. Zohdi e R. (Chunhui) Yang, «Material Anisotropy in Additively Manufactured Polymers and Polymer Composites: A Review», *Polymers*, vol. 13, n. 19, p. 3368, set. 2021, doi: 10.3390/polym13193368.

[35] B. Akhoundi e A. H. Behravesh, «Effect of Filling Pattern on the Tensile and Flexural Mechanical Properties of FDM 3D Printed Products», *Exp Mech*, vol. 59, n. 6, pp. 883–897, jul. 2019, doi: 10.1007/s11340-018-00467-y.

[36] N. Volpato e J. A. Foggiatto, «IMPLEMENTAÇÃO NO PROCESSO DE MODELAGEM POR FUSÃO E DEPOSIÇÃO (FDM)», p. 104.

[37] «Deposition strategies and resulting part stiffnesses in fused deposition modeling», *Journal of manufacturing science and engineering*, vol. v. 121, n. n. 1, pp. 93–103, 1999.

[38] M. M. Mbow, P. R. Marin, e F. Pourroy, «Extruded diameter dependence on temperature and velocity in the fused deposition modeling process», *Prog Addit Manuf*, vol. 5, n. 2, pp. 139–152, jun. 2020, doi: 10.1007/s40964-019-00107-4.

[39] Ken Douglas, «3D Printer Heated Bed – The Advantages», 27 de julho de 2021. https://all3dp.com/2/3d-printer-heated-bed-advantages/ (acedido 16 de janeiro de 2022).

[40] M. Spoerk, J. Gonzalez-Gutierrez, J. Sapkota, S. Schuschnigg, e C. Holzer, «Effect of the printing bed temperature on the adhesion of parts produced by

fused filament fabrication», *Plastics, Rubber and Composites*, vol. 47, n. 1, pp. 17–24, jan. 2018, doi: 10.1080/14658011.2017.1399531.

[41] M. Pivar, D. Gregor-Svetec, e D. Muck, «Effect of Printing Process Parameters on the Shape Transformation Capability of 3D Printed Structures», *Polymers*, vol. 14, n. 1, p. 117, dez. 2021, doi: 10.3390/polym14010117.

[42] Akande, Stephen & Dalgarno, Kenny & Munguia, Javier, «Quality assurance and process monitoring of fused deposition modelling made parts», pp. 31–35, 2014.

[43] S. A. Tronvoll, S. Popp, C. W. Elverum, e T. Welo, «Investigating pressure advance algorithms for filament-based melt extrusion additive manufacturing: theory, practice and simulations», *RPJ*, vol. 25, n. 5, pp. 830–839, jun. 2019, doi: 10.1108/RPJ-10-2018-0275.

[44] L. M. Galantucci, I. Bodi, J. Kacani, e F. Lavecchia, «Analysis of Dimensional Performance for a 3D Open-source Printer Based on Fused Deposition Modeling Technique», *Procedia CIRP*, vol. 28, pp. 82–87, 2015, doi: 10.1016/j.procir.2015.04.014.

[45] Facundo Arceo, «3D Print Speed vs Quality; Best Settings!», *3D Solved*. https://3dsolved.com/3d-printing-speed-vs-quality/

[46] «Calibrating maximum volumetric rate», *Bob's project notebook*. https://projects.ttlexceeded.com/3dprinting_techniques_calibrating_volumetric_rate.html (acedido 16 de janeiro de 2022).

[47] «Original Prusa i3 MK3S+ 3D printer». https://www.prusa3d.com/product/original-prusa-i3-mk3s-3d-printer-3/#Features (acedido 25 de janeiro de 2022).

[48] P. J. Nuñez, A. Rivas, E. García-Plaza, E. Beamud, e A. Sanz-Lobera, «Dimensional and Surface Texture Characterization in Fused Deposition Modelling (FDM) with ABS plus», *Procedia Engineering*, vol. 132, pp. 856–863, 2015, doi: 10.1016/j.proeng.2015.12.570.

[49] C. Abeykoon, P. Sri-Amphorn, e A. Fernando, «Optimization of fused deposition modeling parameters for improved PLA and ABS 3D printed structures», *International Journal of Lightweight Materials and Manufacture*, vol. 3, n. 3, pp. 284–297, set. 2020, doi: 10.1016/j.ijlmm.2020.03.003.

[50] S. Ahn, M. Montero, D. Odell, S. Roundy, e P. K. Wright, «Anisotropic material properties of fused deposition modeling ABS», *Rapid Prototyping Journal*, vol. 8, n. 4, pp. 248–257, out. 2002, doi: 10.1108/13552540210441166.

[51] A. K. Sood, R. K. Ohdar, e S. S. Mahapatra, «Experimental investigation and empirical modelling of FDM process for compressive strength improvement», *Journal of Advanced Research*, vol. 3, n. 1, pp. 81–90, jan. 2012, doi: 10.1016/j.jare.2011.05.001.

[52] A. DeCicco e J. Faust, «Effects of Build Parameters on Additive Materials», p. 193.

[53] E. G. Gordeev, A. S. Galushko, e V. P. Ananikov, «Improvement of quality of 3D printed objects by elimination of microscopic structural defects in fused deposition modeling», *PLoS ONE*, vol. 13, n. 6, p. e0198370, jun. 2018, doi: 10.1371/journal.pone.0198370.

[54] Guessasma, Belhabib, e Nouri, «Microstructure and Mechanical Performance of 3D Printed Wood-PLA/PHA Using Fused Deposition Modelling: Effect of Printing Temperature», *Polymers*, vol. 11, n. 11, p. 1778, out. 2019, doi: 10.3390/polym11111778.

[55] T. J. Coogan e D. O. Kazmer, «Prediction of interlayer strength in material extrusion additive manufacturing», *Additive Manufacturing*, vol. 35, p. 101368, out. 2020, doi: 10.1016/j.addma.2020.101368.

[56] A. Pandzic, D. Hodzic, e A. Milovanovic, «Effect of Infill Type and Density on Tensile Properties of PLA Material for FDM Process», em *DAAAM Proceedings*, 1.ª ed., vol. 1, B. Katalinic, Ed. DAAAM International Vienna, 2019, pp. 0545–0554. doi: 10.2507/30th.daaam.proceedings.074.

[57] T. J. Coogan e D. O. Kazmer, «Modeling of interlayer contact and contact pressure during fused filament fabrication», *Journal of Rheology*, vol. 63, n. 4, pp. 655–672, jul. 2019, doi: 10.1122/1.5093033.

[58] J. Yin, C. Lu, J. Fu, Y. Huang, e Y. Zheng, «Interfacial bonding during multi-material fused deposition modeling (FDM) process due to inter-molecular diffusion», *Materials & Design*, vol. 150, pp. 104–112, jul. 2018, doi: 10.1016/j.matdes.2018.04.029.

[59] I. Calafel *et al.*, «Searching for Rheological Conditions for FFF 3D Printing with PVC Based Flexible Compounds», *Materials*, vol. 13, n. 1, p. 178, jan. 2020, doi: 10.3390/ma13010178.

[60] «Fluidity and Viscosity», *Tudo sobre plásticos*. https://www.tudosobreplasticos.com/en/propriedades/fluidez.asp (acedido 19 de janeiro de 2022).

[61] D. Vaes e P. Van Puyvelde, «Semi-crystalline feedstock for filament-based 3D printing of polymers», *Progress in Polymer Science*, vol. 118, p. 101411, jul. 2021, doi: 10.1016/j.progpolymsci.2021.101411.

[62] C.McIlroy, R.S.Graham, «Modelling flow-enhanced crystallisation during fused filament fabrication of semi-crystalline polymer melts», vol. Volume 24, pp. 323–340, dezembro de 2018.

[63] J. Chen e D. E. Smith, «A Low-Cost Approach for Characterizing Melt Flow Properties of Filaments Used in Fused Filament Fabrication Additive Manufacturing», p. 13.

[64] T. J. Coogan e D. O. Kazmer, «In-line rheological monitoring of fused deposition modeling», *Journal of Rheology*, vol. 63, n. 1, pp. 141–155, jan. 2019, doi: 10.1122/1.5054648.

[65] B. T. Atwood e W. R. Schowalter, «Measurements of slip at the wall during flow of high-density polyethylene through a rectangular conduit», *Rheol Acta*, vol. 28, n. 2, pp. 134–146, mar. 1989, doi: 10.1007/BF01356974.

[66] Saadat A, Nazockdast H, Sepehr F, Mehranpour M, «Linearand nonlinear melt rheology and extrudate swell of acrylonitrile-butadiene-styrene and organoclay-filled acrylonitrile-butadiene-styrene nanocomposite», *Polym Eng Sci 50(12):2340–2349*, 2010.

[67] ALANKAR AGRAWAL, «Computational and mathematical analysis of dynamics of fused deposition modelling based rapid prototyping technique for scaffold fabrication», Índia, 2014.

[68] B. P. Heller, D. E. Smith, e D. A. Jack, «Effects of extrudate swell and nozzle geometry on fiber orientation in Fused Filament Fabrication nozzle flow», *Additive Manufacturing*, vol. 12, pp. 252–264, out. 2016, doi: 10.1016/j.addma.2016.06.005.

[69] N. Shadvar, E. Foroozmehr, M. Badrossamay, I. Amouhadi, e A. S. Dindarloo, «Computational analysis of the extrusion process of fused deposition modeling of acrylonitrile-butadiene-styrene», *Int J Mater Form*, vol. 14, n. 1, pp. 121–131, jan. 2021, doi: 10.1007/s12289-019-01523-1.

[70] Vinay Kumar, Rupinder Singh, Inder Preet S. Ahuja, «Use of Thermosetting Polymers for Smart Civil Structures», *Reference Module in Materials Science and Materials Engineering*, 2020. [Em linha]. Disponível em: https://doi.org/10.1016/B978-0-12-820352-1.00067-5.

[71] S. Wang, L. Capoen, D. R. D'hooge, e L. Cardon, «Can the melt flow index be used to predict the success of fused deposition modelling of commercial poly(lactic acid) filaments into 3D printed materials?», *Plastics, Rubber and Composites*, vol. 47, n. 1, pp. 9–16, jan. 2018, doi: 10.1080/14658011.2017.1397308.

[72] Eom, Lee, e Lee, «Evaluation of Thermal Properties of 3D Spacer Technical Materials in Cold Environments using 3D Printing Technology», *Polymers*, vol. 11, n. 9, p. 1438, set. 2019, doi: 10.3390/polym11091438.

[73] E. Fuenmayor *et al.*, «Material Considerations for Fused-Filament Fabrication of Solid Dosage Forms», *Pharmaceutics*, vol. 10, n. 2, p. 44, abr. 2018, doi: 10.3390/pharmaceutics10020044.

[74] D. Dimonie e N. Dragomir, «Melt Rheology of Renewable Polymers and of New Materials Based on them as Tool in Controlling the 3D/4D Printability», *Mater. Plast.*, vol. 57, n. 4, pp. 77–87, jan. 2021, doi: 10.37358/MP.20.4.5408.

[75] R. Singh, R. Kumar, I. Farina, F. Colangelo, L. Feo, e F. Fraternali, «Multi-Material Additive Manufacturing of Sustainable Innovative Materials and Structures», *Polymers*, vol. 11, n. 1, p. 62, jan. 2019, doi: 10.3390/polym11010062.

[76] A. Dey, I. N. Roan Eagle, e N. Yodo, «A Review on Filament Materials for Fused Filament Fabrication», *JMMP*, vol. 5, n. 3, p. 69, jun. 2021, doi: 10.3390/jmmp5030069.

[77] 3d Matter, «Compare the main FDM 3D printing plastics - PLA, ABS, PET, Nylon, TPU (Flexible) and PC - by material properties and find the best option for your application.», *HUBS*. https://www.hubs.com/knowledge-base/fdm-3d-printing-materials-compared/ (acedido 4 de fevereiro de 2022).

[78] «Polymers For Material Extrusion Additive Manufacturing: Part-1», *Additive manufacturing Inc*. https://aminception.com/blog/viewblogs (acedido 4 de fevereiro de 2022).

[79] A. Joseph Arockiam, Karthikeyan Subramanian, R. G. Padmanabhan, Rajeshkumar Selvaraj, Dilip Kumar Bagal, e S. Rajesh, «A review on PLA with different fillers used as a filament in 3D printing», *Materials Today: Proceedings*, p. S221478532106329X, out. 2021, doi: 10.1016/j.matpr.2021.09.413.

[80] A. R. Torrado Perez, D. A. Roberson, e R. B. Wicker, «Fracture Surface Analysis of 3D-Printed Tensile Specimens of Novel ABS-Based Materials», *J Fail. Anal. and Preven.*, vol. 14, n. 3, pp. 343–353, jun. 2014, doi: 10.1007/s11668-014-9803-9.

[81] B. Meng, J. Deng, Q. Liu, Z. Wu, e W. Yang, «Transparent and ductile poly(lactic acid)/poly(butyl acrylate) (PBA) blends: Structure and properties», *European Polymer Journal*, vol. 48, n. 1, pp. 127–135, jan. 2012, doi: 10.1016/j.eurpolymj.2011.10.009.

[82] Jasim Ahmed, «Thermal Properties of Polylactides and Stereocomplex», *Glass Transition and Phase Transitions in Food and Biological Materials17/*, 17 de fevereiro de 2017. Acedido: 20 de março de 2022. [Em linha]. Disponível em: https://doi.org/10.1002/9781118935682.ch12

[83] S. G. Ji, J. H. Hwang, D. Cho, e H.-J. Kim, «Influence of electron beam treatment of jute on the thermal properties of random and two-directional jute/poly(lactic acid) green composites», *Journal of Adhesion Science and Technology*, vol. 27, n. 12, pp. 1359–1373, jun. 2013, doi: 10.1080/01694243.2012.697365.

[84] D. Garlotta, «A Literature Review of Poly(Lactic Acid)», p. 22.

[85] A. Lanzotti, M. Grasso, G. Staiano, e M. Martorelli, «The impact of process parameters on mechanical properties of parts fabricated in PLA with an open-source 3-D printer», *Rapid Prototyping Journal*, vol. 21, n. 5, pp. 604–617, ago. 2015, doi: 10.1108/RPJ-09-2014-0135.

[86] «Polylactic Acid (PLA)», *Prospectoor*. https://www.ulprospector.com/plastics/en/generics/34 (acedido 20 de março de 2022).

[87] Amar K. Mohanty, Manjusri Misra, Lawrence T. Drzal, *Natural Fibers, Biopolymers, and Biocomposites*, vol. 1st edition. 2005, 2005. [Em linha]. Disponível em: https://doi.org/10.1201/9780203508206

[88] L. Běhálek, P. Lenfeld, M. Seidl, J. Bobek, e A. Ausperger, «FRICTION PROPERTIES OF COMPOSITES WITH NATURAL FIBRES, SYNTHETIC AND BIODEGRADABLE POLYMER MATRIX», p. 6, 2012.

[89] «The Complete 3D Printer Nozzle Buyer's Guide». https://www.3dsourced.com/guides/3d-printer-nozzle/ (acedido 15 de janeiro de 2022).

[90] «Could This Be The Ultimate 3D Printer Nozzle?», *Fabbaloo*. https://www.fabbaloo.com/2018/02/could-this-be-the-ultimate-3d-printer-nozzle (acedido 15 de janeiro de 2022).

[91] «Tudo sobre bicos de impressora 3D (I): Classificação e recomendações», *filament2print*. https://filament2print.com/gb/blog/56_nozzles-guide-classification-recommendations.html (acedido 15 de janeiro de 2022).

[92] «Our Tungsten Carbide Nozzle is finally available», *dyzedesign*. https://dyzedesign.com/2019/01/our-tungsten-carbide-nozzle-is-finally-available/ (acedido 15 de janeiro de 2022).

[93] «ZODIAC V6 [PRO] 3D PRINTER NOZZLE - 0.4 MM», *Plasticz*. https://www.plasticz.nl/en/v6-pro-3d-printer-nozzle-04-mm.html (acedido 15 de janeiro de 2022).

[94] «How Long Does a 3D Printer Nozzle Last?», *3DP master*. https://3dpmaster.com/how-long-does-a-3d-printer-nozzle-last/ (acedido 15 de janeiro de 2022).

[95] filament2print, «All about 3D printer nozzles (II): When to change the nozzle». https://filament2print.com/gb/blog/57_nozzles-guide-when-change-it.html (acedido 15 de janeiro de 2022).

[96] «E3D-Lite6 Documentation». https://wiki.e3d-online.com/E3D-Lite6_Documentation (acedido 19 de março de 2022).

[97] R. A. Buswell, W. R. Leal de Silva, S. Z. Jones, e J. Dirrenberger, «3D printing using concrete extrusion: A roadmap for research», *Cement and Concrete Research*, vol. 112, pp. 37–49, out. 2018, doi: 10.1016/j.cemconres.2018.05.006.

[98] F. Bos, R. Wolfs, Z. Ahmed, e T. Salet, «Additive manufacturing of concrete in construction: potentials and challenges of 3D concrete printing», *Virtual and Physical Prototyping*, vol. 11, n. 3, pp. 209–225, jul. 2016, doi: 10.1080/17452759.2016.1209867.

[99] Honghyu Kwon, «Experimentation and analysis of contour crafting (CC) process using uncured ceramic materials», University of Southern California, California, USA, 2002.

[100] M. E. A. Papon, A. Haque, e M. A. R. Sharif, «Effect of Nozzle Geometry on Melt Flow Simulation and Structural Property of Thermoplastic Nanocomposites in Fused Deposition Modeling», apresentado na American Society for Composites 2017, nov. 2017. doi: 10.12783/asc2017/15339.

[101] W. Muhamad, «NOZZLE DESIGN FOR FUSED DEPOSITION MODELLING 3D PRINTING OF CARBON FIBRE REINFORCED POLYMER COMPOSITE COMPONENT USING SIMULATION METHOD», p. 13, 2020.

[102] T. Beran, T. Mulholland, F. Henning, N. Rudolph, e T. A. Osswald, «Nozzle clogging factors during fused filament fabrication of spherical particle filled polymers», *Additive Manufacturing*, vol. 23, pp. 206–214, out. 2018, doi: 10.1016/j.addma.2018.08.009.

[103] «Bondtech CHT high flow nozzle reviewed», 23 de outubro de 2021. https://www.cnckitchen.com/blog/bondtech-cht-high-flow-nozzle-reviewed (acedido 18 de janeiro de 2022).

[104] «20 principais erros de impressão e como os resulver. Guia completo!», *3DLAB*. https://3dlab.com.br/20-principais-erros-de-impressao/ (acedido 5 de março de 2022).

[105] «3 Soluções para “over extrusion” extrusão excessiva em impressão 3D», *Magma*. https://magma3d.com.br/2020/04/07/over-extrusion-extrusao-excessiva/ (acedido 5 de março de 2022).

[106] «Guia visual para resolver problemas impressão 3D pela Bitfab», *bitfab*. https://bitfab.io/pt-pt/blog/problemas-impressao-3d/#_El_pie_de_elefante (acedido 12 de fevereiro de 2022).

[107] BuildTak, «What is bed adhesion?», *all3dp*. https://all3dp.com/2/3d-printer-bed-adhesion-all-you-need-to-know/ (acedido 5 de março de 2022).

[108] «3D Printing: Elephant’s Foot – Easy Fixes», *all3dp*, 17 de junho de 2021. https://all3dp.com/2/elephant-s-foot-3d-printing-problem-easy-fixes/ (acedido 5 de março de 2022).

[109] Jackson O’Connell, Hironori Kondo, «3D Print Ghosting & Ringing: 3 Easy Fixes», *all3dp*, 6 de fevereiro de 2022. https://all3dp.com/2/3d-printer-ringing-3d-print-ghosting/ (acedido 5 de março de 2022).

[110] L. Santana, J. Lino Alves, e A. da Costa Sabino Netto, «DIMENSIONAL ANALYSIS OF PLA AND PETG PARTS BUILT BY OPEN SOURCE EXTRUSION-BASED 3D PRINTING», apresentado na COBEF 2019, 2019. doi: 10.26678/ABCM.COBEF2019.COF2019-0078.

[111] L. Santana, J. L. Alves, e A. da C. S. Netto, «Effect of the angle of the laid-up filaments on the surfaces on the coefficient of static friction between parts manufactured by extrusion-based 3D printing», *Proceedings of the Institution of*

Mechanical Engineers, Part L: Journal of Materials: Design and Applications, vol. 235, n. 6, pp. 1351–1367, jun. 2021, doi: 10.1177/1464420720978997.

[112] Francisco Forte Alvim de Castro, «Análise da influência da pigmentação na qualidade de peças impressas por FFF em PLA e PETG», Mestrado, Universidade do Porto, Porto, 2021. Acedido: 4 de janeiro de 2022. [Em linha]. Disponível em: https://hdl.handle.net/10216/135101

[113] Impressoras3D.com, «Como nivelar ou calibrar a base da imrpessora 3D», *impressora3D.com*, 24 de fevereiro de 2020. https://www.impresoras3d.com/pt/como-nivelar-ou-calibrar-a-base-da-impressora-3d/ (acedido 20 de março de 2022).

[114] «First layer calibration (i3)», *Prusa Knowledge base*. https://help.prusa3d.com/en/article/first-layer-calibration-i3_112364 (acedido 12 de fevereiro de 2022).

[115] «Prusa i3 MK2 MK3 MK3S Mini V6 Brass Nozzle Replacement - 1.75mm x 0.40mm», *Amazon*. https://www.amazon.com/Prusa-MK3S-Brass-Nozzle-Replacement/dp/B08LC5BZRG (acedido 12 de fevereiro de 2022).

[116] «V6/V5 brass nozzles», *Lukas Pomykal*. http://www.lpomykal.cz/v6-v5-brass-nozzles/ (acedido 13 de fevereiro de 2022).

[117] «Nozzles», *Evolt*. https://evolt.pt/product-category/impressao-3d/acessorios/nozzles/page/4/?_material=aco-endurecido&_diametro_do_nozzle=o-0-4-mm (acedido 12 de fevereiro de 2022).

[118] «Hardened and tempered Vanadium HSS nozzles by Slice Engineering», *Bondtech*. https://www.bondtech.se/product/vanadium-nozzle/ (acedido 12 de fevereiro de 2022).

[119] «Vanadium – Boiling – Melting Point – Thermal Conductivity – Expansion». https://material-properties.org/vanadium-thermal-properties-melting-point-thermal-conductivity-expansion/ (acedido 13 de fevereiro de 2022).

[120] «Vanadium nozzle problems. Is Tungsten Carbide the way to go?», *Prusaprinters forum*. https://forum.prusaprinters.org/forum/english-forum-general-discussion-announcements-and-releases/vanadium-nozzle-problems-is-tungsten-carbide-the-way-to-go/ (acedido 13 de fevereiro de 2022).

[121] «Nozzle E3D V6 0.6mm». https://www.prusa3d.com/product/nozzle-e3d-v6-0-6-mm/ (acedido 12 de fevereiro de 2022).

[122] «0.8mm latão nozzle v6 original m6×1×7.5×12.5 1.75mm (e3d genuíno compatível com mk2.5s, mk3s, mk2/s, mini) - e3d», *Evolt*. https://evolt.pt/produto/0-8mm-latao-nozzle-v6-original-m6x1x7-5x12-5-1-75mm-e3d-genuino-compativel-com-mk2-5s-mk3s-mk2-s-mini-e3d/ (acedido 12 de fevereiro de 2022).

[123] «1mm latão nozzle (compativel com e3d)- Aimsoar», *Evolt*. https://evolt.pt/produto/1mm-brass-nozzle-compativel-com-e3d-aimsoar/ (acedido 12 de fevereiro de 2022).

[124] A. C. G. Teixeira, «Caracterização de Propriedades Termo-Elétricas de Metal Duro», p. 87.

[125] Frandsen, M. V. & Williams, W. S., «Thermal Conductivity and Electrical Resistivity of Cemented Transition-Metal Carbides at Low Temperatures.», *Journal of the American Ceramic Society 74*, 1991.

[126] «Tungsten carbide material properties», *Imetra*. https://www.imetra.com/tungsten-carbide-material-properties/ (acedido 13 de fevereiro de 2022).

[127] «Implementing a Superellipse», *Geeksforgeeks*. https://www.geeksforgeeks.org/implementing-a-superellipse/ (acedido 13 de fevereiro de 2022).

[128] Tucab, «Fil3D PLA 3D850». 2021.

[129] L. Ford, «Ingeo Biopolymer 3D850 Technical Data Sheet», p. 5.

[130] Lucas Carolo, «Best 3D Printer Nozzle- Buyer's Guide». https://all3dp.com/2/3d-printer-nozzle-size-material-what-to-know-which-to-buy/ (acedido 28 de janeiro de 2022).

[131] ASTM International, «Standard Test Methods for Flexural Properties of Unreinforced and Reinforced Plastics and Electrical Insulating Materials». 2010. [Em linha]. Disponível em: DOI: 10.1520/D0790-10

[132] A. Y. Al-Maharma, S. P. Patil, e B. Markert, «Effects of porosity on the mechanical properties of additively manufactured components: a critical review», *Mater. Res. Express*, vol. 7, n. 12, p. 122001, dez. 2020, doi: 10.1088/2053-1591/abcc5d.

[133] «Max volumetric speed», *Prusa Knowledge base*. https://help.prusa3d.com/en/article/max-volumetric-speed_127176 (acedido 26 de janeiro de 2022).

[134] «7 modelos para ajudar a calibrar sua impressora 3D», *3D lab*. https://3dlab.com.br/calibrar-sua-impressora-3d/ (acedido 22 de janeiro de 2022).

[135] CreativeTools, «#3DBenchy - the Tool to Calibrate and Test Your 3D Printer». https://www.instructables.com/3DBenchy-The-tool-to-calibrate-and-test-your-3D-pr/ (acedido 27 de janeiro de 2022).

[136] *MakerBot*. https://www.thingiverse.com/thing:763622/files (acedido 22 de janeiro de 2022).

[137] «Burn marks and layer issues», *Ultimaker comunnity of 3D printing experts*. https://community.ultimaker.com/topic/23099-burn-marks-and-layer-issues/ (acedido 12 de fevereiro de 2022).

[138] T. Tichý, O. Šefl, P. Veselý, K. Dušek, e D. Bušek, «Mathematical Modelling of Temperature Distribution in Selected Parts of FFF Printer during 3D Printing Process», *Polymers*, vol. 13, n. 23, p. 4213, dez. 2021, doi: 10.3390/polym13234213.

[139] Robert Wilson, *Mathematical Modelling of Temperature Distribution in Selected Parts of FFF Printer during 3D Printing Process"*. 1975.

[140] «Slice engineering». https://www.sliceengineering.com/ (acedido 14 de abril de 2022).

[141] M. Alhijjaj, J. Nasereddin, P. Belton, e S. Qi, «Impact of Processing Parameters on the Quality of Pharmaceutical Solid Dosage Forms Produced by Fused Deposition Modeling (FDM)», *Pharmaceutics*, vol. 11, n. 12, p. 633, nov. 2019, doi: 10.3390/pharmaceutics11120633.

[142] G. Hsiang Loh, E. Pei, J. Gonzalez-Gutierrez, e M. Monzón, «An Overview of Material Extrusion Troubleshooting», *Applied Sciences*, vol. 10, n. 14, p. 4776, jul. 2020, doi: 10.3390/app10144776.

Anexo A – Calibration parameters

Table 20- Taguchi DOE.

	C1	C2	C3	C4	C5	C6	C7	C8	C9	C10	C11	C12	C13	C14	C15	C16
Print speed(mm/s)																
Infill	15.1	40	40	40	19.3	7.24	36	36	23.2	23.2	4.63	12.3	19.7	16.7	8.92	3.34
Perimeters	13.9	20	20	20	19.3	7.22	20	20	20	20	5.02	13.4	16.7	19.7	10.5	3.93
First layer perimeter	13.9	20	20	20	19.3	7.22	20	20	20	20	5.02	19.6	19.7	19.7	10.5	3.93
First layer infill	20.0	20	20	20	20	11.8	20	20	20	20	7.37	13.4	20	20	13.9	5.20
Road width (mm)																
External perimeters extrusion width	1.12	1.12	1.12	1.12	1.12	1.12	1.12	1.12	1.12	1.12	1.12	1.12	1.12	1.12	1.12	1.12
Perimeters extrusion width	1.12	1.12	1.12	1.12	1.12	1.12	1.12	1.12	1.12	1.12	1.12	1.12	1.12	1.12	1.12	1.12
Infill extrusion width	1.12	1.12	1.12	1.12	1.12	1.12	1.12	1.12	1.12	1.12	1.12	1.12	1.12	1.12	1.12	1.12

continues

Solid infill extrusion width	1.12	1.12	1.12	1.12	1.12	1.12	1.12	1.12	1.12	1.12	1.12	1.12	1.12	1.12	1.12
Top infil extrusion width	1.00	1.00	1.00	1.00	1.00	1.00	1.00	1.00	1.00	1.00	1.00	1.00	1.00	1.00	1.00

IKSAD GLOBAL
INSTITUTE OF ECONOMIC DEVELOPMENT AND SOCIAL RESEARCH

Certificate
OF PARTICIPATION

This certificate is proudly presented to

Joana TRIBUZI MELO

with the paper entitled

INTERNATIONAL CAPPADOCIA SCIENTIFIC RESEARCH CONGRESS
held on 15-17 December 2021 / Cappadocia-Nevşehir
Mustafa Cappadocia Resort Hotel

in oral and technical presentation,
recognition and appreciation of research contributions to

3D PRINTER NOZZLE: EFFECTS OF ITS DIAMETER AND MATERIAL ON THE QUALITY OF EXTRUDED FILAMENT AND FFF-PRINTED PARTS

Prof. Dr. Mustafa TALAS
Chairman of Organizing Board

www.cappadociacongress.org

Anexo 1- Certificate of participation in an international conference.